12-2022

Fabrication and Characterization of Force Spun Polymeric Nanofiber for Drug Delivery and Tissue Engineering Applications

Salahuddin Ahmed
The University of Texas Rio Grande Valley

FABRICATION AND CHARACTERIZATION OF FORCE SPUN POLYMERIC NANOFIBER FOR DRUG DELIVERY AND TISSUE ENGINEERING APPLICATIONS

A Thesis

by

SALAHUDDIN AHMED

Submitted in Partial Fulfillment of the

Requirements for the Degree of

MASTER OF SCIENCE IN ENGINEERING

Major Subject: Mechanical Engineering

The University of Texas Rio Grande Valley

December 2022

FABRICATION AND CHARACTERIZATION OF FORCE SPUN POLYMERIC NANOFIBER FOR DRUG DELIVERY AND TISSUE ENGINEERING APPLICATIONS

A Thesis

by

SALAHUDDIN AHMED

COMMITTEE MEMBERS

Dr. Karen Lozano
Chair of Committee

Dr. Robert Gilkerson
Committee Member

Dr. Rogelio Benitez
Committee Member

December 2022

ABSTRACT

Ahmed, Salahuddin, Fabrication and characterization of force spun polymeric nanofiber for drug delivery and tissue engineering applications. Master of Science in Engineering (MSE) December, 2022, 82 pp., 7 tables, 29 figures, 194 references.

This study focuses on the development and characterization of polymeric nanofiber for drug delivery and tissue engineering applications. In this study, poly(lactic-co-glycolic) acid (PLGA), Poly-vinyl alcohol (PVA), and Pullulan(PL) were used as the base polymers to develop the nanofiber. Bioactive components Oleanolic acid(OA), Oxymatrine(OM), and Salvianolic Acid(SA) were incorporated in PLGA, PVA, and PL, respectively, via solution mixing. The nano fiber systems were developed using the Forcespinning® method. Morphological, thermo-physical, and biological properties of the fiber mats were analyzed. The composite fiber system containing OA showed a very high drug loading efficiency. The composite fiber system containing high concentration of OM(33%) and SA(25% and 33%) showed effective inhibition against the proliferation of HCT116 colon cancer cells.

DEDICATION

All praise to the almighty Allah; without his blessings, I wouldn't be able to make it until this point. I want to dedicate this work to my parents, A.K.M. Ilias and Shafinaz Parvin, who have always shown me their love, support, and my siblings, Anika Parvin and Saima Sultana, for their love and affection.

ACKNOWLEDGMENTS

I would like to express my sincere gratitude and appreciation to my dissertation supervisor Dr. Karen Lozano for guiding my research in advanced nanomaterials technology. I would like to express my gratitude and special appreciation to Dr. Lozano for her encouragement, guidance, and support throughout my study in the USA. Her motivation has inspired me to achieve my goals. Moreover, her ability and dedication to work helped me to become a better student and person.

I would also like to thank Dr. Victoria Padilla for her guidance, training, and helping me to analyze different experimental results. I would also like to thank Dr. Robert Gilkerson and Dr. Megan Keniry for their kind support in performing the biological experiments and guidance. I would like to thank Dr. Ali Ashraf for his kind support and guidance. I also would like to thank my thesis committee member Dr. Rogelio Benitez for his support. I would also like to thank Dr. Eman Ibrahim for training me on fabrication and different characterization techniques and my lab partners Alexa Villereal, Narcedalia Anaya Barbosa, Casandra Lira, Kithzia Gomez, and Kollol Sarker Jogesh for their effort and suggestions to complete my work.

This project is supported by the NSF PREM award under grant No. DMR 2122178.

TABLE OF CONTENTS

Page

ABSTRACT iii

DEDICATION iv

ACKNOWLEDGMENTS v

TABLE OF CONTENTS vi

LIST OF TABLES viii

LIST OF FIGURES ix

CHAPTER I. INTRODUCTION 1

CHAPTER II. PROCESSING-STRUCTURE-PROPERTY RELATIONSHIPS OF OLEANOLIC ACID LOADED PLGA FIBER MEMBRANES. 4

2.1 Introduction 4

2.2 Materials and Methods 8

2.2.1 Materials 8

2.2.2 Solution Preparation 8

2.2.3 Development of Fiber Membranes 8

2.2.4 Fiber Characterization 9

2.2.5 Cell Interaction studies 10

2.3 Results 11

2.4 Discussions 21

CHAPTER III. OXYMATRINE LOADED CROSSLINKED PVA NANOFIBROUS SCAFFOLD: DESIGN, CHARACTERIZATION, AND ANTI-CANCER PROPERTIES 23

3.1 Introduction 23

3.2 Materials and Method 27

3.2.1 Materials 27

3.2.2 Solution Preparation 27

3.2.3 Development of nanofiber membranes 28

3.2.4 Crosslinking of nanofiber 28
3.2.5 Nanofiber characterization 29
3.2.6 Cell Viability Studies 29
3.2.7 In vitro anticancer activity 29
3.3 Results 30
3.4 Discussion 44

CHAPTER IV. SALVIANOLIC ACID-LOADED NANOFIBER AND ITS BIOACTIVE EFFECTS ON FIBROBLAST AND HCT116 COLON CANCER CELLS 46
4.1 Introduction 46
4.2 Materials and Method 50
4.2.1 Materials 50
4.2.2 Solution Preparation 51
4.2.3 Development of Nanofiber 51
4.2.4 Fiber Characterization 51
4.2.5 Cell viability study 52
4.2.6 Invitro anti cancer studies 52
4.3 Results 53
4.4 Discussion 61
CHAPTER V. CONCLUSION 62
CHAPTER VI. FUTURE PROSPECTS 63
REFERENCES 64
BIOGRAPHICAL SKETCH 82

LIST OF TABLES

Page

Table 2.1 TGA data of OA powder, PLGA control fiber, PLGAOA20 and PLGAOA33 composite fiber 13

Table 2.2 Various concentrations and drug loading efficiency of the formulations 20

Table 3.1 Concentrations of the components in the nanofiber samples. 28

Table 3.2 Statistical analysis of fiber diameters for 100 fibers from PVA-OM fiber samples.....33

Table 3.3 Statistical analysis of bead size for 50 fibers from PVA-OM fiber samples. 33

Table 3.4 Degradation steps for OM loaded nanofibers 40

Table 3.5: The melting temperature and melting enthalpy of crosslinked PVA and OM loaded PVA nanofibers. 41

LIST OF FIGURES

Page

Figure 2.1: Chemical structure of Poly(lactic-co-glycolic) acid and Oleanolic Acid.....7
Figure 2.2: Schematics showing the FS method used to prepare the fiber membranes 9
Figure 2.3: SEM micrographs of the developed fibrous materials: PLGA control (a), PLGAOA20 (b), PLGAOA33(c) and fiber distribution of PLGA control (d), PLGAOA20 (e), and PLGAOA33 (f). 12
Figure 2.4: TGA analysis of Oleanolic Acid powder, PLGA control, and Oleanolic Acid loaded PLGA nanofiber membrane; PLGAOA20 and PLGAOA33. 14
Figure 2.5: DTG analysis of Oleanolic Acid powder, PLGA control, and Oleanolic Acid loaded PLGA nanofiber membrane; PLGAOA20 and PLGAOA33.....15
Figure 2.6: DSC Thermogram of Oleanolic Acid powder (a) PLGA control, PLGAOA20, PLGAOA33 composite nanofiber and PLGAOA20, PLGAOA33 film (b).....16
Figure 2.7: Fourier-transform infrared (FTIR) spectrum of Oleanolic Acid Powder, PLGA control, PLGAOA20, and PLGAOA33 composite nanofiber membranes 18
Figure 2.8: XRD pattern of Oleanolic Acid Powder(a), PLGA control, PLGAOA20, and PLGAOA33 composite nanofiber 19
Figure 2.9. Confocal imaging of OA-containing fibers seeded with 3T3 mouse embryonic fibroblasts. 21
Figure 2.10. MTT assay of cell viability in the presence of control and OA-containing nanofibers. 21
Figure 3.1: The chemical structure of PVA (a) and Oxymatrine (b) 27

Figure 3.2: SEM micrograph of crosslinked PVA nanofiber and OM loaded crosslinked PVA nanofiber. CA5PVA9 (a), CA5PVA9OM20 (b), CA5PVA9OM33(c), CA10PVA9 (d), CA10PVA9OM20 (e), CA10PVA9OM33(f) 31

Figure 3.3: Distribution of 100 fiber diameter (a) and 50 bead size (b) in PVA-OM nanofiber formed during FS. 32

Figure 3.4: SEM images of CA5PVA9 (a), CA5PVA9OM20 (b) and CA5PVA9OM33 (c), CA10PVA9 (d), CA10PVA9OM20 (e) and CA10PVA9OM33 (f) after water absorption 34

Figure 3.5: EDS spectra of CA5PVA9 (a), CA5PVA9OM20 (b) and CA5PVA9OM33 (c).....35

Figure 3.6: EDS spectra of CA10PVA9 (d), CA10PVA9OM20 (e) and CA10PVA9OM33 (f) .36

Figure 3.7: DSC(a) and TGA-DTG(b) curve of OM powder.....37

Figure 3.8: TGA curve of uncrosslinked and crosslinked PVA control(a), 20% OM loaded fiber (c), 33% OM loaded fiber(e). Corresponding DTG curve of uncrosslinked and crosslinked PVA control(b), 20% OM loaded fiber (d), 33% OM loaded fiber(f).....39

Figure 3.9: DSC curve of uncrosslinked PVA, Crosslinked PVA, OM loaded crosslinked PVA nanofiber. Crosslinked with 5% Citric Acid(a), crosslinked with 10% Citric Acid (b) 40

Figure 3.10: FTIR spectra of OM, Uncrosslinked PVA, Crosslinked PVA, OM loaded crosslinked PVA nanofiber. Crosslinked with 5% Citric Acid (a), Crosslinked with 10% Citric Acid (b).....42

Figure 3.11: MTT assay of cell viability in the presence of control and OM-containing nanofibers.....43

Figure 3.12: MTT assay of anticancer studies of control and OM-containing nanofibers and bare OM 44

Figure 4.1: Chemical structure of Pullulan(a), Chitosan(b), Salvianolic Acid B (c).....50

Figure 4.2: SEM micrographs and fiber distribution of the developed fibrous materials: PL-CS control (a), PL-CS-SA(L) (b), PL-CS-SA(H) (c).....54

Figure 4.3: Fourier transform infrared (FTIR) spectra of PL powder, CS powder andSA powder(a), PL-CS control fiber, PL-CS-SA(L) composite fiber and PL-CS-SA(H)(b) composite fiber 56

Figure 4.4: TGA(a) and DTG(c) analysis of PL, CS, and SA powder samples. TGA(b) and DTG(d) analysis of PL-CS control, PL-CS-SA(L) and PL-CS-SA(H) composite fiber 57

Figure 4.5: DSC analysis of PL, CS, and SA powder samples(a) and PL-CS control, PL-CS-SA(L) and PL-CS-SA(H) composite fiber(b) 58

Figure 4.6: MTT assay of cell viability in the presence of PL-CS control and SA-containing nanofibers.....59

Figure 4.7: Anti-cancer activity of PL-CS control, SA-containing nanofibers and raw SA powder.....60

CHAPTER I

INTRODUCTION

Nanofibers have emerged as an interesting one-dimensional nanomaterials because of their unique physicochemical properties and characteristics such as high specific surface area and surface area-to-volume ratio. The capability of forming networks of highly porous mesh with remarkable interconnectivity between their pores makes nanofibers an attractive choice for a variety of cutting-edge applications. Nanofibers can be developed from wide range of materials, such as natural polymers, synthetic polymers , carbon-based nanomaterials, semiconducting nanomaterials, and composite nanomaterials. The potential functional use of nanofibers includes applications in energy generation and storage, water and environmental treatment, and biomedical fields among others.

This thesis describes the development of polymer based fine fiber membranes and its use in drug delivery and tissue engineering applications. A variety of biocompatible polymer systems and bioactive compounds have been explored in this field. Particularly, this work focuses on the development of fiber based membranes using combinations of poly(lactic-co-glycolic) acid, poly (vinyl alcohol), pullulan, and chitosan with the following bioactive compounds, oleanolic acid, oxymatrine, and salvianolic acid. This thesis has been organized per developed systems as individual chapters, each with its corresponding literature review pertinent and characterization.
Chapter II focuses on the development of oleanolic acid (OA) loaded poly(lactic-co-glycolic) acid fiber membranes were utilizing the Forcespinning technology. OA is a natural pentacyclic triterpenoid compound available in fruits and vegetables and known for its plethora of biological activities. The incorporation of OA into polymeric fine fiber membranes opens promising potential applications for biomedical applications such as a system for transdermal delivery of bioactive agents. In this study, nonwoven fiber membranes were developed with different concentrations of OA and morphological, thermo-physical and biological studies were conducted. Results show a

high yield of fiber membranes with average fiber diameters ranging from 541 to 630 nm depending on the concentration of OA. Developed membranes are composed of long and continuous fibers showing rough surfaces. The developed membranes showed stability in aqueous media. Thermo-physical analysis showed miscibility of the components and negligible effects of processing conditions on the structure and stability of the components. High drug loading efficiency (>80%) was observed and cellular studies showed a non-cytotoxic behavior from the developed fiber membranes on fibroblast cells. The observed structural and thermal stability, and non-cytotoxic behavior of these membranes make them a promising potential vehicle for drug delivery applications.

Chapter III presents the fabrication and characterization of biocompatible, and biodegradable composite nanofibers consisting of poly (vinyl alcohol) (PVA), oxymatrine (OM), and citric acid (CA) using a facile and high-yield centrifugal spinning process known Forcespinning®. The effects of varying concentration of OM and CA on fiber diameter and molecular crosslinking respectively were investigated. The morphological and thermo-physical properties, as well as water absorption on the nanofibers were characterized using scanning electron microscopy, Fourier transform infrared spectroscopy, differential scanning calorimetry and thermogravimetric analysis. In vitro cell viability studies and in vitro anticancer studies were conducted. Results show a high yield of long fibers embedded with beads. Fiber average diameters ranged between 462 and 528nm depending on OM concentration. The thermal analysis results show that the fibers are stable in room temperature. The anticancer study revealed that PVA nanofiber membrane with high concentrations of OM can suppress the proliferation of HCT116 colorectal cancer cells. The study provides a comprehensive investigation of OM embedded into nanosized PVA fibers and the prospective application of these membranes as a drug delivery system.

Chapter IV investigates the feasibility of centrifugal spinning for producing fibrous membranes containing pullulan, chitosan, and danshen extract. The danshen extract composed of 20wt% salvianolic acid B (SA); a bioactive component that defined as a super herb due to its low toxicity and various pharmacological effects. Citric acid was added to the mixture as a crosslinking agent and promote its use in an aqueous medium. The influence of the danshen concentration (20 wt% and 33 wt%) on fiber morphology, thermal behavior, and biochemical effect was analyzed. The developed nonwoven composite membranes consist of long, continuous and homogeneous

fibers with sparse scattering of beads, with an average fiber diameter varying between 384 ± 123 nm and 644 ± 141 nm depending on the danshen concentration. The nanofibers showed adequate aqueous stability after crosslinking. Thermal analysis proved that SA was loaded into nanofibers without compromising their structural integrity. Cell-based results indicate that the developed nanofiber membranes promote cell growth and are not detrimental to fibroblast cells. Anticancer studies reveal a promising inhibition to proliferation of HCT116 colon cancer cells. The developed systems show potential as innovative systems to be used as a bioactive chemotherapeutic drug that could be placed on the removed tumor site to prevent colon cancer microdeposits from developing.

CHAPTER II

PROCESSING-STRUCTURE-PROPERTY RELATIONSHIPS OF OLEANOLIC ACID LOADED PLGA FIBER MEMBRANES

2.1 Introduction

Fine fiber based nonwoven membranes have shown multiple promising potential applications. Fine fiber refers to nano, submicron and single digit micron fiber systems, these have found promising applications in a wide number of fields namely filtration, batteries, cosmetics, and biomedical fields among others. Within the biomedical area, its use has been explored in wound care, tissue regeneration, and drug delivery. Drug is crucial to medical treatment. Medicinal agents, natural or synthetic, have a therapeutic effect when their concentrations in blood are higher than their minimal effective level. However, each medicine has its biological half-life and cannot sustain an effective concentration for an extended period. Simply raising the dosage will push the drug into a toxic response zone. On the other hand, giving the patient the same dose of drug numerous times over a period of time (e.g., three/four times a day) might be inconvenient. (Meng et al. 2011) Targeted drug delivery systems have been developed to maximize the therapeutic effects and minimize its toxic effects by delivering the drug to the target sites and reducing the exposure to the non-targeted sites. Controlled release of drugs at target areas promotes maintenance of needed drug concentration while reducing side effects given a reduction in overall amount, and ultimately improves patients' quality of life. (Malik et al. 2015), (Mir, Ahmed, and Rehman 2017)

Nanotechnology-based drug delivery systems which use nanoparticles, hydrogels, and nanofibers are gaining increasing interest due to their ability to deliver drugs at a specific location

with specific pharmacokinetics. Nanofiber membranes are promising systems to be used as scaffolds due to their unique properties, for example, high surface-to-volume ratio, tunable porosity, structural stability and the ability to conform. These properties also make fine fiber membranes highly promising to hold active ingredients and be used as drug delivery systems. The high surface to volume ratio of the nanofiber provides a large contact area for the dissolution of the active ingredient. (Malik et al. 2015) Nanofibers also can encapsulate substances protecting these from adverse atmospheric conditions therefore retaining their therapeutic effect for longer periods of time. Liu et al. (Yang and Tianjin 2014) developed self-assembling peptide nanofibers loaded with curcumin for tumor targeting drug delivery. Their results revealed promising potential as an effective treatment for cancer. Mondal et al. (Mondal et al. 2014) reported high loading levels of enzymes in TiO_2 as a result of the high mesoporosity associated with the nanofiber membrane. Jankovic et el. (Janković et al. 2013) reported that due to the high elasticity, PVA and PEO nanofiber membranes are suitable as scaffolds for tissue regeneration. Han et al. (Han et al. 2011) reported on the ability of nanofibers to protect enzymes from environmental damage.

Electrospinning and centrifugal spinning or Forcespinning® (FS) are two effective technologies to produce fine fiber membranes. The most commonly reported methods to fabricate nanofibers with potential to carry active ingredients and ultimately be used as drug delivery systems are basically variations of the traditional electrospinning and include direct blend electrospinning (H. Peng et al. 2008), coaxial electrospinning (Shoba et al. 2017), and emulsion electrospinning (Moydeen et al. 2018). Although electrospinning is the most popular method it suffers from low yield and specific needs given the use of high electric fields which limits the use of some melt/solution systems. The FS technology overcomes existent limitations (Sarkar et al. 2010), it has been proven to be a feasible option for mass production of nanofiber membranes from a broad range of melt/solutions systems as it does not add the need of an electric field and therefore special dielectric requirements. The method uses centrifugal forces to process the polymer melt or solution. (Padron et al. 2013)

There are several polymeric systems that have shown promising potential to hold active ingredients, for example poly(vinyl alcohol) (PVA) (X. Zhang, Tang, and Zheng 2016), poly(ethylene oxide) (PEO) (Eskitoros-Togay et al. 2019), poly(ε-caprolactone) (PCL) (Eskitoros-Togay et al. 2019), poly(acrylic acid) (PAA) (Khampieng, Wnek, and Supaphol 2014), cellulose

acetate (CA) (Gouda, Hebeish, and Aljafari 2014), poly(L- lactic acid) (PLA) (Parwe et al. 2014), poly(lactic-co-glycolic acid) (PLGA) (Almajhdi et al. 2014), poly(acrylonitrile) (PAN) (Semnani et al. 2018), and poly(urethane) (PU) (Akduman, Özgüney, and Kumbasar 2016) have been extensively studied as drug carrier substrates. Poly(lactic-co-glycolic) acid (PLGA) is a highly stable, biodegradable, and biocompatible polymer that can be subjected to the modification of surface properties to provide better interaction with biological materials. PLGA is approved for pharmaceutical application by the United States Food and Drug Administration (FDA). (Gentile et al. 2014) PLGA is a copolymer having two endogenous metabolite monomers, lactic acid and glycolic acid (shown in Figure 2.1a), which are rapidly metabolized by the body via the Krebs cycle, resulting in negligible systemic toxicity when used for drug administration or biomedical applications. (Danhier et al. 2012) It has proven to be one of the most promising materials to be used as a drug carrier due to its ability to prevent drug degradation (Danhier et al. 2012), ease of processing, and compatibility with a wide variety of drugs, e.g., hydrophilic or hydrophobic small molecules or macromolecules (Mir, Ahmed, and Rehman 2017). PLGA has also been proved to increase the efficiency of the loaded drug, for example, Guimarães et al. (Guimarães et al. 2015) reported that PLGA-daunorubicin nanofiber membranes display increased cytotoxicity against A431 tumor cells while preserving equivalent cytotoxicity against fibroblast cells when compared to free daunorubicin. Z.X. Meng et al. (Meng et al. 2011) synthesized PLGA/gelatin nanofibers and showed promising potential to be used in practical application given the structural stability of the developed membranes combined with the surface bioactivity and controlled degradation.

In this study, oleanolic acid (OA) (3/3-hydroxy-olea-12-en-28-oic acid) (figure 2.1b) was used as the active ingredient, OA is a pentacyclic triterpenoid compound found in a set of medicinal herbs, fruits, and vegetables in the form of free acid or aglycones for triterpenoid saponins linked with one or more sugar moieties that form glycosides. (Shanmugam et al. 2014),(Jie 1995) OA has been isolated from more than 1600 plant species. (Pollier and Goossens 2012) Structurally, it contains five- and six-membered rings and is relatively non-toxic. (Khwaza, Oyedeji, and Aderibigbe 2018) Oleanolic acid and its derivatives exhibit several interesting biological activities such as: anticancer, (Fukumura et al. 2009),(Tian et al. 2017) anti-inflammatory, (Dharmappa et al. 2009) antioxidant, (X. Wang et al. 2010) antifungal, (H. Zhao et al. 2013) antiviral, (Mengoni et al. 2002),(Kong et al. 2013) antidiabetic, (X. Wang et al. 2013),(D. Gao et al. 2007) antitumor, (Qingchao Liu et al. 2013) and antimicrobial (S. Kim et al. 2015)

activities. Wang et al. (Z. hong Wang et al. 2010) reported that OA suppressed renal aldose reductase activity and enhanced glyoxalase I activity, which resulted in the decrease of renal advanced glycation end-products (AGE) formation and improved renal functions. According to modern pharmacology studies, OA has a liver-protective action, which reduces liver tissue inflammation, improves liver cell regeneration, and rapidly repairs necrotic areas. (Pollier and Goossens 2012) Despite having various fascinating biological features, OA has poor water solubility and this limits its application in clinical and cosmetic related applications. To improve the therapeutic efficiency of OA, different kinds of nanocarriers have been developed. Y. Wang et al. (Y. Wang et al. 2019) developed carboxylated cellulose-g-poly(L-lactide) copolymer nanoparticles to deliver oleanolic acid. H.Fu et al. (Fu et al. 2021) developed OA-loaded nanofibers using the electrospinning method for attenuating particulate matter-induced oxidative stress in keratinocytes. Fan et al. (Fan et al. 2021) developed low molecular weight supramolecular hydrogels for the loading of oleanolic acid. Gao et al. (M. Gao et al. 2016) developed oleanolic acid-loaded PLGA-TPGA nanoparticles to enhance liver cancer chemotherapy.

This study explores the fabrication of oleanolic acid-loaded PLGA nanofibers systems. The effect of OA concentrations (20 wt% and 33 wt%) and processing parameters on the morphological and thermo-physical properties of nanofiber membranes developed via FS was studied. Scanning electron microscopy (SEM), thermogravimetric analysis (TGA), differential scanning calorimetry (DSC), powder x-ray diffraction (PXRD), Fourier-transform infrared spectroscopy (FTIR), and cytotoxicity analyses are presented.

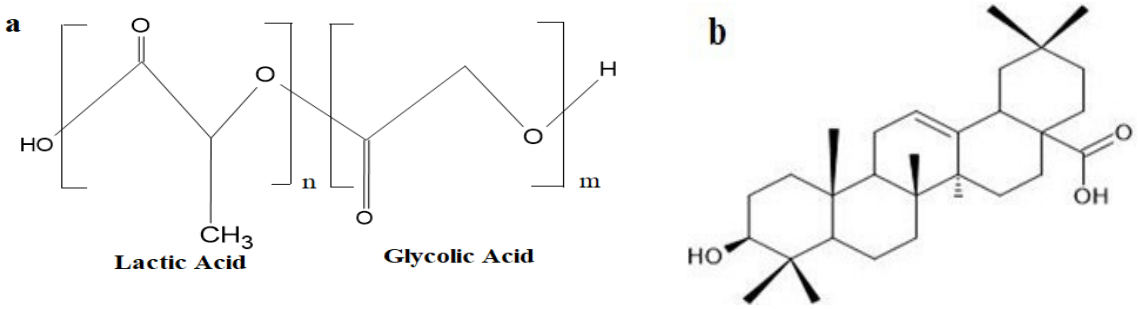

Figure 2.1: Chemical structure of Poly(lactic-co-glycolic) acid and Oleanolic Acid

This study explores the fabrication of oleanolic acid-loaded PLGA nanofibers systems. The effect of OA concentrations (20 wt% and 33 wt%) and processing parameters on the morphological and thermo-physical properties of nanofiber membranes developed via FS was studied. Scanning electron microscopy (SEM), thermogravimetric analysis (TGA), differential scanning calorimetry

(DSC), powder x-ray diffraction (PXRD), Fourier-transform infrared spectroscopy (FTIR), and cytotoxicity analyses are presented.

2.2 Materials and Methods

2.2.1 Materials

Span80 was purchased from Sigma Aldrich (St.Louis,MO). PLGA (Purasorb® PDLG 8531) (85:15) was purchased from Corbion (Netherlands). Deionized (DI) water (18.20 MΩ cm) was filtered using a Barnstead MicroPure ST® (Thermo Fisher Scientific). The polymer solution was made with ACS-grade chloroform, which was purchased from Fisher Scientific. The Oleanolic Acid powder (98% pure) was bought from Jiaherb Phytochem (China). All chemicals were used in analytical grade without any further treatment.

2.2.2 Solution Preparation

A control solution containing 3 wt% of PLGA was prepared. Span 80 was used as the surfactant, 0.066 g were added to 8 mL of chloroform; this mixture was agitated for 2 hours with a magnetic stirrer (Thermo Scientific, Cimarec+ series), 0.3542 g of PLGA were then added to the mixture and stirred at 600 rpm overnight. Multiple systems with different concentrations of OA were prepared and tested for fiber production, systems containing 20 and 33 wt% of OA were selected as the most promising ones. To prepare the 20 and 33 wt% OA solutions, 0.0885 g and 0.1745 g of OA were added to the PLGA control solution respectively. The 20 and 33 wt% OA solutions were labeled as PLGA-OA20 and PLGA-OA33, respectively. The solutions were agitated overnight for homogenization.

2.2.3 Development of Fiber Membranes

Fiber membranes were developed using a Forcespinning® apparatus, the Cyclone-1000M (FiberRio Technology Corp, McAllen, U.S.A.). A cylindrical spinneret equipped with two 30-gauge needles inserted into exit nozzles on both sides was filled with 2 mL of the prepared solution. The spinneret was made to rotate at an angular velocity of 9000 rpm at 23°C and 55-58% relative humidity. Under these conditions, the fluid was expelled from the rotating spinneret as jets that upon solvent evaporation resulted in fibers which were deposited on eight collectors spaced 18 cm apart as seen in Figure 2.2. A 10cm x 10cm hollow frame was used to collect the fibers from the

area in between the collectors. The nanofibers were wrapped with aluminum foil before being kept in a plastic bag with desiccants for moisture control.

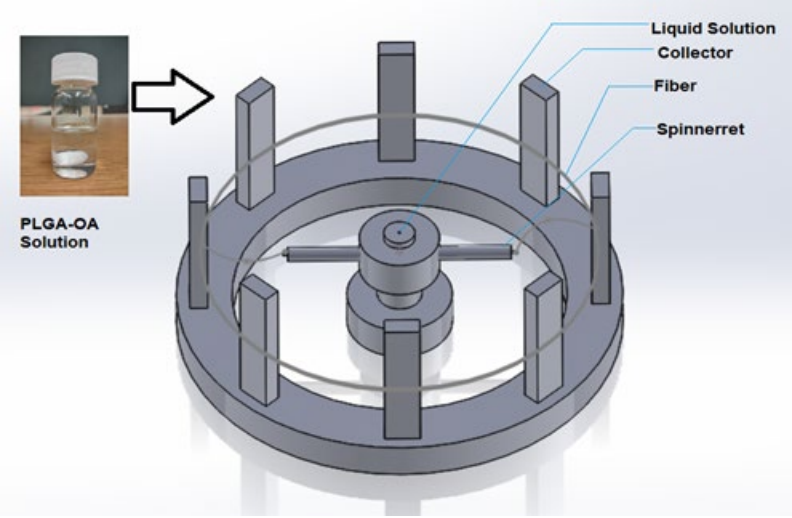

Figure 2.2: Schematics showing the FS method used to prepare the fiber membranes

2.2.4 Fiber Characterization

Fiber morphology was analyzed using a scanning electron microscope (Sigma VP, Zeiss Evo LS10, Jena, Germany). The magnification ranged from 150X to 5500X, and a voltage of 1 kV was used throughout the process. The obtained images were analyzed using ImageJ software (Version-1.8.0) to evaluate average fiber diameter. The average fiber diameter was calculated by measuring the fiber diameter of 100 different randomly selected fibers.

The Fourier transform infrared spectra was carried out using a Nicolet iS5 spectrometer in the attenuated total reflection (ATR) mode. Samples of 1 cm x 1 cm were used and sixteen scans were collected in the range of 400-4000 cm^{-1} with a resolution of 4 cm^{-1}.

Thermo-physical properties of the developed fiber membranes were analyzed using thermogravimetric analysis and differential scanning calorimetry. TGA was carried out using a Netzsch 209. For the analysis, approximately 10 mg of each sample were heated from 25 °C to 900 °C at a heating rate of 10 °C/min in a nitrogen environment. DSC was carried out using a Netzsch 214. OA powder of approximately 10 mg was placed in aluminum crucibles and heated from 25 °C to 320 °C at a rate of 10 °C/min, then held under isothermal conditions at 320 °C for 6 min. Subsequently, samples were cooled down to 25 °C at a rate of 10 °C/min and left under

isothermal condition for 2 min. A second heating cycle was followed under same conditions as the first heating cycle. The fiber samples, each weighing about 10 mg, were put into aluminum crucibles and heated at a rate of 10°C/min from 25°C to 270°C, where they were maintained under isothermal conditions for 6 minutes. Samples were then cooled down to 25°C at a rate of 10°C/min, and they were kept in an isothermal condition for 2 min. The initial heating cycle's conditions were followed for a second heating cycle.

Powder XRD (PXRD) patterns of the OA powder and fine fibers were recorded with a Bruker D8 Advance X-ray diffractometer under a wavelength of 2θ range from 7° to 75° in increments of 0.2° at a rate of 2° min^{-1} under a power setting of 40 kV and 40 mA.

The drug loading efficiency, of OA, within the fiber was determined by quantifying the absorption of clear supernatant using UV-vis spectrometer (Cary60, Agilent Technology, Santa Clara, CA). The supernatants were prepared by dissolving 10.5mg of each sample in 10mL of chloroform and sonicate for 1 hour. The corresponding calibration curve was obtained by testing five OA solutions with the concentration ranging from 1 g/L to 5 g/L. The absorbance value of OA was measured using a UV–vis spectrophotometer at 270 nm.

The drug loading efficiency of the membrane was calculated using the following formula:

Drug loading efficiency= $\frac{w_a}{w_t} * 100\%$

Where, w_t is the amount of OA used in the solution to develop in the membrane, w_a is the actual amount of OA in the membrane.

2.2.5 Cell interaction studies

To examine the interaction of mammalian cells with PLGA-based fibers, samples were crosslinked for 5 minutes under UV light, followed by wetting in phosphate-buffered saline (PBS). NIH 3T3 mouse embryonic fibroblasts (MEFs) were seeded onto the fibers and given Dulbecco's Modified Eagle's Medium (DMEM, Gibco) supplemented with 10% fetal bovine serum and antibiotic/antimycotic (Gibco), followed by incubation at 37 degrees C in 5% CO_2. After growth for two days, samples were fixed with 4% paraformaldehyde in PBS, followed by incubation with phalloidin-Alexa488 (Invitrogen Molecular Probes) in PBS (to visualize the actin cytoskeleton)

and diaminophenylindole (DAPI) (to visualize cell nuclei). Samples were mounted with 50% glycerol in PBS and imaged on an Olympus Fluoview FV10i confocal microscope.

To examine cell viability, 25,000 3T3 cells were seeded in each well of a 24-well plate in the presence of control or OA-containing nanofibers for 72 hrs. 50 microliters of MTT Reagent (Sigma) was added to each well and incubated for 4 hrs., after which the media was removed and 200 microliters DMSO added. Plates were run on a BioRad plate reader for absorbance at 595 nm.

2.3 Results

Different solutions of OA loaded PLGA systems were prepared ranging from 1 to 50 wt% (1, 3, 5, 15, 20, 33, and 50 wt%). Fibers were fabricated at speeds ranging from 6500 to 10000 rpm. As the goal was to maximize fiber yield with the highest possible concentration of OA and smallest possible fiber diameter, samples containing 20 wt% and 33 wt% of OA were selected as the optimum systems for detailed morphological, thermo-physical analysis, and cellular studies. Fibers with average diameters in the 100 nm range were observed under certain processing parameters though yield was low and those systems were not selected for subsequent characterization. SEM micrographs of the selected fiber systems are shown in Figure 2.3 together with their respective diameter histograms. It can be observed that throughout the fiber, surface was heterogenous (rough surface). The developed PLGA fiber membrane used as control as well as the OA-loaded PLGA systems show long, continuous, twisted, and bead-free fiber membranes.As can be seen from the fiber diameter histograms, the PLGA control fibers show an average fiber diameter of 537 nm with a large standard deviation of 220 nm. The fiber diameter ranged from 190 nm-1200 nm. The mean fiber diameter of the PLGA-OA20 sample was found to be 542 nm with a standard deviation of 165 nm, as for the PLGA-OA33, the mean fiber diameter was 630 nm with a standard deviation of 192 nm. This tendency of increasing fiber diameter (from nano to micro range) upon addition of drugs has already been stated in the literature. (J Biomed Mater Res - 2004 - Katti - Bioresorbable nanofiber-based systems for wound healing and drug delivery Optimization.pdf n.d.; Raimi-Abraham et al. 2015) When compared to the PLGA control system, the OA loaded fibers were observed to have a less twisted morphology.

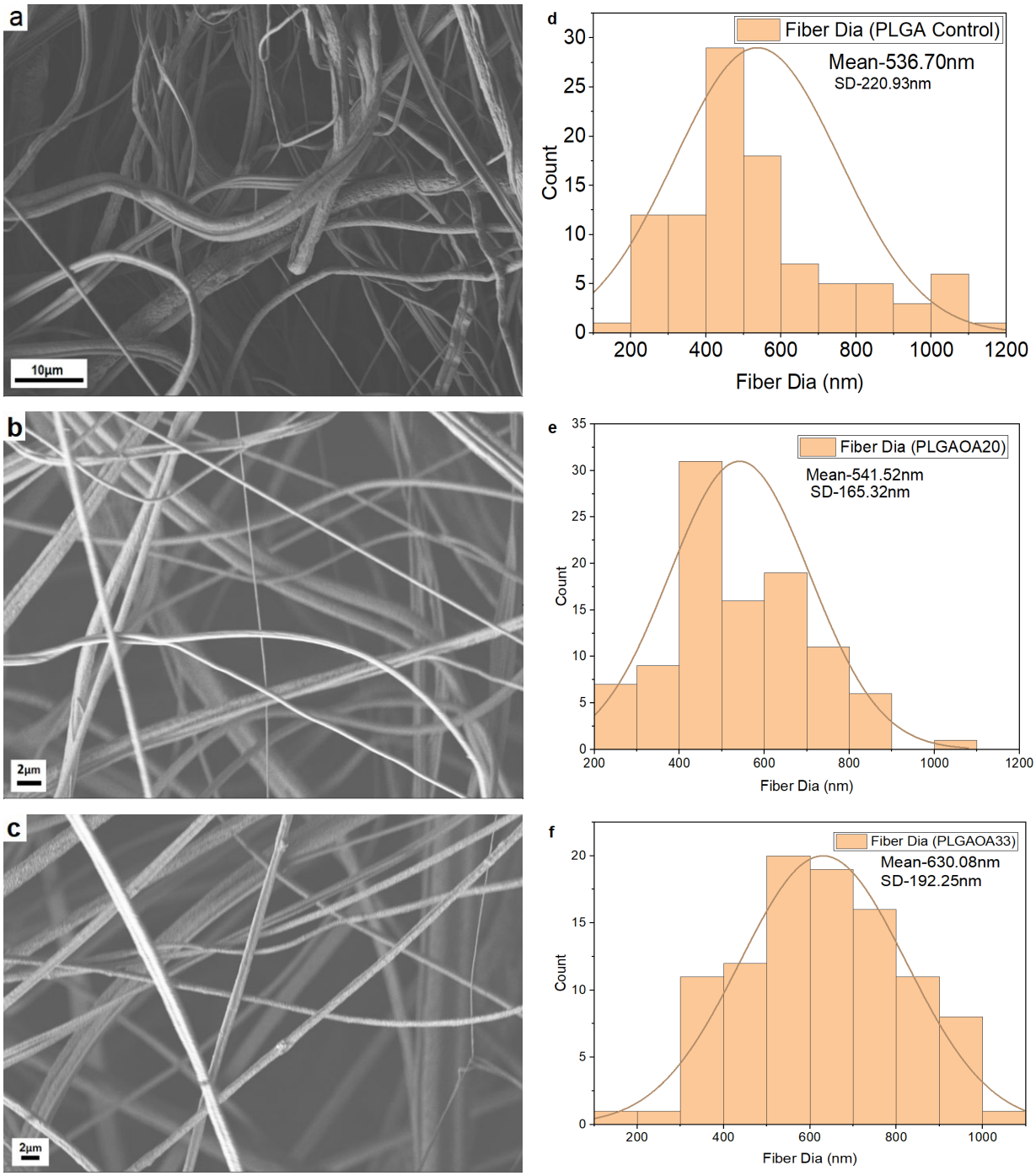

Figure 2.3: SEM micrographs of the developed fibrous materials: PLGA control (a), PLGAOA20 (b), PLGAOA33(c) and fiber distribution of PLGA control (d), PLGAOA20 (e), and PLGAOA33 (f).

The TGA and DTG thermograms represented in Figures 2.4 and 2.5 show the thermal stability of the oleanolic acid powder, PLGA control fiber system, and OA loaded PLGA fibers. As can be observed from these thermograms, the oleanolic acid powder shows a 2.41% weight loss at 100°C, due to the loss of absorbed water. Between 100°-160°C, there is a weight loss of 1.38%. This weight loss could be due to the loss of residual solvate in the oleanolic acid powder. The onset temperature of degradation for the OA sample is 275°C, exhibiting a one-step degradation process. A total 97.3% degradation of the oleanolic acid is mostly completed at 410°C with 2.7% left over as residual carbon. From the corresponding DTG curves shown in Figure 2.5, it can be observed that the maximum weight loss rate of the control OA sample occurred at 383°C. After 410°C, there is a negligible amount of degradation. These results compare well with a detailed degradation analysis conducted by Xiao et al where they state that the decomposition mechanism of OA starts with side groups breaking from the main molecular skeleton followed by chain scission among six-membered rings. They conducted TGA analysis and confirmed the study with infrared spectrum of evolved gases. (Xiao, Guo, and Guo 2014)

As for degradation of pure PLGA nanofibers, the onset temperature of degradation is observed at 220 °C, and a two-step degradation process occurs as seen in Figure 2.4. The first step occurs between 220 °C and 350 °C and 79% of the polymer is lost. This degradation is attributed to the lactic acid compound. The second step occurs between 350 – 520 °C where 20.6% is lost and

Table-2.1. TGA data of OA powder, PLGA control fiber, PLGAOA20 and PLGAOA33 composite fiber

Sample	T_{on}	$T_{10\%}$	$T_{50\%}$	T_{max}
OA powder	275°C	317.3°C	367.7°C	410°C
PLGA control	220°C	264.2°C	307.7°C	520°C
PLGAOA20	225.9°C	270.5°C	325.5°C	450°C
PLGAOA33	222.8°C	269.7°C	337.1°C	450°C

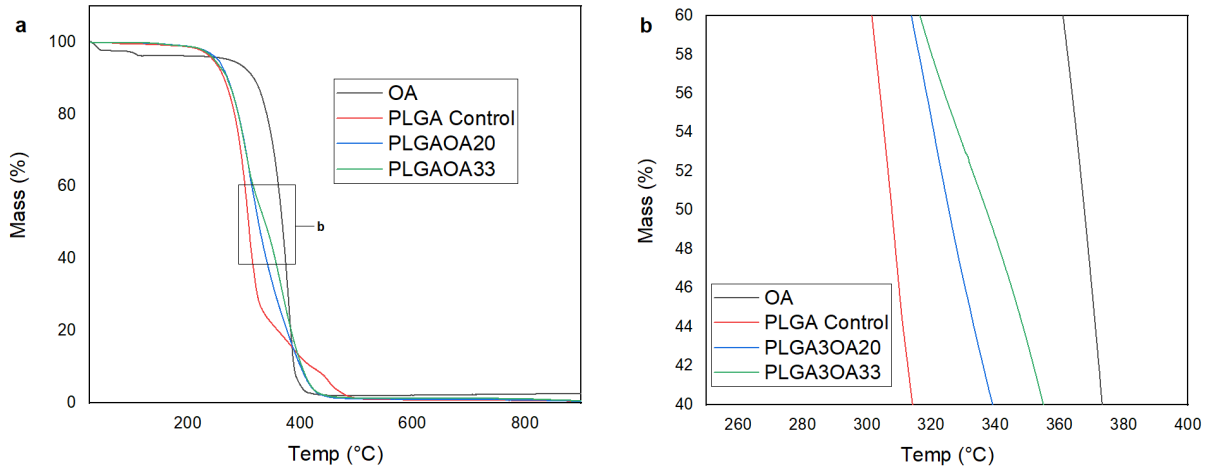

Figure 2.4: TGA analysis of Oleanolic Acid powder, PLGA control, and Oleanolic Acid loaded PLGA nanofiber membrane; PLGAOA20 and PLGAOA33.

attributed to the glycolic acid compound of the copolymer. Oleanolic acid loaded PLGA fiber show a decrease in thermal stability compared to OA powder. The onset temperature of degradation is now 225.9 °C and 222.8 °C for PLGAOA20 and PLGAOA33, respectively with the maximum weight loss rate at 312°C and 302.8°C. The small decrease in onset temperature of degradation in PLGAOA33 compared to PLGAOA20 can be attributed to the higher amount of hydroxyl group from OA. (Akgün et al. 2019; Maiza et al. 2015) The onset decomposition temperature (T_{on}), temperature at 10% ($T_{10\%}$) and 50% ($T_{50\%}$) weight loss and temperature of maximum decomposition rate (T_{max}) of OA powder, PLGA control fiber, PLGAOA20 and PLGAOA33 composite fiber is shown in Table 2.1.

Figure 2.6 depicts the DSC thermograms for the developed systems. Figure 2.6(a) focuses on the first and second heating cycles for the oleanolic acid powder. It shows two endothermic peaks, one at 160.5°C and a second one at 311.1 °C. An exothermic peak at 179.4°C is also observed. Samples were held isothermal at 320 °C, then cooled down to room temperature, on the second heating cycle, only the second endothermic peak is observed now at 308 °C. The first small endothermic and exothermic peaks are due to processing induced effects, such as residual solvent and meso-ordering effects as well as to a transition from metastable to crystalline state. (N. Gao et al. 2017) OA is highly crystalline and this is depicted by the second large endothermic peak at 311.1°C. The second heating cycle exhibits only one endothermic peak, the melting peak of OA which shifted

to 308°C indicating OA is in fact crystalline since all processing induced effects were deleted during the first heating and isothermal states.

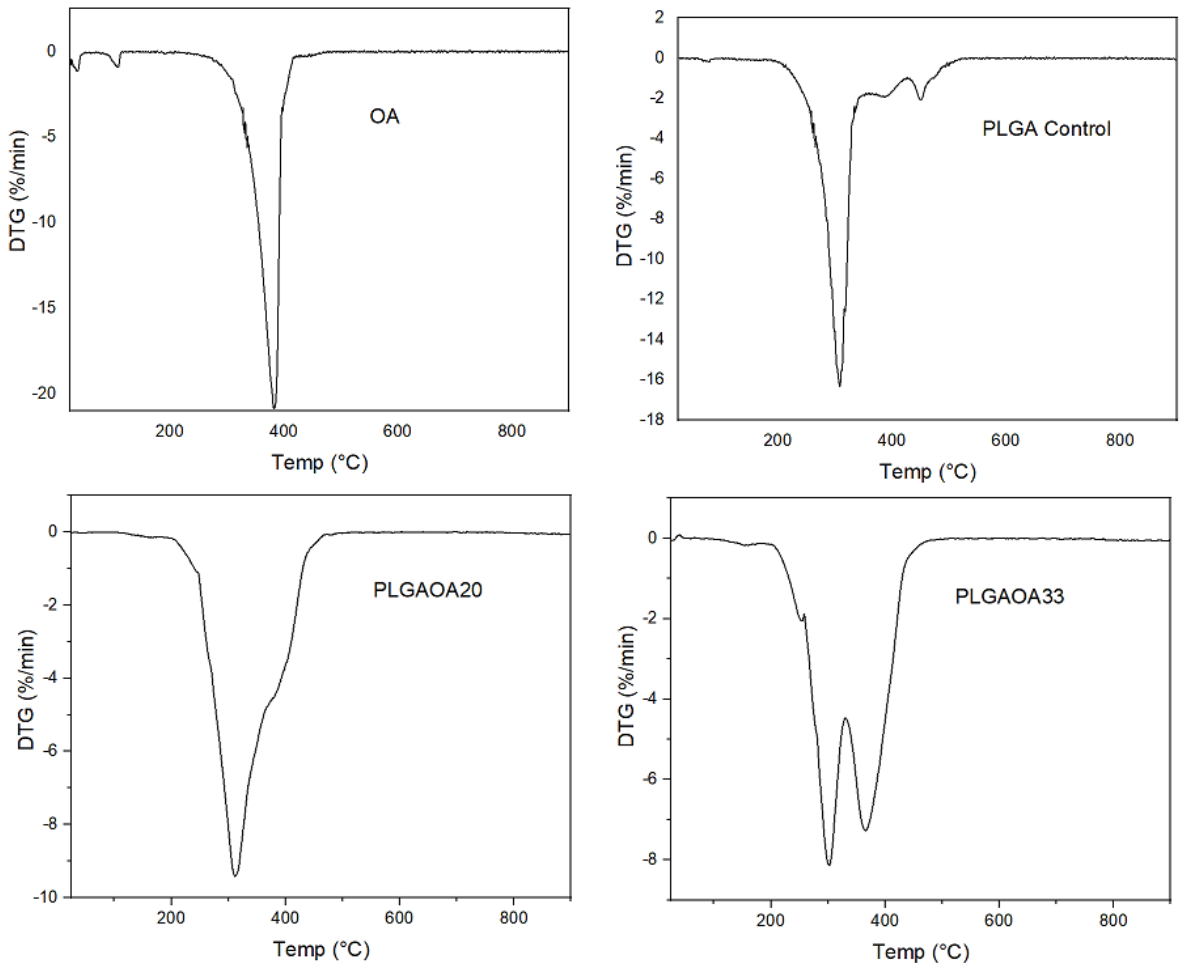

Figure 2.5: DTG analysis of Oleanolic Acid powder, PLGA control, and Oleanolic Acid loaded PLGA nanofiber membrane; PLGAOA20 and PLGAOA33.

Figure 2.6(b) shows the DSC thermogram of PLGA control fibers, PLGAOA20, and PLGAOA33 fibers, it should be noted that thermograms for two more samples are included in this graph, PLGAOA20 and PLGAOA33 films. Films were prepared to better understand the

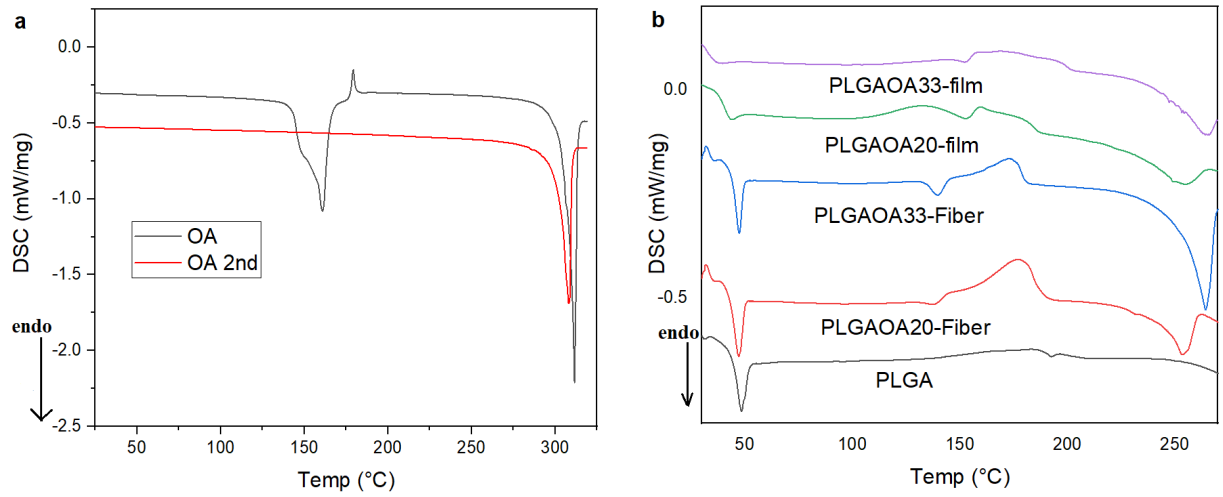

Figure 2.6: DSC Thermogram of Oleanolic Acid powder (a) PLGA control, PLGAOA20, PLGAOA33 composite nanofiber and PLGAOA20, PLGAOA33 film (b)

processing induced effects of PLGA phase transitions. Film samples were prepared by drop casting developed solutions onto glass slides. PLGA fibers depict the structure of an amorphous polymer with a glass transition temperature (T_g) at 48 °C, however a small endothermic melting peak is observed at 192.7°C which is attributed to the melting of the meso-ordered phase due to molecular alignment during fiber formation. OA loaded PLGA fibers exhibited DSC profiles with a series of thermal transitions, similar to those seen for PLGA fibers and OA separately. However, some shifts in the position of these thermal transition peaks and some newly formed signals are observed. These shifts in peak positions suggest interactions between PLGA and OA as well as processing induced morphologies. The glass transition temperatures of PLGAOA20 and PLGAOA33 fibers is shown at 47.4°C and 47.3°C, a small decrease from PLGA control sample and attributed to interaction between PLGA and OA. (Blasi et al. 2007) The PLGAOA20 and PLGAOA33 films showed a lower glass transition temperature, 44°C and 39.4°C respectively. It is worth noting that the T_g of the fibers is shown as a weak endothermic peak rather than a step as seen in the film samples. Fiber samples were subjected to molecular alignment during extensional elongation processes, this generates stresses into the material and some of these are released when heating through T_g and appear as a weak endothermic transition after T_g. All samples show single glass transition temperature which demonstrates miscibility of PLGA and OA. (Shawe et al. 2000) PLGAOA20 and PLGAOA33 fibers showed new endothermic peaks at 138.4°C and 139.9°C, respectively which are due to total elimination of meso-ordered phase induced during fiber

formation. The exothermic of OA at 177 °C is also seen for all composite samples. Endothermic peaks are visible at 253.6°C for PLGAOA20 and 263.9°C for PLGAOA33 and attributed to melting of small OA crystals. No peaks besides T_g were visible in the second heating cycle of the composite fibers indicating PLGA amorphous state and its effect on the ability of OA to crystallize. (Wegiel et al. 2013), (Irene et al. 2014)

The FTIR spectra of OA powder, PLGA control, and OA-loaded PLGA nanofiber systems are shown in Figure 2.7. For OA, the peak bands around 3500cm^{-1} (between 3676-3320 cm^{-1}) are due to O-H stretching. The peak at 2940 cm^{-1} is for CH_3-(aliphatic) asymmetric stretching vibration, 2868 cm^{-1} is for CH_3- (aliphatic) symmetric stretching. (Ghosh, Kar, and Bera 2016) The sharp peak at 1689 cm^{-1} is due to carboxylic C=O stretching vibration. The other significant peaks are 1461 cm^{-1} for asymmetric CH_3- deformation peak, 1375 cm^{-1} for C-H deformation,1272 cm^{-1} for C-O stretching. As for PLGA, the intense band observed at 1752 cm^{-1} for PLGA spectra is due to the stretching vibration of carbonyl groups present in two monomers. The characteristic peaks at 2998, 2953, and 2858 cm^{-1} are due to C-H, C-H_3, and C-H_2 functional group stretching. The medium bands at 1261 and 1185 cm^{-1} can be attributed to the asymmetric and symmetric C-C(=O)-O stretches. The peaks at 860 cm^{-1} and 802 cm^{-1} result from the C-H bending.

In comparison to PLGA control fibers and OA powder, differences in band intensities and shifting in wavenumbers were detected for the PLGAOA20 and PLGAOA33 fiber samples. For instance, the pronounced peak of PLGA at 802 cm^{-1} is diminished in PLGA-OA composite fibers. The C-H stretching band of -CH_2 in OA diminished in the composite nanofiber. The significant peaks at 1029 cm^{-1} present in bare PLGA shifted to 1042 cm^{-1} and became less pronounce in PLGA-OA composite fibers. The asymmetric C-C(=O)-O band at 1261 cm^{-1} in PLGA control shifted to 1267cm^{-1} for the PLGA-OA composite fibers. The band intensity significantly decreased with the increase of OA. These shifts might be caused by weak hydrogen bonding, van der Waal's force attraction, or dipole-dipole interactions.(Basu et al. 2012)

The PLGAOA20 and PLGAOA33 composite nanofibers show peaks at 1689cm^{-1}, which are absent in the PLGA control fiber, a characteristic of carboxylic C=O, which suggest the encapsulation of OA in PLGA nanofiber. The peak in PLGAOA33 is more pronounced than in PLGAOA20, indicating the higher concentration in the PLGAOA33 sample.

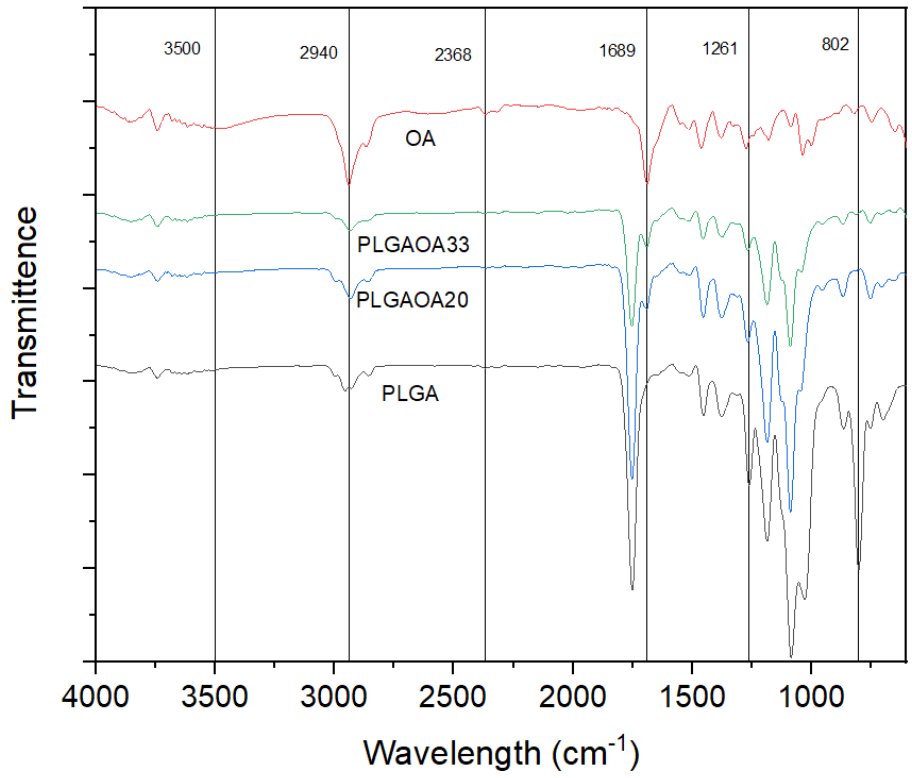

Figure 2.7: Fourier-transform infrared (FTIR) spectrum of Oleanolic Acid Powder, PLGA control, PLGAOA20, and PLGAOA33 composite nanofiber membranes.

Figure 2.8 shows the XRD pattern of OA powder, PLGA fibers and PLGA-OA composite fibers. Characteristic diffraction peaks of OA appeared at 12.06°, 12.78°, 14.56°, and 16.82° indicating the crystalline state of OA. The observed pattern for OA matches previously reported studies which explain the parallel stacking of OA molecules due to the H-bonding between carboxylic groups, alcohol groups, or carboxylic and alcohol groups. (Teixeira et al. 2010) For PLGA, the XRD pattern showed no distinct peak indicating the amorphous characteristic nature of this polymer. The XRD pattern of PLGAOA20 and PLGAOA33 showed a single and broad peak with low intensity at 14.44° and 14.74°, respectively. The spacing of these peaks represent average distance between disorderly packed molecules. (Teixeira et al. 2010)

The results show that interaction with PLGA destroys most of the original crystallinity of OA. The reduction of intensity and number of peaks in OA loaded PLGA fiber indicate the maximum OA was entrapped in PLGA as the decrease in intensity of the peaks can be attributed

to the lower level of detecting encapsulated drug dispersed at molecular level. (Venkatesh et al. 2015)

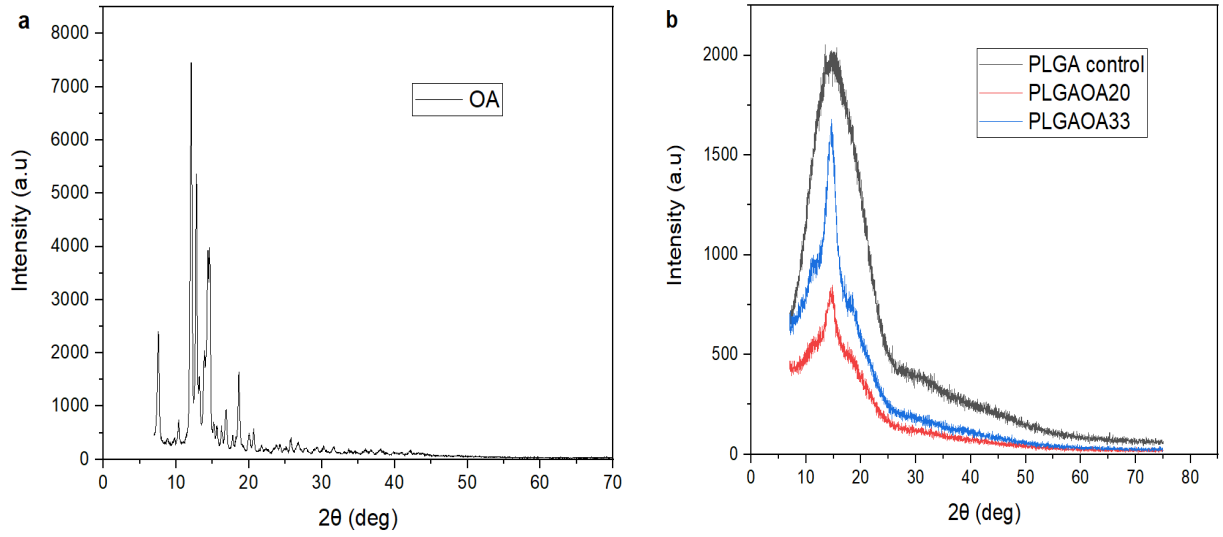

Figure 2.8: XRD pattern of Oleanolic Acid Powder(a), PLGA control, PLGAOA20, and PLGAOA33 composite nanofiber(b)

As mentioned in the introduction section, Oleanolic acid has been intensively studied given its interesting biological activity as: hepatic protection, (Pollier and Goossens 2012) anticancer, (Fukumura et al. 2009) (Tian et al. 2017) anti-inflammatory, (Dharmappa et al. 2009) antioxidant, (X. Wang et al. 2010) antifungal, (H. Zhao et al. 2013) antiviral, (Mengoni et al. 2002) (Kong et al. 2013) antidiabetic, (X. Wang et al. 2013) (D. Gao et al. 2007) antitumor, (Qingchao Liu et al. 2013) and antimicrobial (S. Kim et al. 2015) activities. Though its poor water solubility has limited its applications. The use of PLGA nanofibers as carriers for OA presents an opportunity for the developed membranes to be used as drug delivery carriers. Drug loading efficiency has been used as a method to determine the efficiency of the formulation. Liu et al. (Qi Liu et al. 2021) and Böncü et al. (Böncü and Ozdemir 2022) have studied the drug loading efficiency of polymeric nanofiber and found that it is related to the drug's solubility in the polymer solution. Table 2.2 presents the tested drug loading efficiency of the developed systems. As it was expected, increasing the amount of drug resulted in increased drug loading efficiency. The drug loading efficiency of PLGAOA20 and PLGAOA33 were found to be 81.7% and 82.57%, respectively. The high drug loading efficiency is due to the high solubility of OA in the solution. (Qi Liu et al. 2021)

Cell viability and cytotoxicity of the developed membranes were evaluated in vitro with mouse embryonic fibroblast cells (NIH 3T3). PLGA-OA composite mats were crosslinked via UV irradiation and seeded with 3T3 mouse embryonic fibroblasts, followed by incubation and sample preparation, as previously described. (Barbosa et al. 2021; Rodriguez et al. 2022) Confocal imaging reveals that both PLGAOA20 and PLGAOA33 allow 3T3 cells to adhere and proliferate on the surface of the nanofiber mats, with numerous cell nuclei visible (cyan, DAPI staining) and apparent spreading of the cell body (green, phalloidin-Alexa488) onto the nanofiber matrix.

Table 2.2. Various concentrations and drug loading efficiency of the formulations

Sample	Amount of PLGA	Amount of OA	Theoretical Drug loading (%)	Actual Amount of PLGA	Actual amount of OA	Actual drug loading (%)	Drug loading efficiency
PLGAOA20	0.3542g	0.0885g	20%	8.784mg	1.716mg	16.34%	81.7%
PLGAOA33	0.3542g	0.1745g	33%	7.638mg	2.862mg	27.25%	82.57%

To examine whether OA-loaded nanofibers have detrimental effects on cells themselves, 3T3 cells were incubated in the presence of control PLGA fibers, as well as OA-containing fiber mats. After three days of incubation, MTT assays were used to determine cell viability. 3T3 cells grew equally well in the presence of all three fiber types, with no statistically significant differences between the control and OA-containing fibers. These results demonstrate that OA does not confer any cytotoxic effects on mammalian cell growth and viability.

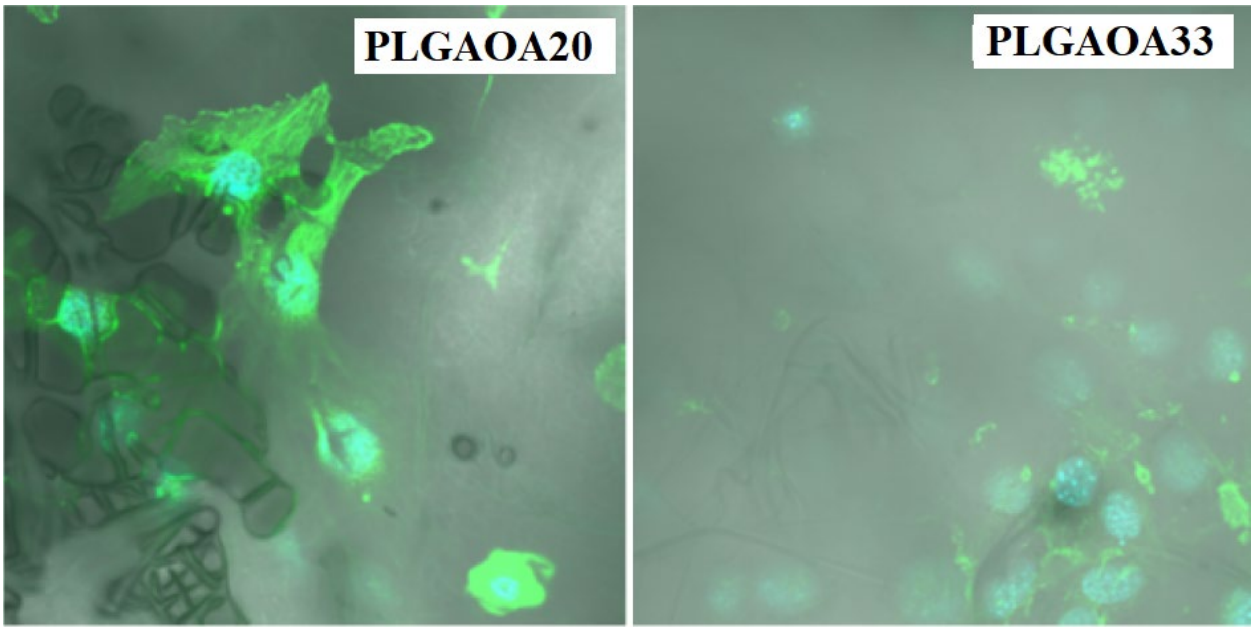

Figure 2.9: Confocal imaging of OA-containing fibers seeded with 3T3 mouse embryonic fibroblasts.

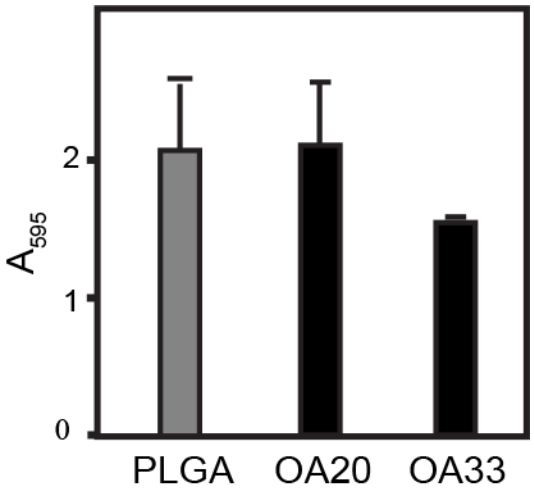

Figure 2.10: MTT assay of cell viability in the presence of control and OA-containing nanofibers.

2.4 Discussions

In this study, Oleanolic acid loaded PLGA fine fiber membranes were prepared using the Forcespinning method. Different concentrations of OA were developed, 20 and 33 wt% OA loadings were selected for comprehensive structural, thermo-physical, and biological analysis. Ease of processing with high yield of fiber membranes was obtained. The findings revealed that

developed membranes effectively incorporated oleanolic acid and demonstrated adequate structural integrity for potential use as transdermal bioactive agent delivery systems. High drug loading efficiency (>80%) was observed and cellular studies showed a non-cytotoxic behavior from the developed fiber membranes on fibroblast cells.

CHAPTER III

OXYMATRINE LOADED CROSSLINKED PVA NANOFIBROUS SCAFFOLD: DESIGN, CHARACTERIZATION, AND ANTI-CANCER PROPERTIES

3.1 Introduction

Within biomedical fields, nanofibers have sparked much interest given their high surface area, nano-porosity, and ability to effectively incorporate biomolecules and drugs making these an effective system for targeted drug delivery [1]. Nanofibers have shown to exhibit promising potential given improved gradual drug release properties compared to drugs loaded in cast films. Taepaiboon et al. (Taepaiboon, Rungsardthong, and Supaphol 2007) demonstrated its potential as drug delivery systems by developing cellulose acetate electrospun nanofibers loaded with vitamins A and E and used for transdermal drug delivery. The nanofibers showed gradual drug release compared to the burst release observed from cellulose acetate casted films. Nanofibers have also shown ability to increase the efficacy of loaded drugs. Compared to free daunorubicin, Guimares et al. (Guimarães et al. 2015) found that PLGA-daunorubicin nanofiber membranes have improved cytotoxicity against A431 tumor cells while maintaining equal cytotoxicity against fibroblast cells.

Nanofibers have been fabricated by several methods such as template synthesis (S. Liu et al. 2020), self-assembly (Liao et al. 2016), electrospinning (Xue et al. 2017), and forcespinning (Sarkar et al. 2010). The most common approaches for fabricating nanofibers for drug delivery systems are direct blend electrospinning (Amarjargal et al. 2019), coaxial electrospinning (Pant, Park, and Park 2019), and emulsion electrospinning (Sanchez et al. 2020). Although electrospinning is the most widely used process for producing nanofibers, it has several disadvantages, including low yield and a low dielectric requirement due to the usage of strong electric fields. The Forcespinning method (Sarkar et al. 2010), which is based on the use of centrifugal force to develop nanofiber, has been proven to be a viable alternative for the mass

production of nanofiber membranes from a wide range of melt/solutions systems since it eliminates the need for an electric field and hence specific dielectric requirements. Forcespinning has been shown effective to increase yield and as an attractive industrial system (J of Applied Polymer Sci - 2012 - Padron - Production and characterization of hybrid BEH-PPV PEO conjugated polymer.pdf n.d.).

A wide variety of polymers or copolymers such as poly(vinyl alcohol) (PVA) (Cui et al. 2018), poly(ethylene oxide) (PEO) (Gatti et al. 2013), Polylactic acid (PLA) (Chi et al. 2020), Poly(lactic-co-glycolic) acid (PLGA) (Hu et al. 2013), cellulose acetate (Taepaiboon, Rungsardthong, and Supaphol 2007), polycaprolactone (PCL) (Kamath et al. 2020), Collagen (X. Zhang, Tang, and Zheng 2016), and Poly(vinylpyrrolidone) (PVP) (Rahmani et al. 2021) have been extensively studied as nanofiber based drug delivery systems. Particularly, polyvinyl alcohol, a semicrystalline synthetic polymer with a hydroxyl group in its structure, has been one of the systems of choice for nanofiber based drug delivery systems (Kadajji and Betageri 2011; S. I. Song and Kim 2004). It is a translucent, white, or cream-colored granular powder without any odor or taste (Saxena 2004). It is soluble in highly polar and hydrophilic solvents, such as water, dimethyl sulfoxide (DMSO), ethylene glycol (EG), and n-methyl pyrrolidone (NMP), slightly soluble in ethanol and insoluble in other inorganic solvents (Saxena 2004; Tacx et al. 2000).Due to its biocompatible, bio-degradable, non-toxic nature and good thermal and chemical stability(Taepaiboon, Rungsardthong, and Supaphol 2006), it is widely used as a food barrier (Molki et al. 2019) as well as in biomedical applications such as wound dressing (Bahadoran, Shamloo, and Nokoorani 2020), tissue engineering (L. Peng et al. 2019), and drug delivery (Taepaiboon, Rungsardthong, and Supaphol 2006). Reddy et al. (Reddy et al. 2016) developed a 5-fluorouracil loaded chitosan–PVA/sodium montmorillonite (Na^+MMT) nanocomposite which showed an improved microbial inhibition zone when compared to chitosan and chitosan/ Na^+MMT nanocomposite films. Lou et. el (Lou et al. 2019) developed TiO_2 coated vitamin B2 loaded PVA nanofiber. The nanofiber exhibited steady drug release of vitamin B2. Fathollahipour et al. (Fathollahipour et al. 2015) developed PVA/chitosan nanofibrous core-sheath nanocomposite containing gelatin nanoparticles as a duel drug delivery system. Cui et al. (Cui et al. 2018) developed polyvinyl alcohol/chitosan composite nanofibers for transdermal drug delivery. Kim et al. (J. H. Kim et al. 2016) developed *Juniperus chinensis* extracts loaded PVA nanofibers and these were noted to exhibit antibacterial activity against both Gram-positive and Gram-negative

bacteria. The hydrophilic nature of PVA makes it attractive to produce and study nanofiber systems. However, for drug delivery applications, the morphology of the fiber is quickly destroyed upon swelling caused by water absorption, resulting in a burst release of loaded drug. Therefore, PVA nanofiber-based systems require a post-treatment to decrease the solubility of PVA in water. One way to prevent the burst release of drugs from nanofibers is to chemically crosslink PVA. Citric acid is considered to be a green crosslinker that can impart improved mechanical properties and water stability(Nataraj et al. 2018). Nataraj et al. (Nataraj, Reddy, and Reddy 2020) studied the effect of crosslinking PVA electrospun nanofibers with citric acid for biomedical application. They observed an increase in melting temperature and an improved stability of the nanofiber in cell culture media.

Oxymatrine (OM), a tetracyclo-quinolizidine alkaloid, as shown in Figure-3.1, extracted from the dried roots of a traditional Chinese herb, *Sophora flavescens*, was demonstrated to have high anti-inflammatory and tissue protective properties (Y. Liu et al. 2014). The chemical formula is $C_{15}H_{24}N_2O_2$, and the molecular weight is 264.36 g/mol. It is generally found as amorphous white powder or in the form of white needle prismatic crystals (Lu, Xiang, and Xia 2016). OM is water-soluble (Xiong et al. 2016). It exhibits several biological activities and has been widely used in China to treat cancer, heart illnesses (viral myocarditis), and skin diseases (psoriasis and eczema) (Xiong et al. 2016). Oxymatrine possesses various pharmacological effects such as antiviral (Ma et al. 2013), anti-inflammation (Guzman et al. 2013), antifibrosis (X. Liu et al. 2020), analgesic (Hanqing Liu et al. 2010), antiarrhythmic (Phytotherapy Research - 2010 - Yong-gang - Antiarrhythmic effects and ionic mechanisms of oxymatrine from Sophora.pdf n.d.), antioxidant (P. Zhao et al. 2015), hepatoprotective (Wen et al. 2014) etc. It can impede cell proliferation (C. Wu et al. 2015) and as a result it is used for treating tumors (Ying et al. 2015), hepatitis (Y. P. Wang et al. 2011), and cirrhosis (Jiang et al. 2018). Due to the antiproliferation effects, OM treatment successfully reduces proliferation of cells in skin lesions and improves the symptoms of psoriasis Vulgaris (H. J. Shi et al. 2019). The chemotherapeutic potential of oxymatrine has led to its use in the treatment of breast cancer (Jie Wu et al. 2017), prostate cancer (C. Wu et al. 2015), pancreatic cancer (H. Chen et al. 2013), glioblastoma (Dai et al. 2018), etc. However, because of OM's short half-life and poor dispersion, it has limited biological availability (Wang, Y., Meng, G.D.L., Zheng, W.Y., Liu 2003). OM is partially metabolized into matrine by intestinal bacteria in vivo, decreasing the oxymatrine's bioavailability and activity (Yue et al. 2010). When

experimented on rats, oxymatrine's slight liposolubility resulted in limited permeation through intestinal epithelial cells and little gastrointestinal (GI) tract absorption (Yue et al. 2010). The oral bioavailability of OM solution is reported to be low; only 19.4%(Xiong et al. 2016). High doses of OM are needed to enhance the therapeutic outcome, which leads to adverse effects on non-targeting tissues and cells (C. S. Wu et al. 2005). A variety of studies have reported on the use of OM as targeted drug delivery system to improve the therapeutic effectiveness and decrease the negative side effects (Upadhyay et al. 2010). Yue et al. (Yue et al. 2010) developed an oxymatrine-phospholipid complex that enhanced oxymatrine absorption, lowered oxymatrine metabolism, and improved oxymatrine bioavailability in vivo. Chai et al. (Chai et al. 2012) developed OM liposomes that attenuated hepatic fibrosis by targeting its stellate cells. Jin et al. (Jin et al. 2011) developed OM mixed micellar nanoparticles that delayed the drug release and enhanced the cytotoxicity of OM against cancer cells. Liu et al. (M. Liu et al. 2017) developed OM-loaded hydrogenated soybean phosphatidylcholine (HSPC) liposomes that significantly enhanced OM's bioavailability and liver targeting capability in higher concentration levels and for a longer therapeutic duration.

Colorectal cancer (CRC) is the third most prevalent cancer worldwide. Although considerable progress has been made in the treatment of CRC over the past years, it is still the third leading cause of cancer related death in The United State and fourth leading cause of cancer related death around the world. (McGuire 2016; Siegel et al. 2014) 5-fluorouracil (5-FU) and its derivatives are currently used for the initial chemotherapy of CRC. (J. Chen et al. 2015; Y. Zhang, Talmon, and Wang 2015) Although majority of the patients respond well to this chemotherapy, the relapse rate is still high due to increasing resistance to chemotherapeutic agents. (Jing et al. 2016) The search for new chemotherapeutic agents has become very important. OM has proven to inhibit the invasion of CRC cells by modulating epithelial-mesenchymal transition (EMT) (L. Liang and Huang 2016) and suppress the viability of interferon γ-stimulated CRC cells(Hua et al. 2021).

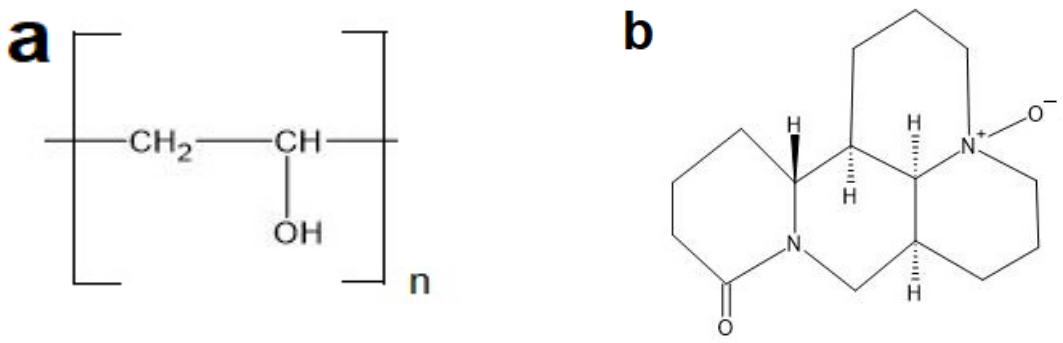

Figure 3.1: The chemical structure of PVA (a) and Oxymatrine (b)

Despite the attractiveness of OM and its multiple reports showing its use in drug delivery systems in liposomes, films and nanoparticles; to the knowledge of the authors, there are no studies reporting the use of OM-loaded nanofibers. In the present study, the PVA nanofibers loaded with OM were developed using the forcespinning method and citric acid as a crosslinker agent. The morphological, thermal properties, and hydrophilicity of the crosslinked PVA composite nanofibers were evaluated. The cell viability studies, and in vitro anticancer activity were evaluated.

3.2 Materials and method

3.2.1 Materials

Poly(vinyl alcohol) (27–96 medium hydrolyzed grade) was purchased from Kuraray Poval^{TM}. Citric Acid (CA) was bought from Sigma–Aldrich (St Louis, USA). Deionized (DI) water was produced from a Smart2Pure water purification system. Oxymatrine (98% pure) was obtained from Jiaherb Phytochem (China). All compounds were utilized in analytical grade without additional purification.

3.2.2 Solution preparation

Citric acid solutions containing 5 and 10 wt % of citric acid were prepared using deionized water. The mixture was homogenized using a magnetic stirrer for 30 minutes. 0.45g of PVA was added to the mixture, and the mixture was stirred at 600 rpm at 85°C using an oil bath for 1 hour. The solution was then stirred at 600 rpm for another 4 hours at room temperature. A total of six solutions (three solutions with 5% citric acid (CA5PVA9) and three solutions with 10% citric acid (CA10PVA9)) were prepared. 0.1125g of Oxymatrine was added to CA5PVA9 and CA10PVA9 to prepare solutions containing 20 wt % of OM and labeled as CA5PVA9OM20 and

CA10PVA9OM20, respectively. Solutions containing 33 wt % of OM were also prepared by adding 0.2216 grams of OM and labeled as CA5PVA9OM33 and CA10PVA9OM33. The mixtures were stirred overnight to prepare homogeneous solutions. Table-3.1 shows the concentration of the components in the nanofiber samples.

Table-3.1: Concentrations of the components in the nanofiber samples.

Oximatrine (wt.%)	Citric Acid (wt.%)	PVA (wt.%)	Label
0	5	9	CA5PVA9
0	10	9	CA10PVA9
20	5	9	CA5PVA9OM20
20	10	9	CA10PVA9OM20
33	5	9	CA5PVA9OM33
33	10	9	CA10PVA9OM33

3.2.3 Development of nanofiber membranes

The nanofiber membranes were developed using the Cyclone-1000M (FiberRio Technology Corp, McAllen, USA), which consists of a cylindrical spinneret with two nozzles and uses centrifugal forces to produce nanofibers. 2 mL of prepared solution was injected into the spinneret using a 3 mL syringe. The solution was then spun at an angular velocity of 4000 rpm at 23°C with 40-50% humidity. The solution was ejected through two 30-gauge needles placed at the nozzles at both sides of the spinneret and was deposited on eight collectors arranged around the spinneret at a distance of 18 cm from the nozzle. The fibers were collected manually using a 10 cm x 10 cm hollow frame. The collected nanofibers were covered with aluminum foil and preserved using desiccant for moisture control in a plastic bag.

3.2.4 Crosslinking of nanofiber

After nanofibers were collected, the membranes were placed in an oven at 140°C in vacuum for 15 minutes for crosslinking to take place. Samples were then removed from oven and allowed to cool down before further analysis. The cross-linking process allows the composite nanofibers to become water stable.

3.2.5 Nanofiber characterization

The surface morphology of the forcespun nanofibers was captured using a scanning electron microscope (SEM) (Sigma VP, Zeiss Evo LS10, Jena, Germany). The magnification ranged from 150X to 5500X, and a voltage of 1kV was used throughout the process. The obtained images were analyzed using ImageJ software (Version-1.8.0) to evaluate average fiber diameter and bead size. The average fiber diameter was calculated by measuring the fiber diameter of 100 different fibers. The distribution and dispersion of the OM in the fiber was determined using energy dispersive X-ray spectroscopy (EDS, EDAX Octane Super).

Thermal properties were analyzed using thermogravimetric analysis (TGA) and differential scanning calorimetry (DSC). TGA was carried out using Netzsch 209. For the analysis, 10 mg samples were heated from 25°C to 950°C at a heating rate of 10°C/min in a nitrogen environment. DSC was carried out using Netzsch 214. Approximately 10 mg samples were placed in an aluminum crucible and heated from 25°C to 220°C at a rate of 10°C/min, samples were maintained isothermally at 220°C for 6 minutes and then cooled to 25°C at a rate of 10°C/min. The second heating cycle was conducted following same conditions as the first heating cycle.

The Fourier transform infrared (FTIR) spectra was carried out using Nicolet iS5 in the attenuated total reflection (ATR) mode. Samples of 1cm x 1cm were cut and placed in the FTIR machine. 16 scans were collected in the range of 400-4000cm^{-1} with a resolution of 4 cm^{-1}.

3.2.6 Cell Viability studies

NIH 3T3 mouse embryonic fibroblasts (35,000 cells/well) were seeded to a 24 well plate and incubated at 37 °C, 5% CO_2 in a ThermoFisher incubator. After 48 hours of incubation, MTT (3-(4,5-dimethylthiazol-2-yl)-2,5-diphenyltetrazolium bromide) reagent was added (50 microliters per well) and allowed to incubate for 4 additional hours. Following incubation, media was removed, and 200 microliters of dimethyl sulfoxide (DMSO) was added and left for a period of 4 hours. The resulting solutions were analyzed to determine absorbance readings at 595 nm wavelength on a BioRad iMark™ microplate reader.

3.2.7 In vitro anticancer activity

To determine the effect of Oxymatrine embedded with the nanofibers on the growth of human cell cultures, in vitro cytotoxicity testing was carried out using colon cancer HCT116 cells.

12,000 cells were seeded along with nanofiber per well in 24-well plates using Dulbecco's modified Eagle's medium (DMEM) with 10% fetal bovine serum (FBS) and 5% antifungal/antibacterial (Anti/Anti, Thermo Fisher, Waltham, MA, USA). Cells were grown under standard tissue culture conditions (5% CO_2 and 37 °C) for five days. The Trevigen TACS MTT Cell Proliferation Assay Kit (Gaithersburg, MD) was utilized to assess impacts on human cell proliferation and/or viability. Fifty microliters of MTT reagent were added to each well and incubated under 5% CO_2 at 37 °C for another 4 h. Finally, 200 µL of DMSO reagent was added and incubation was continued for an additional 4 h. The optical density (A_{595}) was determined using a Bio-Rad iMark microplate absorbance reader. Samples were carried out in triplicate.

3.3 Results

Forcespinning® technology was chosen because of its ability to produce high yield of nanofibers and therefore develop the process to prepare OM loaded nanofibers that could have practical applications given rapid potential to be transferred to industrial yield. Various concentrations of PVA-OM solutions and processing parameters were studied to produce the nanofiber-based membranes. It should be noted that the goal was to find the parameters that could produce the smallest possible fiber diameter with high yield of fibers (in the order of a gram per minute for the lab scale units). Fibers as small as few tens of nanometers can be obtained with FS though the yield would be as compared to electrospinning, less than a gram per hour. Below 7 wt.% PVA concentration very few fibers were developed. Increasing the concentration of PVA increased the fiber yield. However, it also increased the diameter of the fiber. To optimize the fiber yield with smallest possible fiber diameter 9 wt.% concentration of PVA was selected for further studies. The nanofiber yield was also dependent on rpm and humidity. The optimal parameters for producing the desired OM-PVA nanofiber systems were found to be 4000 rpm at a humidity of 40–50%. OM-loaded PVA systems with concentrations ranging from 1 to 50 wt.% of OM were produced (1, 3, 5, 15, 20, 33, and 50 wt.%). Samples containing 20 wt.% and 33 wt.% of OM were selected for detailed morphological and thermo-physical analysis. SEM micrographs were analyzed to obtain morphological information of the fibers and beads, micrographs and statistical analysis of measured diameters are shown in Figures 3.2 and 3.3. The obtained system exhibited long fibers with embedded beads as illustrated in Figures 3.2(a-f). The CA5PVA9 control sample had the lowest mean fiber diameter, 462.85nm with a standard deviation of 263.77nm. The sample CA10PVA9OM33 had the highest mean fiber diameter, 528.27nm with a standard deviation of

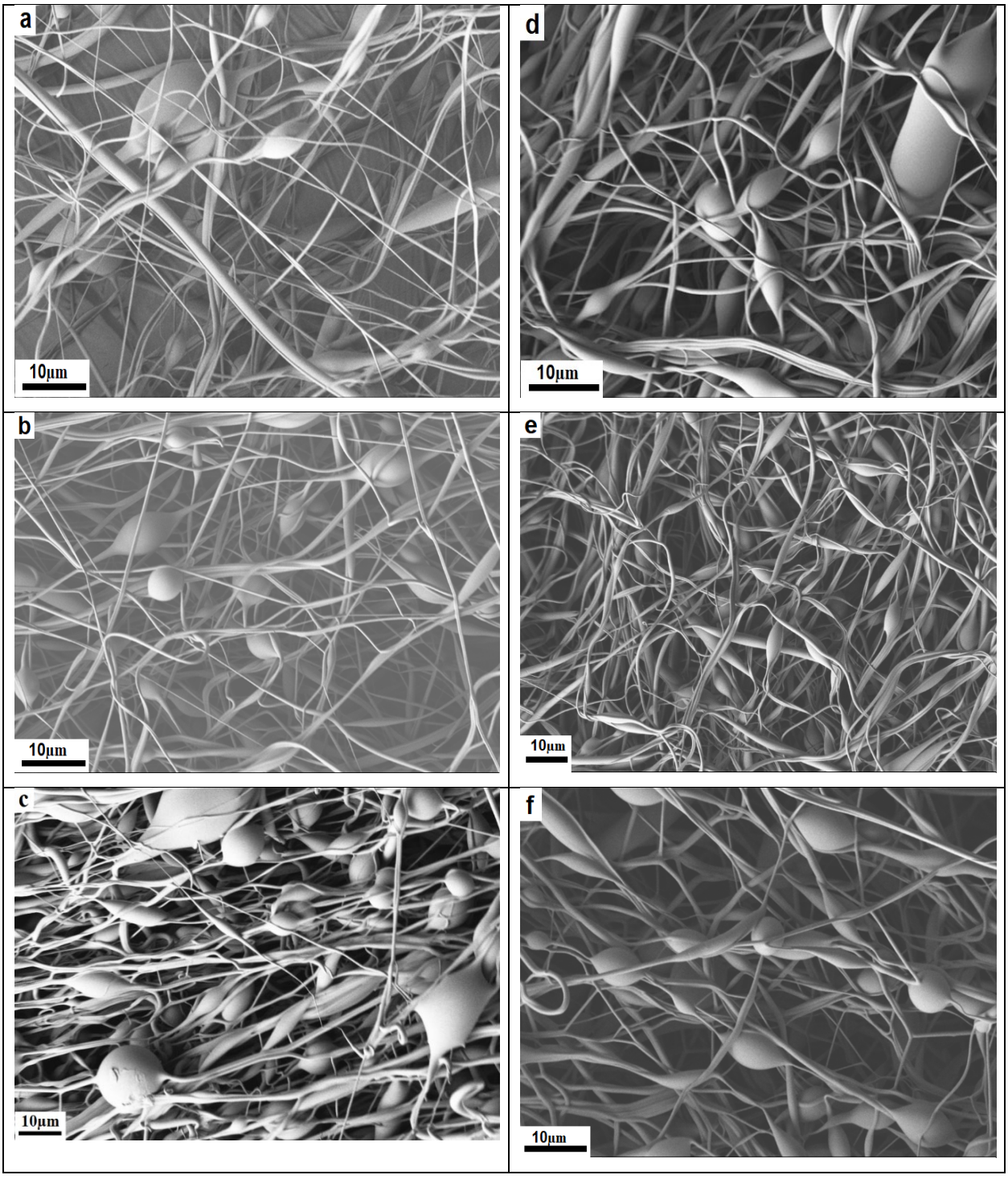

Figure 3.2: SEM micrograph of crosslinked PVA nanofiber and OM loaded crosslinked PVA nanofiber. CA5PVA9 (a), CA5PVA9OM20 (b), CA5PVA9OM33(c), CA10PVA9 (d), CA10PVA9OM20 (e), CA10PVA9OM33(f)

151.93nm. The data reveals that an increase in CA and OM results in an increase in mean fiber diameter. It also reveals a positive correlation between the bead size with the increase in CA and

OM concentration. Both PVA and OM are soluble in water. As a result, the developed membranes were unstable in water.

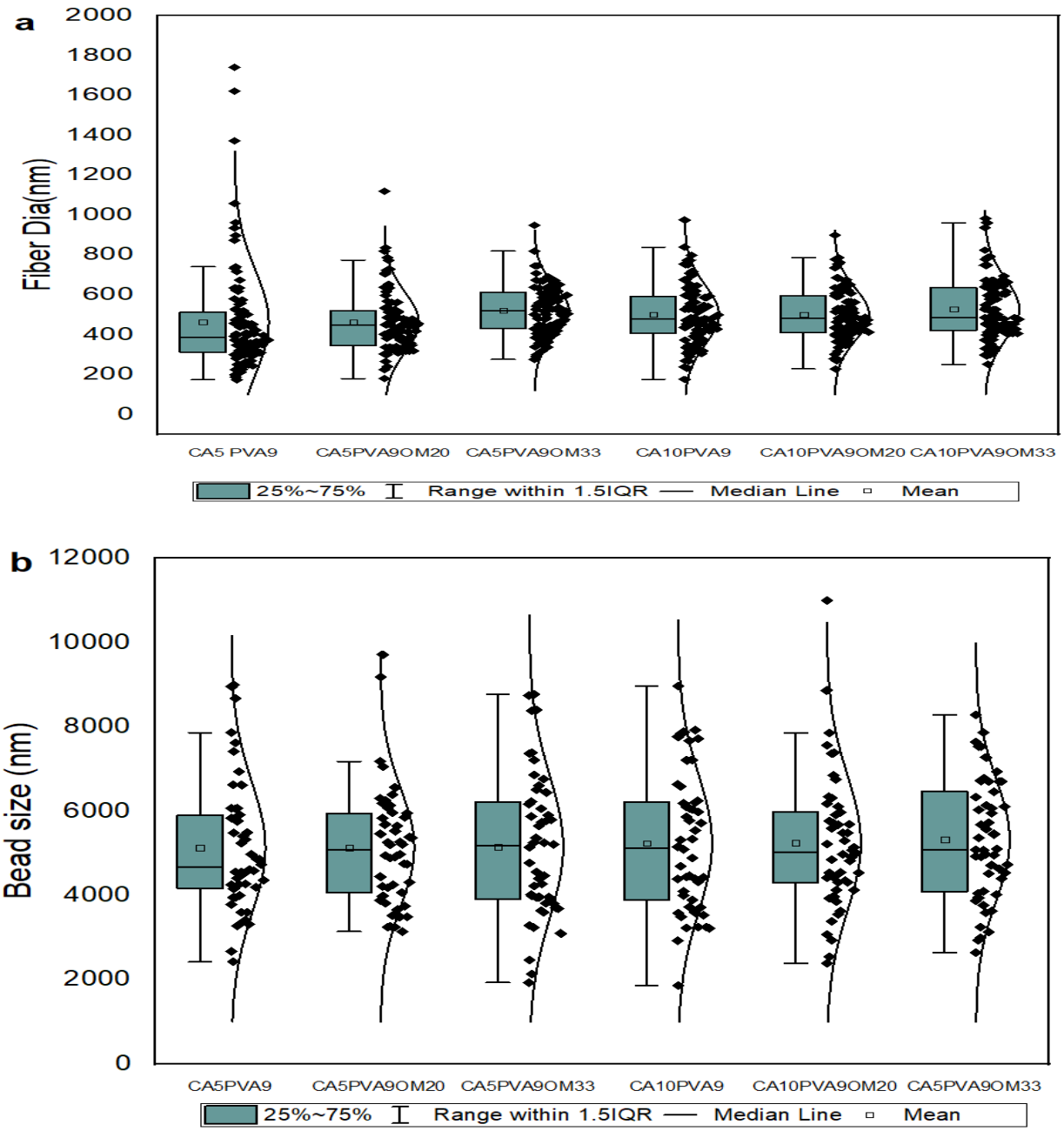

Figure 3.3: Distribution of 100 fiber diameter (a) and 50 bead size (b) in PVA-OM nanofiber formed during FS.

Various concentrations of CA were added to the PVA-OM solutions to study its effect on crosslinking polymer molecules and stability in aqueous medium. The cross-linked membranes

were submerged in water, retrieved, and analyzed under SEM, as shown in Figure 3.4. CA5PVA9 and CA10PVA9 fiber membranes show the best stability in water. The CA5PVA9OM20 showed lowest stability in aqueous medium among the developed samples.

Through energy dispersive X-ray spectroscopy (EDS) spectrum and elemental mapping, the presence of OM in the fibers was confirmed. OM contains nitrogen which is a distinctive element among the components that make up the fiber. Figure 3.5 and 3.6 shows the EDS spectrum of the fiber samples. The EDS spectra showed highest amount of N concentration on the bead of the fiber sample.

Table-3.2: Statistical analysis of fiber diameters for 100 fibers from PVA-OM fiber samples.

Sample	Mean(nm)[a]	Standard Deviation(nm)	Q1-Q3(nm)
CA5PVA9	462.008±26.37	263.77	313.26-511.22
CA5PVA9OM20	462.85±14.82	148.27	344.31-521.26
CA5PVA9OM33	520.67±12.36	123.67	432.28-613.88
CA10PVA9	499.62±14.67	146.75	405.53-480.91
CA10PVA9OM20	501.65±12.96	129.63	411.98-593.86
CA10PVA9OM33	528.07±15.19	151.93	420.44-637.70

[a]=mean±SE

Table-3.3: Statistical analysis of bead size for 50 fibers from PVA-OM fiber samples.

Sample	Mean(nm)[a]	Standard Deviation(nm)	Q1-Q3(nm)
CA5PVA9	5128.16±219.18	1549.84	4162.26-5913.73
CA5PVA9OM20	5138.31±196.44	1389.04	4066.28-5952.95
CA5PVA9OM33	5156.52±239.097	1690.67	3910.61-6222.74
CA10PVA9	5237.94±230.59	1630.51	3895.02-6213.49
CA10PVA9OM20	5244.26±227.38	1607.87	4312.72-5980.67
CA10PVA9OM33	5323.20±2075	1433.23	4098.86-6468.02

[a]=mean±SE

At various CA and OM contents from the corresponding SEM micrographs. Statistical analysis for each concentration represented in a box chart reflects the average fiber diameter 3.3(a) and bead size 3.3(b) in the central 25 - 75% range of the distribution (Q1-Q3). Whiskers on the boxes represent the corresponding maximal- and minimal-interquartile range (IQR) within 1.5IQR. The horizontal line and the dot in each box correspond to the median and the mean (the average fiber diameters(a) and average bead size(b), as shown in Table-3.2 and Table-3.3).

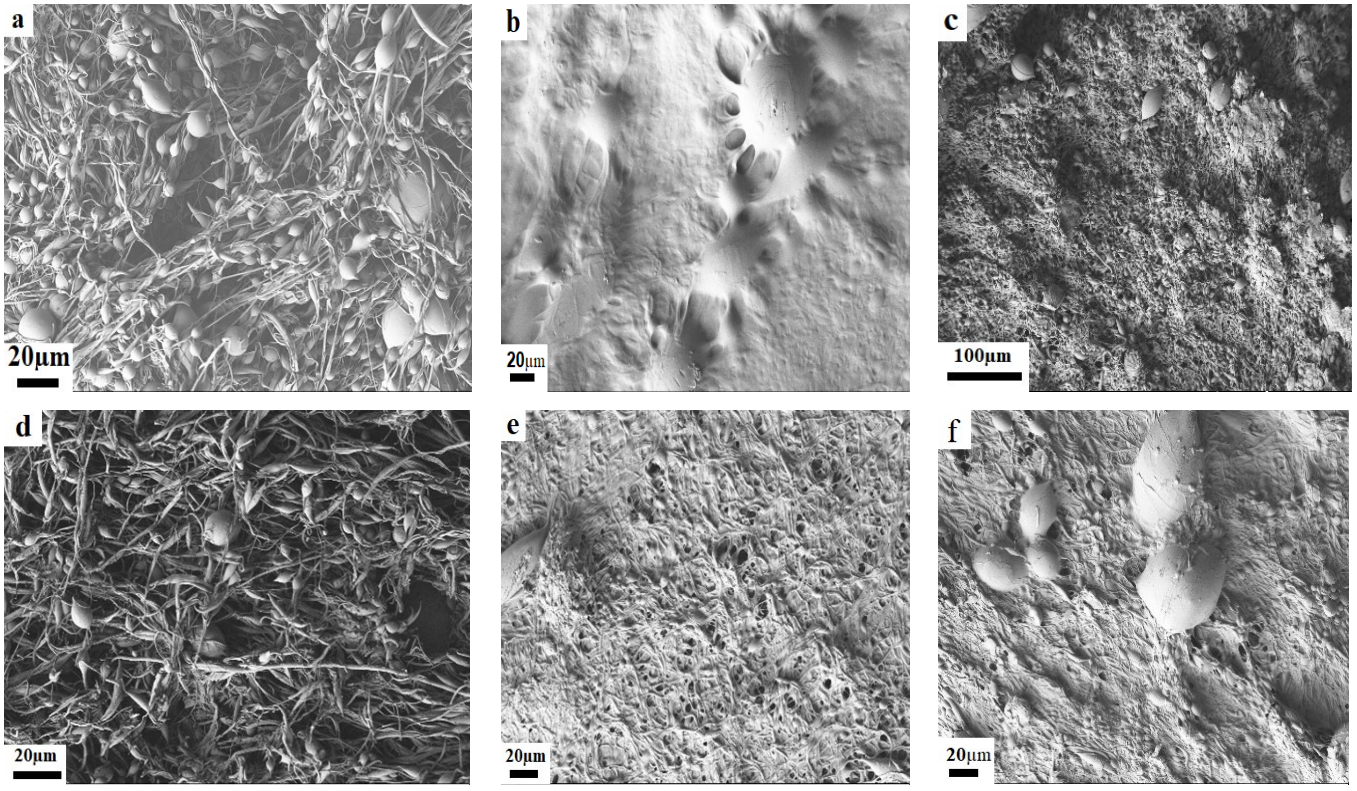

Figure 3.4: SEM images of CA5PVA9 (a), CA5PVA9OM20 (b) and CA5PVA9OM33 (c), CA10PVA9 (d), CA10PVA9OM20 (e) and CA10PVA9OM33 (f) after water absorption

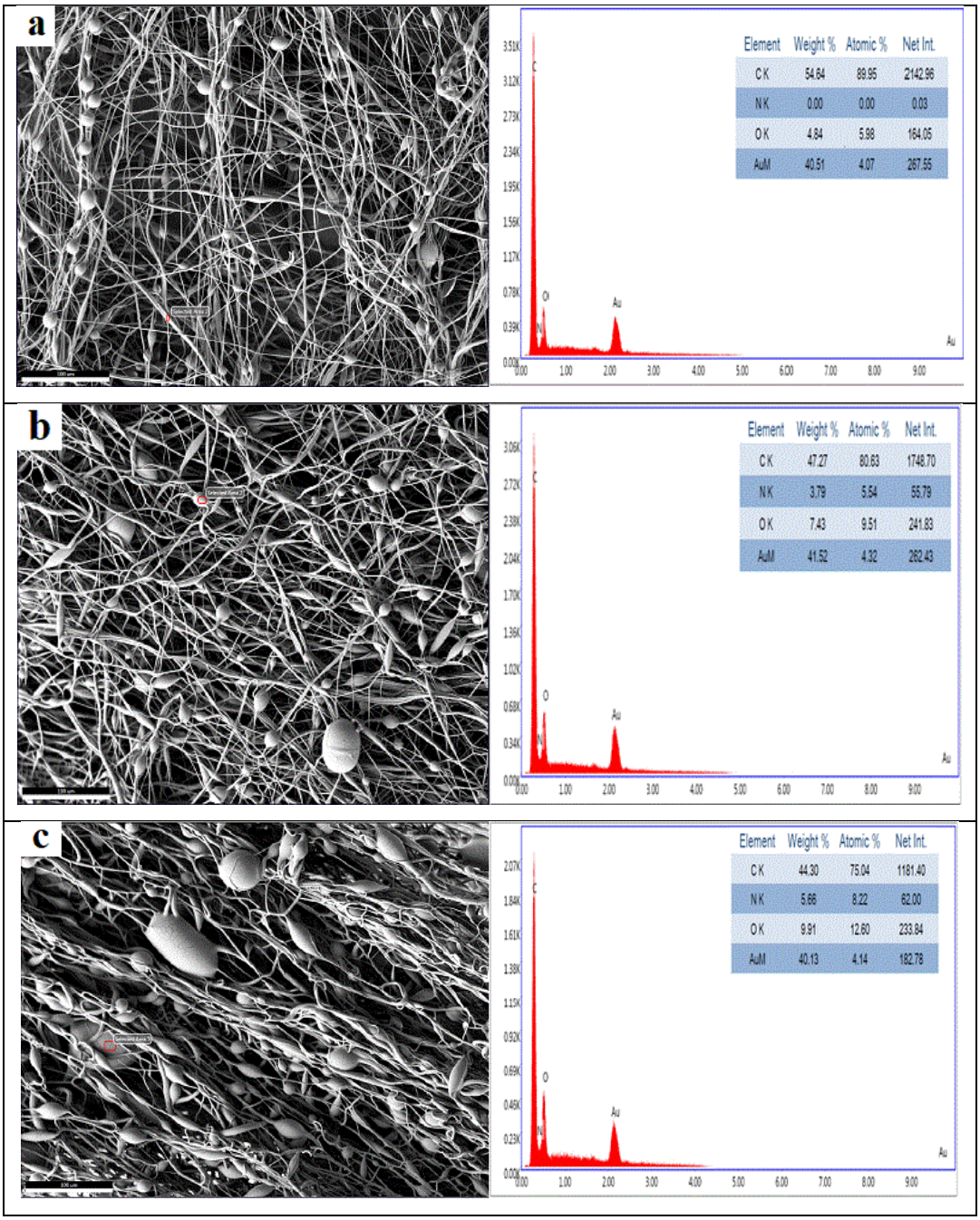

Figure 3.5: EDS spectra of CA5PVA9 (a), CA5PVA9OM20 (b) and CA5PVA9OM33 (c),

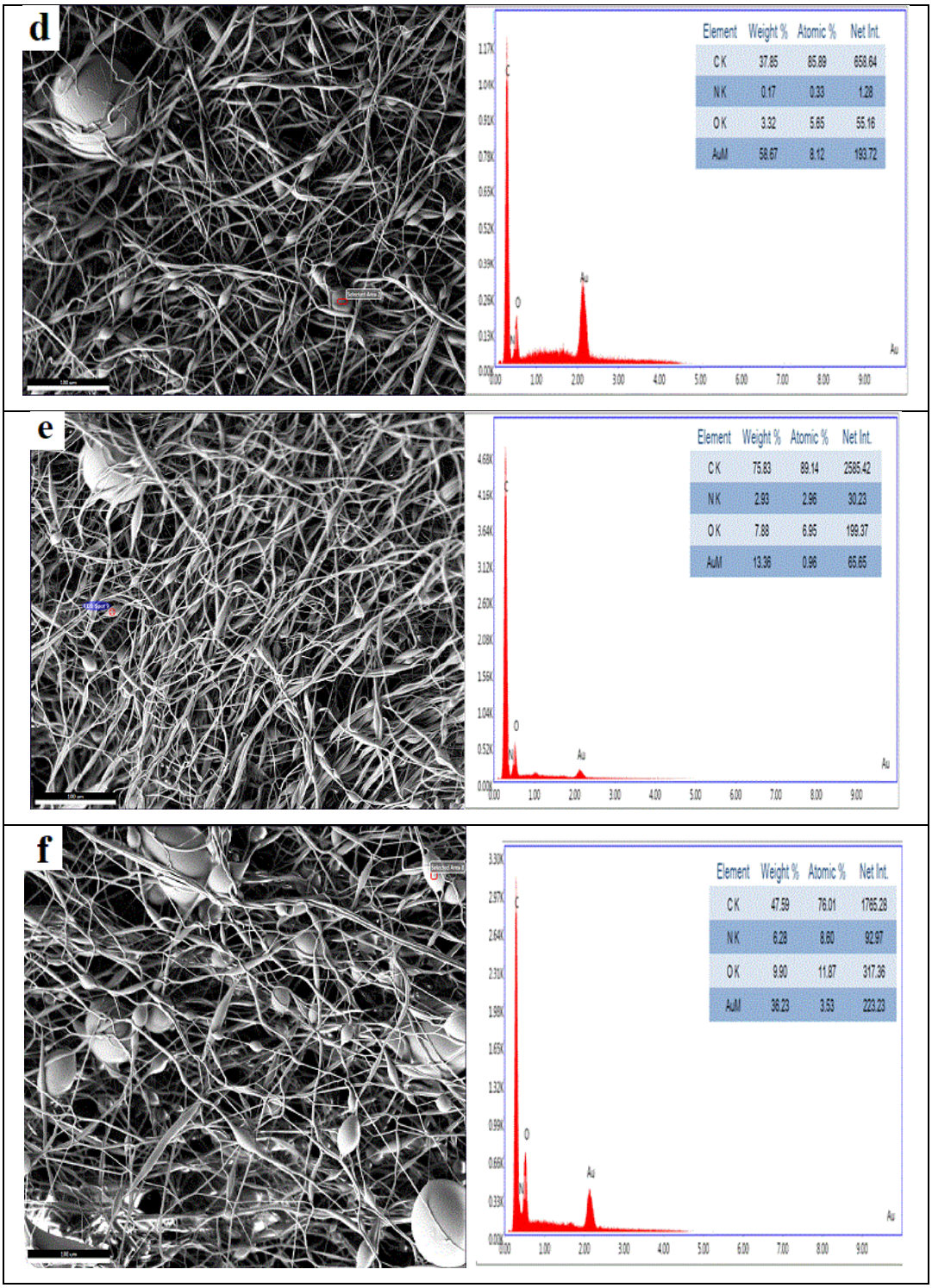

Figure 3.6: EDS spectra of CA10PVA9 (d), CA10PVA9OM20 (e) and CA10PVA9OM33 (f).

Figure 3.7 shows the DSC and TGA-DTG thermograms of oxymatrine. The DSC curve shows an endothermic peak at 169°C which can be attributed to the dehydration process of crystal hydrate. (B. Li et al. 2021) The corresponding TGA curve also shows a mass loss of 5.28% at this

temperature, which corresponds to the hydrated form of oxymatrine (ref). The 2nd endothermic peak at 242.28°C is associated with the melting point of OM and the exothermic peak at 258.4°C represents the decomposition of OM. The DTG curve shows two distinct peaks at the region at 250°C and a maximum decomposition rate at 292°C. The TGA curve shows a total of 91.2% of OM is degraded at 292°C which corresponds with the result reported by Li et al. (B. Li et al. 2022).

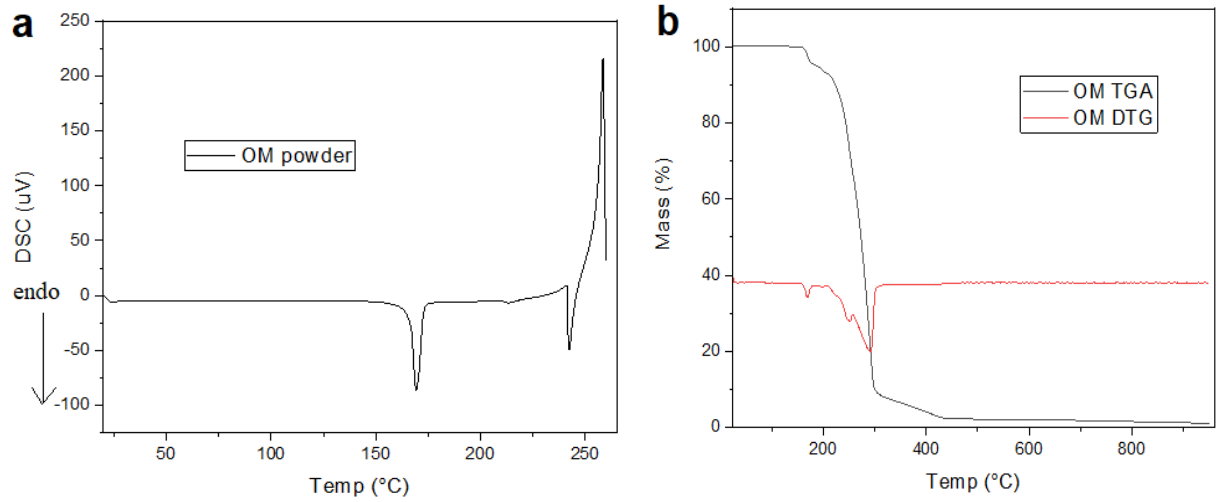

Figure 3.7: DSC(a) and TGA-DTG(b) curve of OM powder.

TGA and DTG curves of raw PVA fiber and crosslinked PVA fibers are shown in Figure 3.8. The curves show weight loss in three stages. The first stage of degradation can be attributed to the evaporation of loosely bound water from the spinning solvent (distilled water). As the crosslinking was done at 140°C, the weight loss in this stage is significantly less in the crosslinked fiber compared to the uncrosslinked fiber. The second stage degradation between 240°C-350°C can be attributed to the thermal decomposition of the side PVA chain, and the products that are composed of small molecular carbon and hydrocarbon (R. Shi et al. 2008; D. Yu et al. 2021). The third decomposition stage between 350°C-470°C is due to the breaking of the main polymer chain of PVA (Estevez-Areco et al. 2018; Santos et al. 2014). The crosslinked PVA samples show higher thermal stability as a result of crosslinked PVA molecular chains (Sonker et al. 2018). In the DTG curve of the PVA nanofibers, the temperature for the maximum weight loss rate of the second degradation stage for uncrosslinked PVA, CA5PVA9, and CA10PVA9 are 280.2°C, 356.8°C, and 362.8°C respectively. The second stage of degradation is due to the degradation of the side chain of PVA polymer; the crosslinking of the side chain increases with the increase of citric acid content

in the sample (D. Yu et al. 2021). The addition of citric acid reduced the weight loss rate, as depicted by the DTG curve. This result shows that the thermal stability of crosslinked nanofiber mats increased as the citric acid concentration increased due to crosslinking and strong hydrogen bonding as a function of CA, these results are consistent with findings reported by Yu et al.(D. Yu et al. 2021) and Shi et al.(R. Shi et al. 2008). The crosslinking process does not affect the main polymer chain of PVA. (D. Yu et al. 2021) As a result, the third stage degradation of crosslinked and uncrosslinked nanofiber mats is identical, as shown in the DTG graph. The melting point of the crosslinked PVA fiber increases with increasing concentrations of citric acid (Figure 3.7a). The uncrosslinked PVA fiber showed an endothermic peak at 65°C which could be assigned as glass transition temperature. This glass transition temperature is lower than the glass transition temperature found in literature. (Freire et al. 2021) The glass transition temperature for 20% and 33% OM loaded uncrosslinked PVA fiber was 59°C and 56°C respectively. The peak for glass transition temperature was vanished in the crosslinked PVA fiber and OM loaded PVA fibers. The endothermic peak for melting of the uncrosslinked PVA fibers was about 197°C, whereas the endothermic peak of the crosslinked fibers CA5PVA9 and CA10PVA9 was around 206°C and 213°C, respectively. The creation of a crosslinked network due to the esterification reaction between CA and PVA increased the molecular weight of PVA, requiring higher temperature to melt crosslinked fibers than control fibers. (Gadhave et al. 2018) Nataraj et al. (Nataraj, Reddy, and Reddy 2020) reported a melting temperature of an uncrosslinked PVA fiber to be 179°C while that one of the crosslinked PVA fiber with 15% CA to be 194°C, which aligns well with results obtained in the present study. The melting enthalpy and crystallinity (not shown) decreased with the crosslinking of the fiber due to effect imparted by addition of citric acid (R. Shi et al. 2008)

The thermal stability of the composite fiber was observed to decrease with the addition of OM (Figures 3.8c and 3.8e). The OM loaded PVA nanofiber showed four stages of thermal degradation. The result shows a decrease in thermal stability with the increasing amount of OM. The degradation steps for OM loaded nanofiber is shown in table-3.4.

The TGA results reveal that increasing the concentration of OM from 20% to 33% significantly decrease the thermal stability of the nanofiber. However, the fiber is stable up to 220°C and can be effectively used for drug delivery.

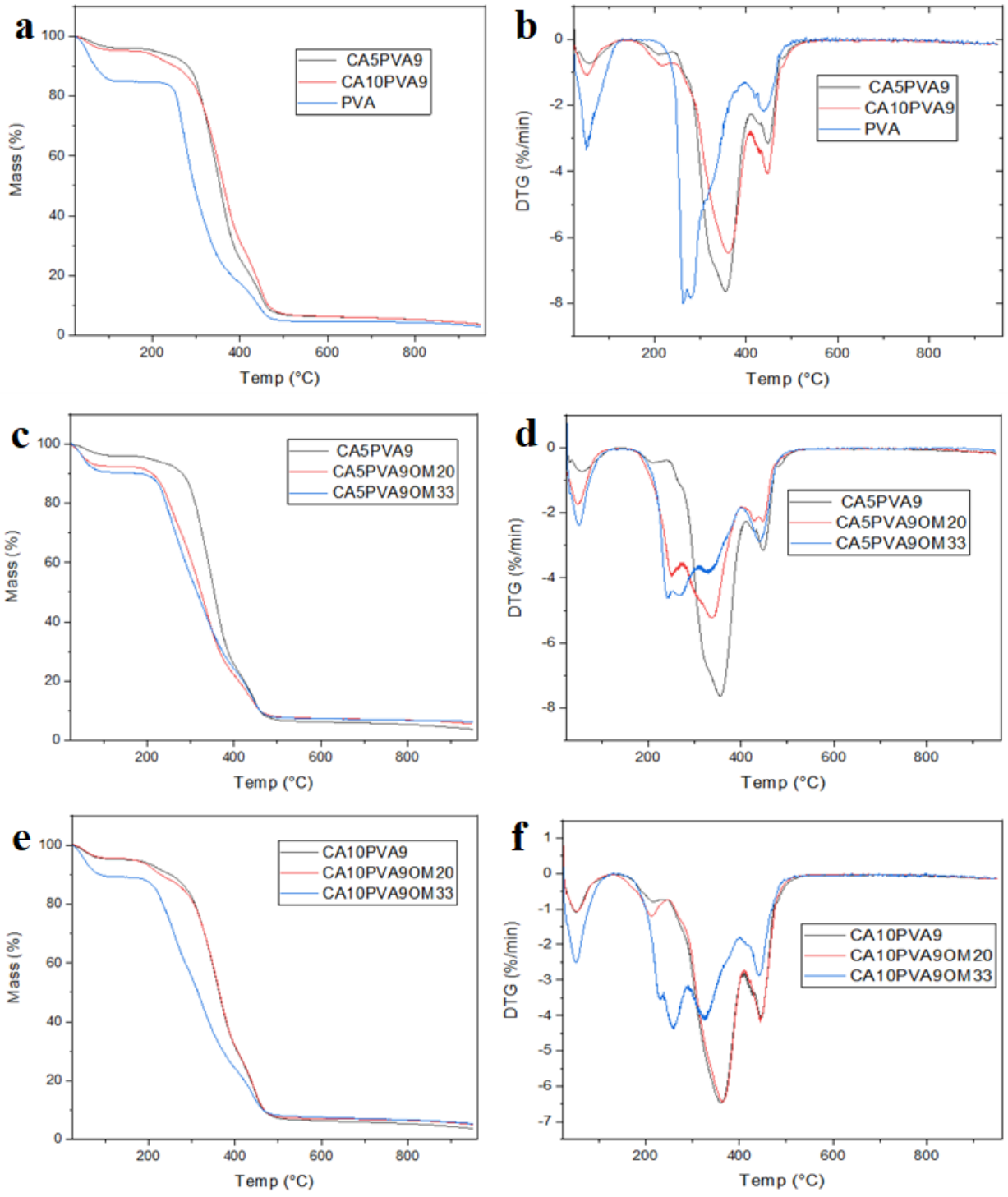

Figure 3.8: TGA curve of uncrosslinked and crosslinked PVA control(a), 20% OM loaded fiber (c), 33% OM loaded fiber(e). Corresponding DTG curve of uncrosslinked and crosslinked PVA control(b), 20% OM loaded fiber (d), 33% OM loaded fiber(f)

Table-3.4: Degradation steps for OM loaded nanofibers

Sample	1st step/ degradation	2nd step/ degradation	3rd step/ degradation	4th step/ degradation
CA5PVA9OM20	25-120°C/ 6.6%	180-280°C/ 20.1%	280-370°C/ 50.55%	370-480°C/ 14.52%
CA5PVA9OM33	25-100°C/ 11.58%,	180-300°C/ 37.42%,	300-360°C/ 29.46%	360-460°C/ 14.82%
CA10PVA9OM20	40-130°C/ 4.52%	150-220°C/ 5.9%	220-400°C/ 60.08%	400-500°C/ 22.5%
CA10PVA9OM33	40-130°C/10.89%	180-300°C/ 31.02%	300-400°C/ 33.5%	400-500°C/ 16.47%

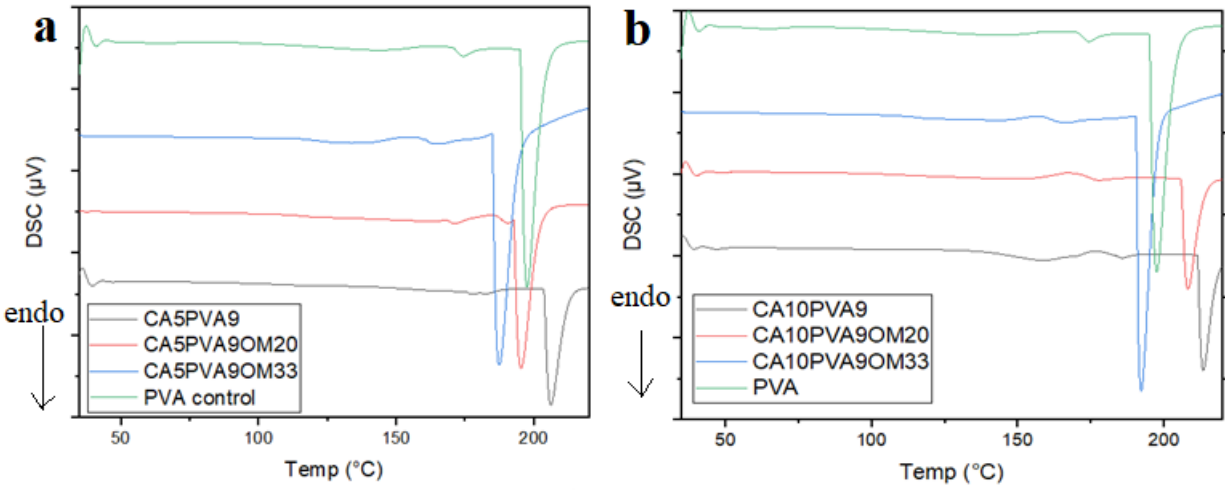

Figure 3.9: DSC curve of uncrosslinked PVA, Crosslinked PVA, OM loaded crosslinked PVA nanofiber. Crosslinked with 5% Citric Acid(a), crosslinked with 10% Citric Acid (b)

The composite PVA-OM nanofiber samples exhibited a lower melting temperature compared to the crosslinked control PVA nanofibers. With the increase of OM content, the melting temperature of OM loaded PVA nanofiber decreased, and the melting enthalpy increased, as depicted in figure-3.8 and table-3.5. It can be due to the high miscibility of OM and PVA.(B. Li et al. 2021) The results suggest that OM is dispersed in the PVA polymer networks, which affect the crystal structure.(Shukry et al. 2014)(B. Li et al. 2022)

Table-3.5: The melting temperature and melting enthalpy of crosslinked PVA and OM loaded PVA nanofibers.

Sample	Melting Temperature(°C)	Melting Enthalpy
CA5PVA9	206.2	86.78 J/g
CA5PVA9OM20	195.3	112.3 J/g
CA5PVA9OM33	187.4	176.4J/g
CA10PVA9	213.5	70.03 J/g
CA10PVA9OM20	208.3	87.98 J/g
CA10PVA9OM33	192.3	163.5 J/g

The FTIR study was carried out to determine distinct functional groups as well as interactions between PVA and OM. figure-3.9 show the FTIR spectra of OM powder, uncrosslinked PVA nanofiber, crosslinked PVA nanofiber, and OM-loaded PVA nanofibers. For uncrosslinked and crosslinked PVA, the broad bands around 3292 cm^{-1} are due to intra and intermolecular hydrogen bonds from -OH stretching. The intensity of this peak is diminished in the crosslinked fiber, which can be attributed to the formation of acetal bridges due to crosslinking.(Mansur et al. 2008) The vibration observed at 2938 cm^{-1} was due to -CH stretching from alkyl groups. The characteristic peaks at 1435 cm^{-1} and 1094 cm^{-1}can be attributed to -CH_2 bending, and C–O stretching respectively.(D. Yu et al. 2021) The broad peak at 1713 cm^{-1} is due to the C=O stretching vibrations. Due to the exposure at a high temperature of 140 °C and the following crosslinking reaction, the band in crosslinked PVA is slightly more intense. (Nataraj, Reddy, and Reddy 2020) This phenomenon suggests that ester groups were formed by the chemical reaction between the hydroxyl groups of PVA and the carboxyl groups of citric acid. (D. Yu et al. 2021)

OM powder showed its characteristic stretching peaks at 2873 cm^{-1}, 2292 $cm^{-1}$and 1602 cm^{-1} which are attributed to the C–H of skeleton ring, N–O coordination bond and C=O group, respectively. The intense carbonyl peak at 1602 cm^{-1} is due to the rigid six-membered ring structure of tertiary amine of OM (B. Li et al. 2021) In OM loaded PVA nanofiber the C-H bonds

of OM shifted to 2906cm^{-1}, 2908cm^{-1}, 2903cm^{-1}, 2905cm^{-1}, for CA5PVA9OM20, CA5PVA9OM33.

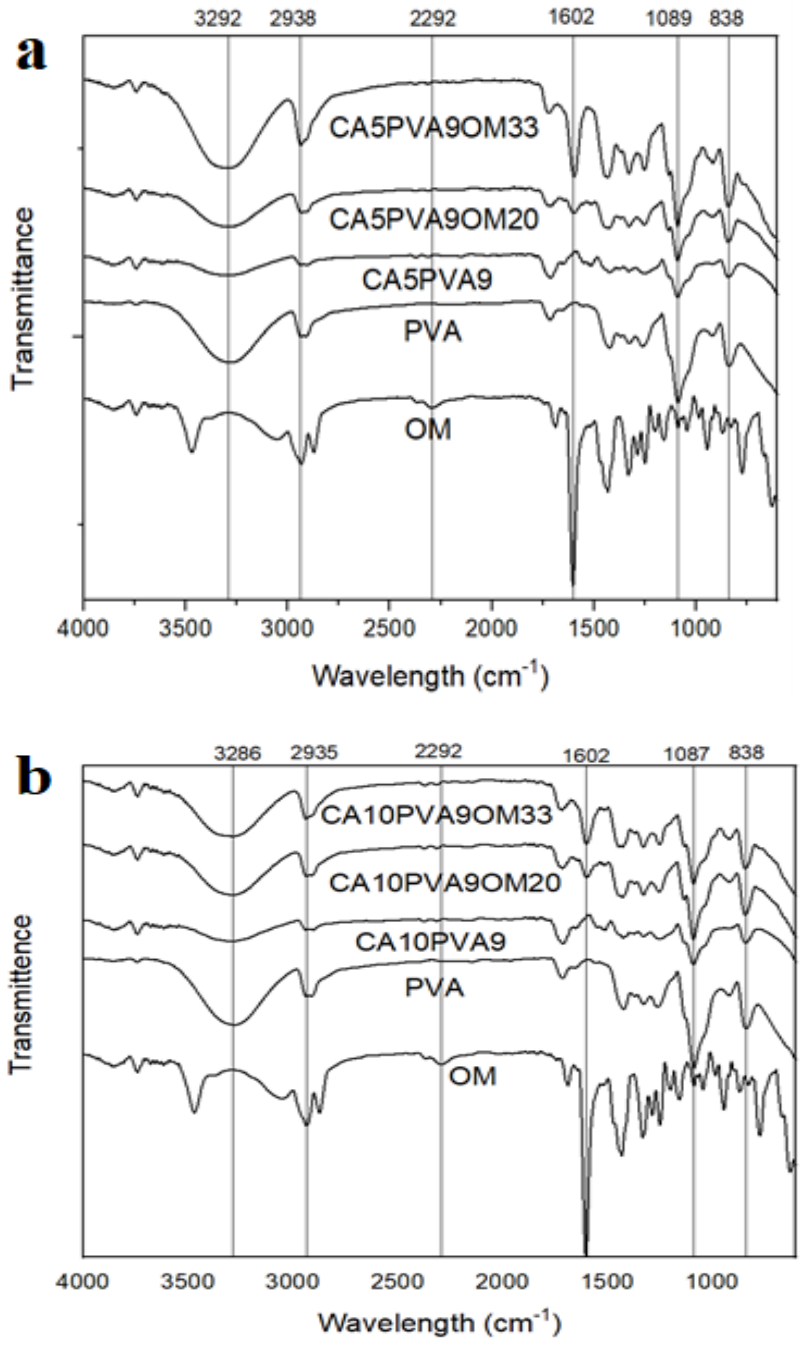

Figure 3.10: FTIR spectra of OM, Uncrosslinked PVA, Crosslinked PVA, OM loaded crosslinked PVA nanofiber. Crosslinked with 5% Citric Acid (a), Crosslinked with 10% Citric Acid (b)

CA10PVA9OM20, CA10PVA9OM33 respectively. We have found overlapping peaks of crosslinked PVA and OM powder in the OM loaded PVA nanofiber at 1445 cm^{-1}. The N-O stretching peak of OM powder disappeared in all OM loaded PVA nanofiber. The uncrosslinked and crosslinked PVA nanofiber showed no peak at 1602 cm^{-1}. The peaks at 1602 cm^{-1} for CA5PVAOM20, CA5PVAOM33, CA10PVAOM20, and CA10PVAOM33 originate from the carbonyl stretching validates the presence of OM in composite nanofiber. The disappearance of N-O coordination bond and in the composite nanofiber may be due to the change of the molecular environment, rather than the formation of hydrogen bond. (Löbmann et al. 2013) Compared to the spectra of CA5PVAOM20 and CA10PVAOM20, the spectra of CA5PVAOM33 and CA10PVAOM33 show more intense peaks at 1602 cm^{-1}, indicating a higher concentration of OM content in the composite nanofiber.

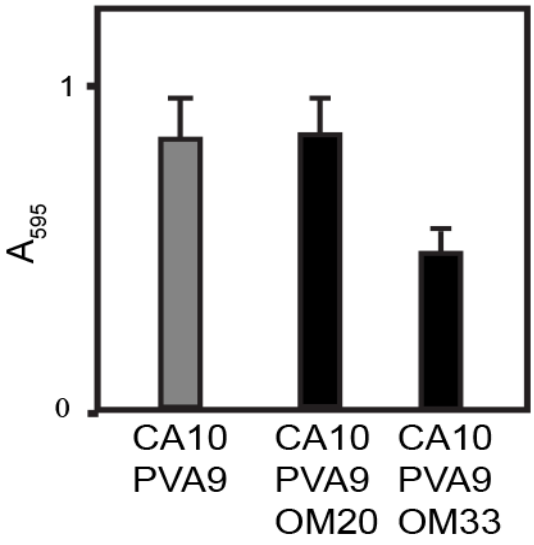

Figure 3.11: MTT assay of cell viability in the presence of control and OM-containing nanofibers.

To examine whether OM-containing fibers have any detrimental effects on cell growth compared to fibers containing CA10PVA9 fibers alone, MTT assays were conducted on NIH 3T3 fibroblast cells grown in the presence of CA10PVA9 control fibers, as well as CA10PVA9 fibers incorporating OM (OM20 or OM33). Following two days incubation in the presence of nanofibers, no statistically significant differences were observed between cell growth in the three fiber matrix environments ($p>0.05$, Student's T-test). These results indicate that OM does not impede short-term cell growth and viability for 3T3 mouse embryonic fibroblast cells when included as part of the fiber matrix.

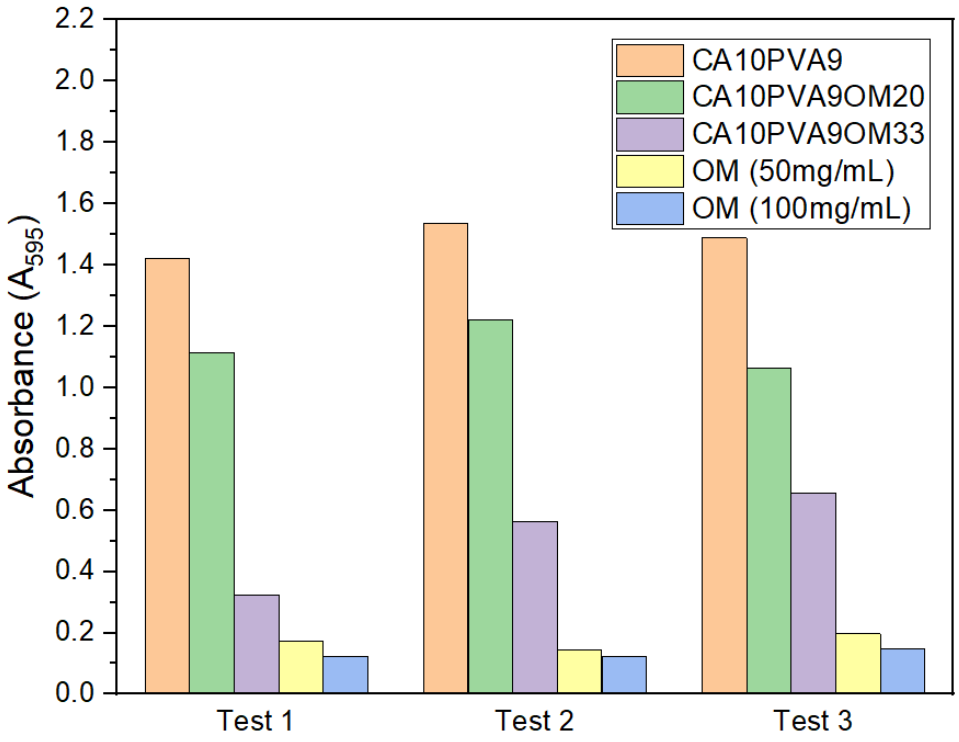

Figure 3.12: MTT assay of anticancer studies of control and OM-containing nanofibers and bare OM

To evaluate the cytotoxic properties of OM loaded nanofiber, MTT assay was performed on human colon cancer cells HCT116. The cytotoxic activity of the control fiber (CA10PVA9) and oxymatrine loaded fibers (CA10PVA9OM20 and CA10PVA9OM33) is shown in figure-3.11. Nanofiber membrane loaded with higher concentration of OM (CA10PVA9OM33) showed strong cytotoxicity against HCT116 colon cancer cells. However, nanofiber membrane loaded with lower concentration of OM (CA10PVA9OM20) had insignificant cytotoxic effect on the colon cancer cells compared to the control nanofibers. It could be interpreted from the results that OM retains its activity even after blending into nanofibrous matrix and is not affected by the forcespinning process. As PVA is a biodegradable polymer, after the drug release is complete, it doesn't need to be surgically removed.

3.4 Discussion

OM loaded PVA nanofiber was fabricated using high yield forcespinning method. The concentrations, RPM were optimized for a high yield with smallest fiber diameter. The nanofibrous

membranes were crosslinked with citric acid to make them more stable in aqueous medium. The high surface area made it a potential candidate for drug loading in high concentration and good thermal stability enabled it to be sterilized before being applied as a targeted drug delivery system. The method used in this work might be applied to create a variety of biocompatible composite nanofibers from other materials for drug delivery purposes. Our cell-based results indicate that while nanofibers containing OM are not cytotoxic to mammalian cells after 48 hrs, longer incubation with high concentration of OM-containing fibers elicits decreased cell viability relative to uncoated nanofibers. These results suggest that OM-containing nanofibers may provide an innovative strategy for targeted delivery of anticancer agents to tumor sites. Lining remaining tissues with nanofibers embedded with chemotherapeutic drugs such as OM after tumor resection has the potential to deter colon cancer microdeposits left behind. These microdeposits are migratory and aggressive. Given that OM was shown to hinder epithelial to mesenchymal transition and viability of colon cancer cells, it is likely that OM would hinder tumor microdeposit invasion further into the underlying connective tissue leading to fewer distant metastases and longer survival times.

CHAPTER IV

SALVIANOLIC ACID-LOADED NANOFIBER AND ITS BIOACTIVE EFFECTS ON FIBROBLAST AND HCT116 COLON CANCER CELLS

4.1 Introduction

Targeted drug delivery systems can increase its therapeutic effect and limit the adverse consequences to non-targeted locations. Nanotechnology-based drug delivery methods, such as nanoparticles(Yao et al. 2020), hydrogels(Nii 2021), and nanofibers(Kajdič et al. 2019), are gaining attraction due to their potential to deliver therapeutics at a specific site with a precise pharmacokinetic profile. The unique properties of nanofiber membranes and scaffolds, makes them highly promising medium for targeted drug delivery. Nanofibers have been proven as an efficient method for delivering both hydrophilic and hydrophobic drugs (B. Song, Wu, and Chang 2012; J. Xu et al. 2011); offering unique ways to increase the rate of dissolution of poorly soluble substances, which reduces the drawbacks of oral bioavailability (D.-G. Yu et al. 2009). Additionally, it has the ability i) to enhance the effectiveness of the loaded drugs, ii) to enable encapsulated drugs to maintain their therapeutic effect for longer periods by shielding them from adverse atmospheric conditions. Xie et al. (J. Xie and Wang 2006) developed anticancer drug paclitaxel-loaded PLGA nanofibers, their system contained the drug in a solid-state solution within polymeric micro and nanofibers and showed a sustained release of the drug for 60 days.

Pullulan, Figure 4.1(a), is a commercially emerging microbially produced biopolymer that is mainly produced by yeast like fungus *Aureobasidium pullulans* in sugar and starch cultures (BERNIER 1958; Ram Sarup Singh and Kaur 2010). It is formed on the surface of microbial cells as an amorphous slime (Catley, Ramsay, and Servis 1986; R. S. Singh and Saini 2008; Ram S. Singh, Saini, and Kennedy 2009; Sutherland 1998). It is

naturally non-toxic, non-immunogenic, non-carcinogenic, and non-mutagenic(Ram Sarup Singh et al. 2017). It is a linear, unbranched, and water-soluble exopolysaccharide with the molecular formula $(C_6H_{10}O_5)_n$ and has a molecular weight ranging from $4.5x10^4$ to $6x10^5$ Da, which is heavily influenced by cultivation parameters (Ram Sarup Singh and Kaur 2010). It has maltotriose repeating units which are connected by α-(1,6) glycosidic bonds (R. S. Singh and Saini 2012). The internal glucose units within maltotriose are connected by a α-(1,4)glycosidic bond (Cheng, Demirci, and Catchmark 2011). It is a white, non-hygroscopic powder that dissolves easily in hot and cold water, as well as diluted alkali. It is insoluble in most of the organic solvents except dimethylsulfoxide and formamide (Kimoto, Shibuya, and Shiobara 1997). Due to its unique physio-chemical properties, pullulan has been used in food (Pınar et al. 2013), pharmaceutical (Mishra, Suneetha, and Rath 2011) and biomedical applications. Due to its inert nature, biocompatibility, low oxygen permeability, and chemical and mechanical properties, pullulan is extensively used for biomedical applications such as targeted drug (Xi et al. 1996) and gene (Grenha and Rodrigues 2013) delivery, medical imaging (Hasegawa et al. 2005), vaccination (Nakahashi-Ouchida, Yuki, and Kiyono 2018), tissue engineering (Fricain et al. 2013), and wound dressing (Wong et al. 2011). Additionally, it has been declared safe by FDA in United States and has GRAS status (Ram Sarup Singh et al. 2021). Fricain et al. (Fricain et al. 2013) developed nano-hydroxyapatite-Pullulan/dextran polysaccharide composite macroporous material for bone tissue engineering. The study revealed that the mineral phase integrated within these natural polysaccharides leads to a chemical and structural architecture, which triggers early calcification and osteoid tissue formation in non-osseous and osseous sites. Liang et al. (Y. Liang et al. 2019) developed multifunctional injectable hydrogels made of chitosan-grafted-dihydrocaffeic acid and oxidized pullulan with pH-sensitivity and mucosal adhesiveness as localized drug carriers. The hydrogel showed sustained release of anticancer or antibacterial drugs for colon cancer therapy. Li et al. (Huanan Li et al. 2011) developed cystamine- carboxymethylpullulan hydrogel incorporated with antimicrobial agents which showed good swelling capacity, high water absorption, outstanding mechanical strength, efficient antimicrobial release activity, and biocompatibility. Pullulan nanofiber membranes have showed potential in wound dressing and skin tissue engineering. Xu et al. (F. Xu et al. 2015)developed a ternary nanofibrous membrane composed of pullulan, chitosan, and tannic acid that showed non-cytotoxicity to the fibroblast cells, antibacterial characteristics, improved cell proliferation and attachment, and high water

stability and absorption. Barbosa et. al (Barbosa et al. 2021)developed nanofibrous membranes containing Aloe vera extract, pullulan, chitosan and citric acid that showed synergistic antibacterial activity against E. coli and capability to promote cell attachment and growth.

Chitosan (CS), Figure 4.1(b), is a modified natural, biodegradable, biocompatible, non-toxic homopolymer of linear nitrogenous polysaccharides (Rishabha et al. 2010). Commercial CS is produced by deacetylating chitin, a naturally occurring polysaccharide, which is the structural component of the exoskeleton of crustaceans (Bansal et al. 2011). It is composed of randomly distributed β-(1 → 4)-linked N-acetyl-d-glucosamine (GlcNAc) and d-glucosamine (GlcN) (Figure 4.1(b)), the latter of which gives it cationic properties at physiological pH. It has an average molecular weight ranging between 3800 and 20,000 Daltons (Roberts 1992). Variety of CS derivatives have been created using free amino and hydroxyl groups with increased solubility which makes CS an attractive compound in biomedical and pharmaceutical processes, such as drug/gene/vaccine delivery(Martínez-Martínez et al. 2018), tissue engineering(G. Tang et al. 2020), wound healing(He Liu et al. 2018), and manufacture of cosmetic products. For example, Alavarse et al.(Alavarse et al. 2017) used a chitosan and poly(vinyl alcohol) (PVA) blend to construct a fiber scaffold with antibiotic tetracycline hydrochloride (TCH). The addition of Chitosan on the PVA solution created a thickening effect, which increased viscosity and formed uniform nanofibers. This blend enhanced mechanical properties because of the inter and intra-molecular hydrogen bonds between the PVA and chitosan chains.

Salvianolic acid B (SA) , Figure 4.1(c), is a bioactive component derived from the Chinese medicinal herb, Danshen, which is the dry root of *Saliva miltiorrhiza*. It is defined as a super herb due to its low toxicity and has been widely used in Chinese pharmacology to treat cardiovascular diseases such as angina pectoris, myocardial infarction and stroke(T. Chen et al. 2011; Ji, Tan, and Zhu 2000; Lin et al. 2019). Salvianolic acid B consists of three parts of Danshensu ($C_9H_{10}O_5$) and one part of dimeric caffeic acid. It has been clinically used to treat cardiovascular diseases (CVDs), pulmonary fibrosis, malignant tumors, cerebrovascular diseases, and chronic wounds by stimulating angiogenesis, re-epithelialization, and cell proliferation (Cao et al. 2012; Lay et al. 2003). It has shown various anti-oxidative (C. S. Liu et al. 2006) and anti-inflammatory (L. X. Xie et al. 2010) effects in different disease models. Treatment with Salvianolic acid B improved their motor function (M. Tang et al. 2006) and reduced brain damage (Y. H. Chen, Du, and Zhang 2000)

after cerebral ischemia in rats. Chen et al. (T. Chen et al. 2011) reported that Salvianolic acid attenuates brain damage and inflammation after traumatic brain injury in rats. Liang et al. (Y. H. Liang et al. 2009)reported that Salvianolic acid B serves as a matrix metalloproteinase inhibitor, which is helpful in the healing of chronic wounds. Studies suggest that Salvianolic acid inhibits cancer initiation and development and its anticancer effect has been demonstrated in both cell cultures and animal models(Hao et al. 2009; Y. Zhao et al. 2010). Zhou et al. (Zhou, Zuo, and Chow 2005) reported that Sal B protects various cells, including nerve cells and hepatocytes, by acting as an antioxidant and scavenger of free radicals. Despite having several biological activities, due to its low efficacy, poor systemic delivery, and low bioavailability, the extensive use of SA has been limited (Hongquan Li et al. 2016). Nanotechnology-based targeted drug delivery systems have been proven to be able to overcome these limitations and improve the bioactivity of Salvianolic acid B (Q. He et al. 2010). Li et al. (Hongquan Li et al. 2016) developed Salvianolic acid loaded phospholipid complex nanoparticles that are more potent than free Salvianolic acid and had an anticancer effect against HNSCC cells. Shoba et al.(Shoba et al. 2017) developed a nanofibrous membrane for wound dressing with salvianolic acid and bromelin that improved keratinocyte cell proliferation, endothelial cell migration, neovascularization, vessel density, and inhibited bacterial growth. Kuang et al. (Kuang et al. 2018) developed internal layer of artificial vascular grafts with SA and heparin that showed sustained release of Salvianolic acid and heparin for 30 days without any burst release.

Colorectal cancer (CRC) is the third most common type of cancer in the world. Even though CRC treatment has come a long way in recent years, it is still the third leading cause of cancer deaths in the United States and the fourth leading cause of cancer deaths worldwide(McGuire 2016; Siegel et al. 2014). 5-fluorouracil (5-FU) and its derivatives are currently used for the initial chemotherapy of CRC(J. Chen et al. 2015; Y. Zhang, Talmon, and Wang 2015). Even though most patients respond well to this chemotherapy, because of the growing level of resistance to the chemotherapeutic agents, the relapse rate is still high(Jing et al. 2016). It has become crucial to find new chemotherapeutic drugs. Salvainolic acid has been shown to effectively reduce multidrug resistance (MDR) in HCT116 colon cancer cells by inhibiting the expression of CD44, SOX2, and ABCG proteins(Guo et al. 2018). Jing et al. (Jing et al. 2016) reported that Salvianolic acid B is an autophagy inducer with potent anticancer activity as a single agent by inducing autophagic cell death in HCT116 CRC cells.

In this study, SA-loaded PL-CS composite nanofiber membranes were developed using the forcespinning® method to avoid the use of electric fields and organic solvents. The forcespinning approach has demonstrated high yield and proven potential to scale up. The influence of SA concentrations and processing parameters on the morphological and thermophysical properties of developed nanofiber membranes were investigated. The results indicate that nanofibers produced by forcespinning can include SA and exhibit structural integrity suitable for prospective usage as bioactive agent delivery systems. The in vitro cell viability studies and in vitro anti cancer properties were evaluated.

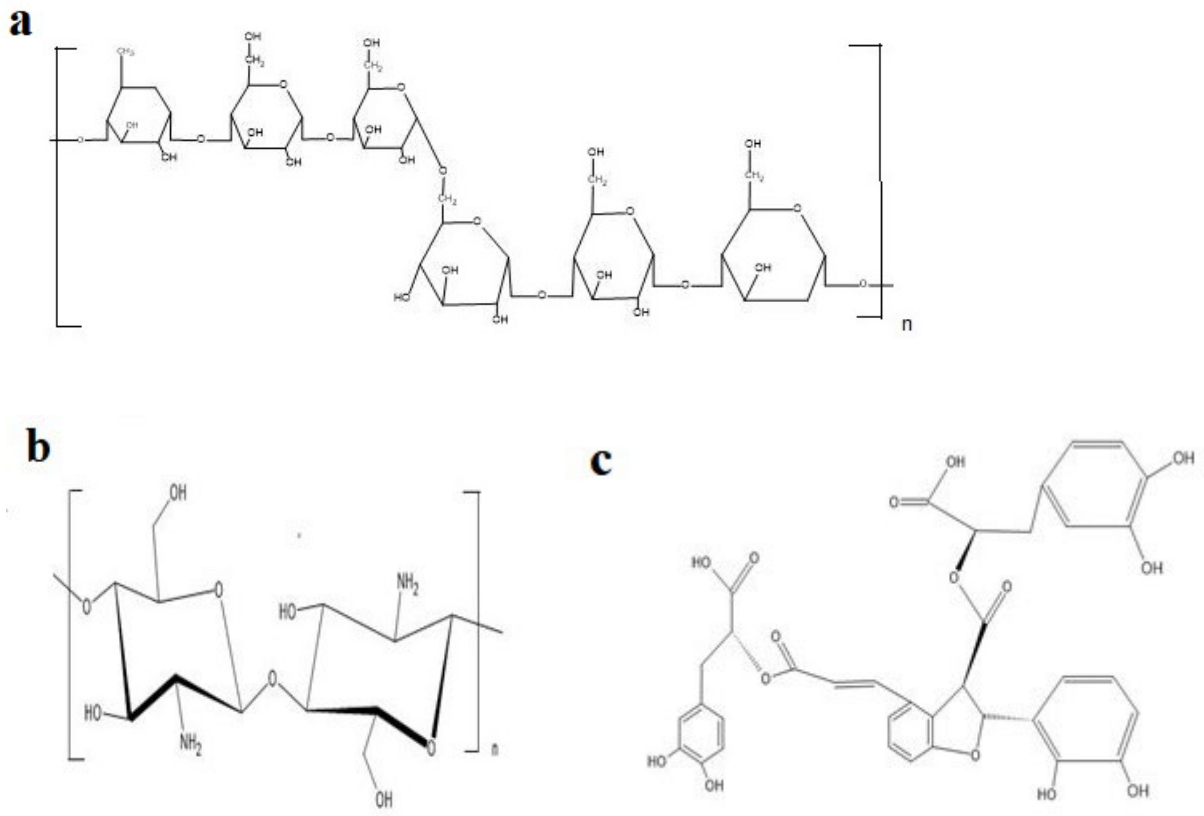

Figure 4.1: Chemical structure of Pullulan(a), Chitosan(b), Salvianolic Acid B (c)

4.2 Materials and Method

4.2.1 Materials

Chitosan (CAS 9012-76-4 (448877-250G), Brookfield viscosity 200 cps), pullulan (CAS 9057-02-7), and citric acid were purchased from Sigma Aldrich (St Louis, USA). Deionized (DI)

water was produced from a Smart2Pure water purification system. Danshen extract containing 20% Salvianolic acid B was acquired from Jiaherb Phytochem (China). This bioactive compound will be identified as SA throughout the manuscript. All of the chemicals were used in analytical grade without any further purification. As for fiber production, the 30-gauge bevel needles from PrecisonGlideTM were obtained from Fisher Scientific.

4.2.2 Solution Preparation

300 mg of citric acid (CA) was added to 10mL of deionized water (DI). The mixture was homogenized at 600 rpm using a magnetic stirrer (Thermo Scientific, Cimarec+ series) for 30 minutes. 50mg of chitosan (CS) was added to the CA solution. The solution was left on the magnetic stirrer overnight at 800rpm for homogenization. 2.2g of pullulan (PL) was added to the mixture to prepare the control (PL-CS) solutions. Three control solutions were prepared. Then, 0.2225g and 0.3925g of SA was added to the control samples to prepare solutions identified as PL-CS-SA(L) to identify the low concentration of SA and PL-CS-SA(H) for the high concentration of SA. The mixtures were stirred overnight to prepare homogeneous solutions.

4.2.3 Development of Nanofiber

The nanofiber membranes were developed using centrifugal force in Cyclone-1000M (FiberRio Technology Corp, McAllen, USA), which consists of a cylindrical spinneret with two nozzles. A 3 mL syringe was used to inject 2 mL of the prepared solution into the spinneret. Spinning was carried out for six minutes at 6500 rpm at ambient temperature and 20-30% relative humidity. Mats from five spinning cycles were collected manually using a 10cm x 10cm hollow frame and stored in sealed bags containing desiccants for moisture control.

Following the collection of nanofiber, the membranes were placed in an oven and heated to 140°C in a vacuum environment for 1 hour and 15 minutes for crosslinking to take place. The composite nanofibers became stable in water after crosslinking process. The samples were then taken out of the oven and allowed to cool down before further analysis.

4.2.4 Fiber Characterization

The surface morphology of the nanofibrous membranes was examined using a field-emission scanning electron microscope (FESEM) (Sigma VP, Zeiss Evo LS10, Jena, Germany).

A voltage of 1kV was applied throughout the procedure, with magnifications ranging from 35X to 15000X. The images were analyzed using ImageJ software (Version-1.8.0) to determine the average fiber diameter. The average fiber diameter was obtained by measuring the fiber diameter of 100 different fibers.

The thermal properties were analyzed using thermogravimetric analysis (TGA) and differential scanning calorimetry(DSC). TGA was carried out using Netzsch 209. For the analysis, 10mg samples were heated from 27°C to 700°C at a heating rate of 10°C/min in a nitrogen environment. DSC was carried out using a Netzsch 214. Each sample of approximately 6 mg was placed in aluminum crucibles and heated from 30 °C to 210°C at a rate of 10 °C/min, then held under isothermal conditions for 6 min. Subsequently, samples were cooled down to 30 °C at a rate of 10 °C/min and left under isothermal condition for 2 min. A second heating cycle was followed under same conditions as the first heating cycle.

The Fourier transform infrared (FTIR) spectra was obtained using a Nicolet iS5 spectrometer in the attenuated total reflection (ATR) mode. .Samples of 1cm x 1cm were cut and placed in the FTIR machine. 16 scans were collected in the range of 400-4000cm^{-1} with a resolution of 4 cm^{-1}.

4.2.5 Cell viability study

35,000 3T3 mouse embryonic fibroblasts were seeded to a 24-well plate in the presence of the nanofiber matierals and incubated for two days. MTT Reagent (50 microliters) was added to each well and incubated for 4 hrs. Media was aspirated and 200 microliters DMSO added. MTT signal was detected at A595 using a BioRad plate reader.

4.2.6 Invitro anti cancer studies

To determine the anti-cancer effect of SA embedded with the nanofibers, in vitro cytotoxicity testing was carried out using human colon cancer HCT116 cell lines. 12,000 cells were seeded along with nanofiber(20mg) per well in 24-well plates using Dulbecco's modified Eagle's medium (DMEM) with 10% fetal bovine serum (FBS) and 5% antifungal/antibacterial (Anti/Anti, Thermo Fisher, Waltham, MA, USA). Cells were grown under standard tissue culture conditions (5% CO_2 and 37 °C) for five days. The effect of human cell proliferation and/or viability was assessed using the Trevigen TACS MTT Cell Proliferation Assay Kit (Gaithersburg, MD).

Fifty microliters of MTT reagent were added to each well and incubated under 5% CO_2 at 37 °C for another 4 h. Finally, 200 µL of DMSO reagent was added and incubation was continued for an additional 4 h. The optical density (A_{595}) was determined using a Bio-Rad iMark microplate absorbance reader. Samples were carried out in triplicate.

4.3 Results

Forcespinning® technology was chosen due to its ability to produce a high yield of nanofibers. Various concentrations of PL-CS-SA solutions were prepared to produce nanofiber. After optimization process, 18 wt. % of PL was selected considering a balance between fiber production yield and fiber diameter. . Regarding the Cs,. 2.2 wt% was selected as the optimum concentration to produce the nanofiber. Due to PL is a hydrophilic polymer, the nanofiber production yield was dependent on humidity as well. The optimal humidity for producing the composite nanofibers was found to be between 40 and 50%. SA-loaded PL-CS systems were developed with SA concentrations ranging from 1 to 50 percent (1, 3, 5, 15, 20, 33, and 50 wt. %). The optimal rpm for fiber production was found to be 6500. Samples with 20 and 33 wt.% of SA were selected for further morphological and thermophysical analysis. SEM images and statistical analysis of the fiber diameter of the developed samples are depicted in Fig. 2. The developed nanofibers had a long, smooth, and continuous fiber morphology with a sparse scattering of beads. The control PL-CS sample had the highest mean fiber diameter, 644 nm, with a standard deviation of 141 nm. With the increasing amount of SA the average fiber diameter decreased. The sample PL-CS-SA(H) had the lowest mean fiber diameter, 385 nm with a standard deviation of 122.85 nm. With the increase in the concentration of SA, the number of beads increased in the system. The fluorescent microscopy results reveal that SA concentrated in the beads of the nanofibers. The with the increasing amount of SA, bead size increased which resulted in the decrease in the diameter of the nanofiber.

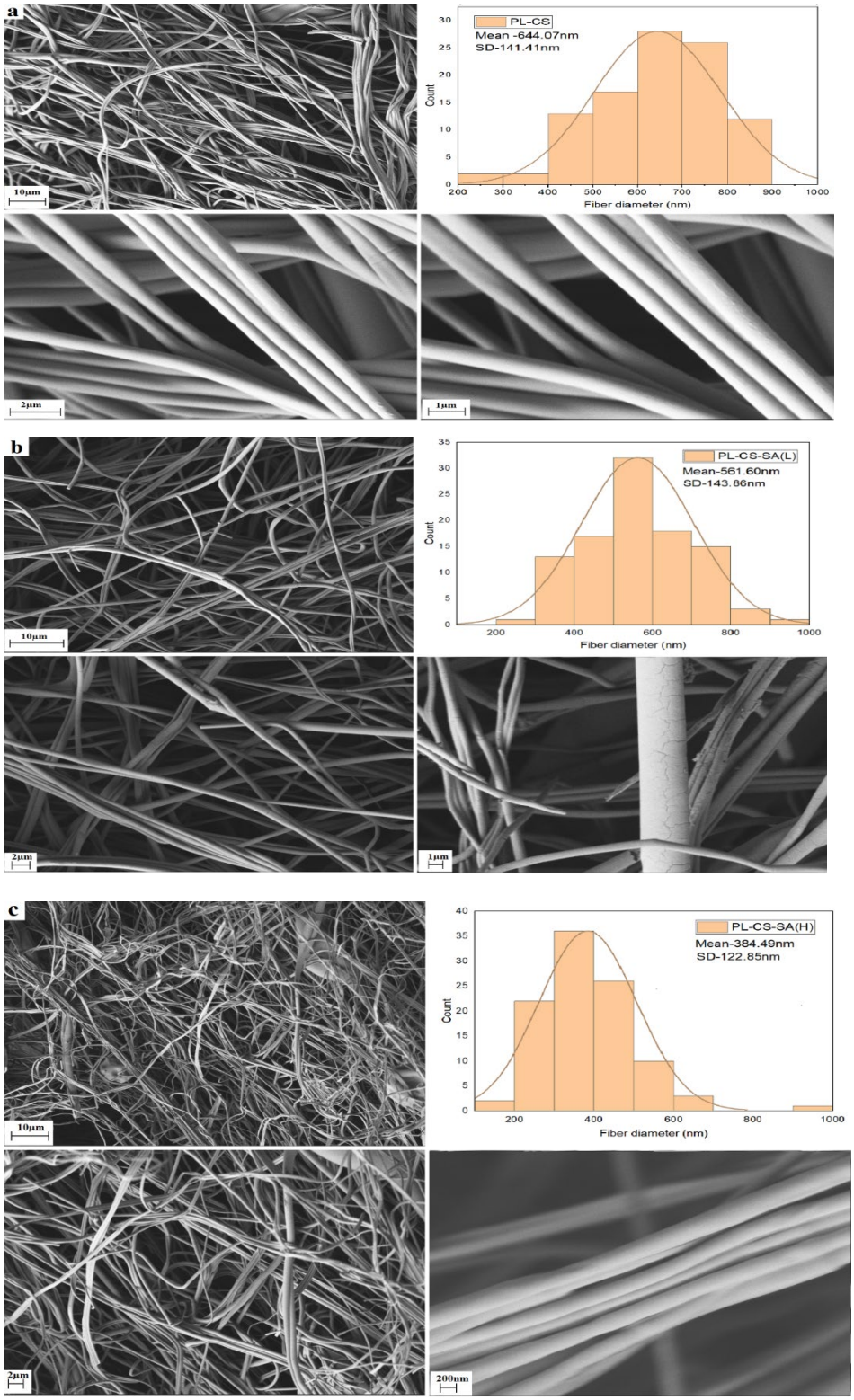

Fig-4.2: SEM micrographs and fiber distribution of the developed fibrous materials: PL-CS control (a), PL-CS-SA(L) (b), PL-CS-SA(H) (c).

The FTIR analysis was carried out to identify different functional groups and the interactions between PL, CS, and SA. Figure 4.3 shows the FTIR spectra of Danshen, Pullulan and chitosan powder, PL-CS control sample, and SA-loaded PL-CS nanofiber. SA showed a wide phenolic hydroxyl group peak at 3305cm^{-1}. The peak at 2926 cm^{-1} can be attributed to the stretching vibrations of $–CH_3$, $–CH_2$ groups. The peak at 1640 cm^{-1} was attributed to the stretching vibrations of C=O groups. The peaks between 1200–900 cm^{-1} are due to the stretching vibration of C–O, displayed by the characteristic absorptions of polysaccharides and glycosides (X. H. Liu et al. 2012). For pullulan, a large peak at 3331 cm^{-1} was attributed to O-H stretching, which was affected by the intermolecular or intramolecular hydrogen bonds. The C-H stretching vibration was associated with the peak at 2927 cm^{-1}, and the peak at 1149 cm^{-1} represents a polysaccharide (1,4) glycosidic bond stretching vibration (Jia Wu et al. 2013). A single band at 1639 cm^{-1} was attributed to O–C–O stretching vibration. The spectra also showed other characteristics, such as the C-O (997 cm^{-1}) and C-O-H bend (1340cm^{-1}) (Barbosa et al. 2021). For chitosan, the broad peak at 3353 cm^{-1} was due to O-H stretching, which overlaps with the N-H stretching in the same region and is also affected by the intermolecular/intramolecular hydrogen bonds (Jia Wu et al. 2013). The absorption band at around 2870 cm^{-1} is due to the asymmetric C–H stretching, a characteristic of polysaccharides. The C=O stretching of amide I band at 1654 cm^{-1} and C–N stretching band of amide III at 1319 cm^{-1} confirmed the presence of residual N-acetyl groups. Characteristic absorption bands at 1564 cm^{-1},1418 cm^{-1}, and 1376 cm^{-1} can be attributed to the NH_2 bending of the primary amine, CH_2 bending, and the distorting vibration of C-CH_3, respectively(Q. Wang et al. 2007)(Barbosa et al. 2021). In addition, the absorption band at 901 cm^{-1} was associated with the structure of the (1,4) glycoside bond, and the band at 1149 cm^{-1} can be attributed to C-O-C stretching vibration in the glucopyranose ring (G. He et al. 2011).

The control PL-CS crosslinked nanofiber showed a new band at 1723 $cm^{-1,}$ which is due to the C=O stretching vibration due to the carbonyl group in CA(Barbosa et al. 2021). The composite nanofibers contained the bands at 754 cm^{-1} and 928 cm^{-1} that show the presence of pullulan's two primary links, the α-(1,4)glycosidic bond and the α-(1,6) glycosidic bond, respectively(Cheng, Demirci, and Catchmark 2010).

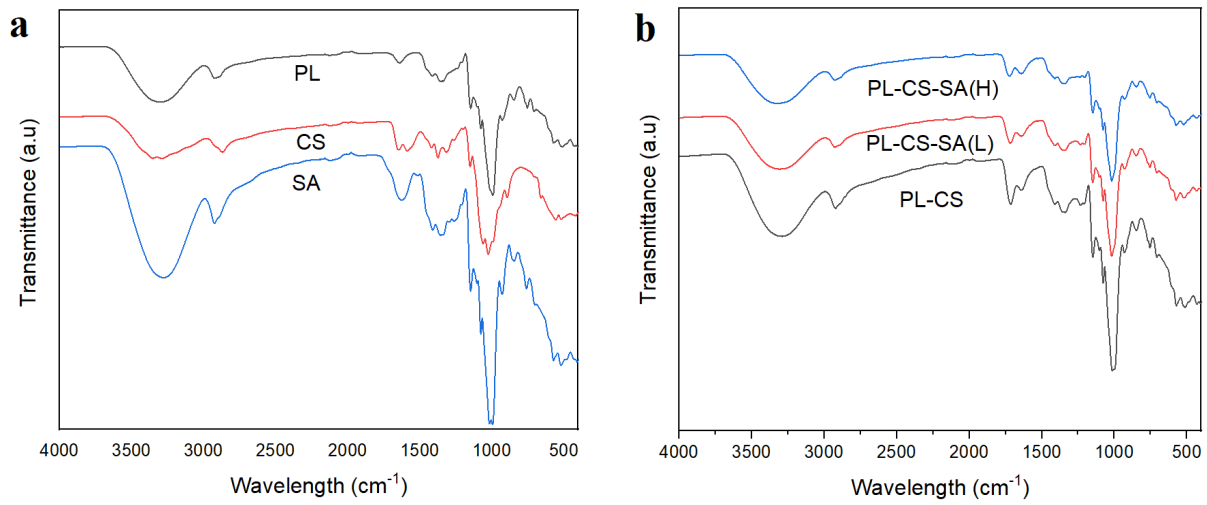

Figure 4.3: Fourier transform infrared (FTIR) spectra of PL powder, CS powder andSA powder(a), PL-CS control fiber, PL-CS-SA(L) composite fiber and PL-CS-SA(H)(b) composite fiber

Compared to the uncrosslinked fiber((supplemental-S3) , the intensity of broad bands around 3305 cm^{-1} for -OH stretching was diminished in the crosslinked fiber, which can be attributed to the formation of acetal bridges due to crosslinking(Mansur et al. 2008). Identical absorption bands were seen with lower intensity with the addition of SA in the nanofiber. Some minor modifications were observed in the spectra with the addition of SA. The result indicates good compatibility of SA in PL-CS composite fiber.

The thermal stability and effect of SA in the crosslinked composite nanofiber membranes were analyzed using athermogravimetric technique. The TGA and DTG thermograms of the samples are shown in Figure 4.4. The SA underwent several degrading stages, beginning with the loss of water content. In the TGA curve, the first step shows a loss of 8.4%. The second and third steps are the large-scale degradation of the SA's molecular framework. The onset temperature of degradation for SA is 200°C followed by a mass loss of 17%, between 200°-250°C.This weight loss could be related to the desorption of the hydroxyl group. The third step of degradation between 250-700°C is due to the degradation of toluene.

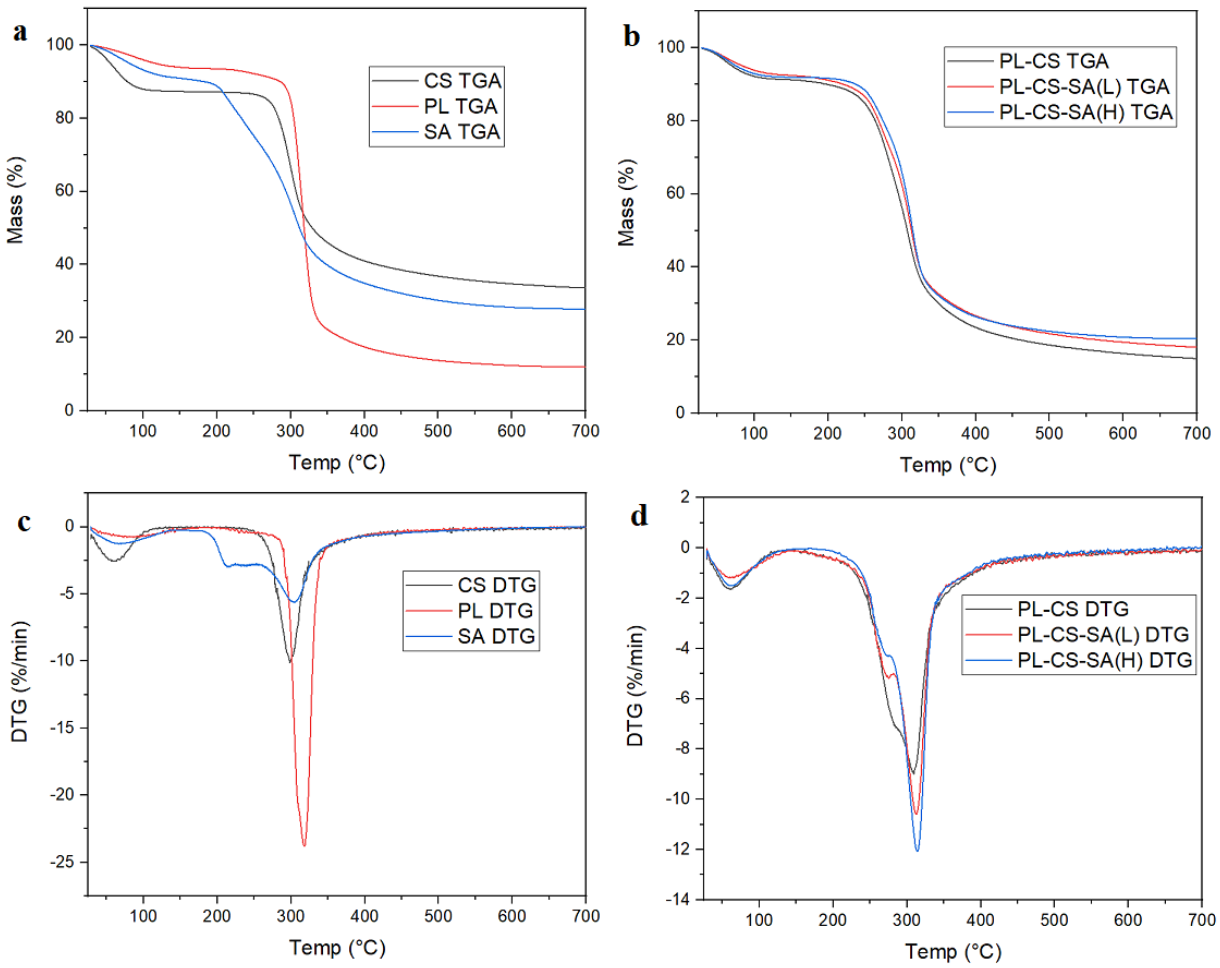

Figure 4.4: TGA(a) and DTG(c) analysis of PL, CS, and SA powder samples. TGA(b) and DTG(d) analysis of PL-CS control, PL-CS-SA(L) and PL-CS-SA(H) composite fiber

From room temperature to 200°C, Pullulan lost around 8% of its weight, which may have been caused by moisture evaporation (originating from the hydrogen bonds in the exopolysaccharide structure). The onset temperature of decomposition of Pullulan was 300°C. A major weight loss appeared between 300-330°C, indicating the degradation of Pullulan's chain structure. (Mirzaee et al. 2020) From the DTG curve, the maximum rate of weight loss was observed at 317°C.

The control PL-CS composite nanofiber membrane showed weight loss over two stages. The first one due to water loss. The second stage was the thermal degradation of the polymers, starting at 210°C. At this point, the material started to decompose as a result of the partial breakdown of the molecular structure and the disintegration of intermolecular connections.

(Lewandowska 2009) With the increase of SA content, the nanofiber membranes exhibited a higher decomposition onset temperature. It indicates that crosslinking between the PL-CS and SA increased the thermal stability of the nanofiber. The increase in SA content also affected the overall decomposition of the nanofiber samples. For the PL-CS control, PL-CS-SA(L), and PL-CS-SA(H), respectively, residual masses of 14.94%, 18.07%, and 20.45% represented the greater SA concentration in the sample.

In DSC, disappearance of endothermic peaks, emergence of new peaks, changes in peak form and its beginning or peak temperature, and relative peak area or enthalpy suggest a possible interaction. Figure 4.5(a) shows the DSC thermogram of raw pullulan, chitosan powder and danshen. Danshen sample showed several endothermic peaks with maximum points at 163°C, 176°C and 184°C. The melting event seen at 163°C was caused by salvianolic acid B, which melting point is approximately this temperature, and the others might be due to the impurities contained in danshen sample (Q. Peng et al. 2008). Pullulan and chitosan powder shows endothermic melting peaks at 201°C and 186°C.

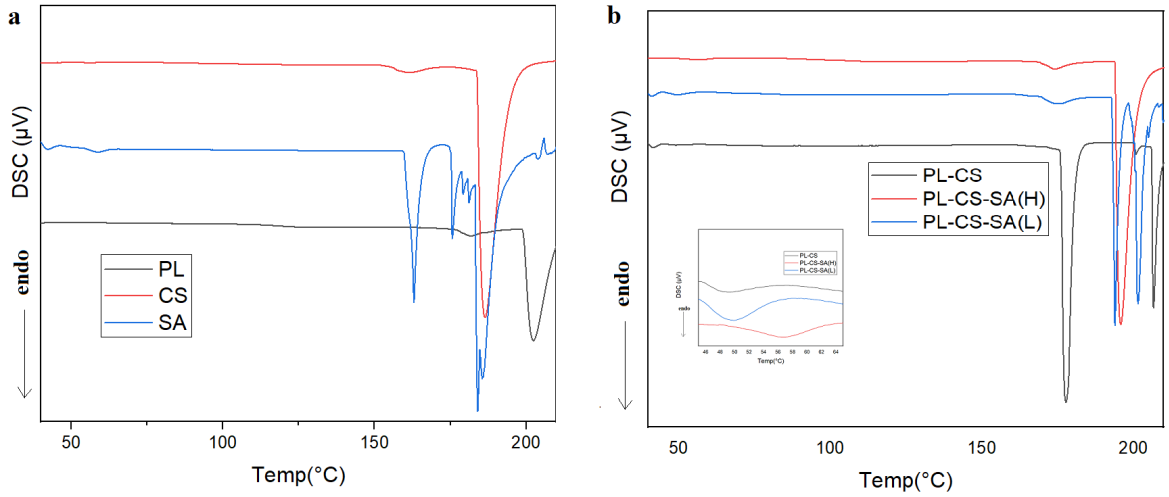

Figure 4.5: DSC analysis of PL, CS, and SA powder samples(a) and PL-CS control, PL-CS-SA(L) and PL-CS-SA(H) composite fiber(b)

Figure 4.5(b) shows the DSC thermogram of PL-CS control fiber, PL-CS-SA(L), and PL-CS-SA(H) fibers. The PL-CS control fiber showed a glass transition temperature (T_g) of 48.8°C. The glass transition temperatures increased with the incorporation of Danshen. The PL-CS-SA(L) and PL-CS-SA(H) fibers had glass transition temperatures of 49.2°C and 56.6°C, respectivelly.

The melting point of the fiber samples also increased with the increase of the Danshen content. Two melting point was observed in PL-CS control fiber. The PL-CS-SA(L) showed several endothermic peaks after 200°C. The PL-CS-SA(H) sample showed only one melting peak. This might be attributed to the fact that with the increase in SA content, the fiber diameter decreases, producing a higher ordered molecules. This leads to an alignment of the molecules in the fiber. The molecules are in a highly ordered form, leading to a single melting point of the fiber sample.

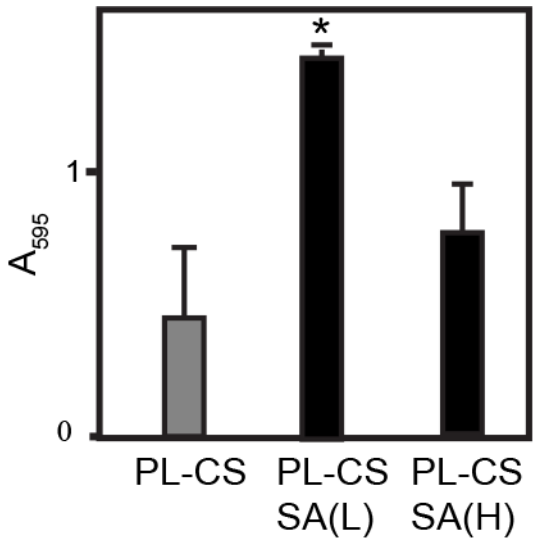

Figure 4.6: MTT assay of cell viability in the presence of PL-CS control and SA-containing nanofibers

To examine the effect of SA on mammalian cell growth, 3T3 cells were grown in the presence of control PL-CS fibers, as well as SA-containing (SA(L) and SA(H)) fibers. Strikingly, an MTT assay demonstrated that SA(L) incorporation actually confers improved cell growth, as compared with fibers composed of PL-CS alone. SA(H) fibers did not show a similar increase in cell presence. These results indicate that SA(L) provides an improved environment for cellular growth compared with fibers composed of PL-CS alone, possibly due to buffering the biochemical environment surrounding the fiber matrix.

To evaluate the anti-cancer properties of SA loaded nanofiber, MTT assay was performed on human colon cancer cells HCT116. The cytotoxic activity of the control fiber (PL-CS) and SA loaded fibers (PL-CS-SA(L) and PL-CS-SA(H)) and bare SA powder is shown in figure-4.7. No inhibition of cell growth is recorded for PL-CS control nanofibers. Nanofiber membrane loaded

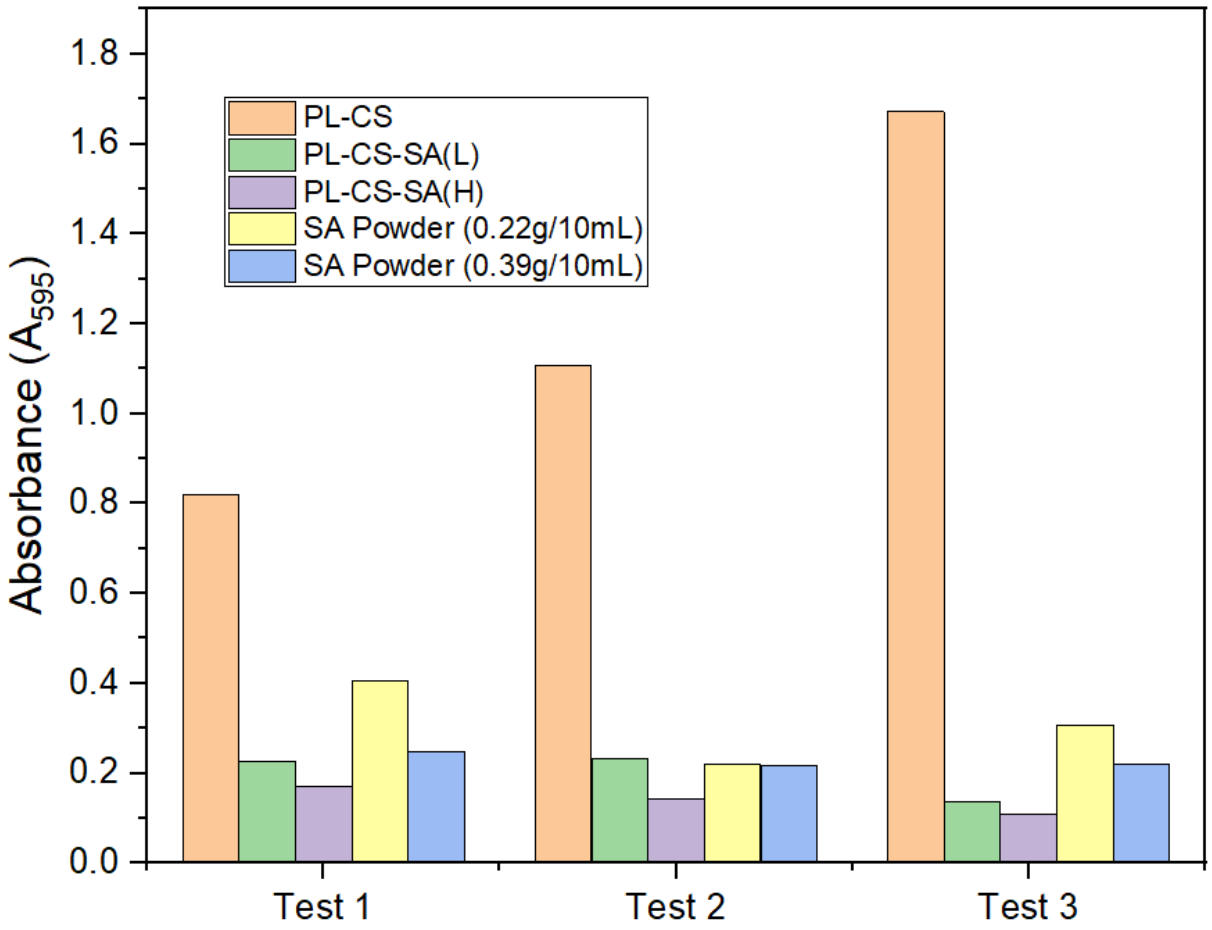

Figure 4.7: Anti cancer activity of PL-CS control, SA-containing nanofibers and raw SA-powder.

with SA (PL-CS-SA(L) and PL-SA-SA(H)) showed strong cytotoxicity against HCT116 colon cancer cells. The average cell inhibition rate for PL-CS-SA(L) and PL-CS-SA(H) is 83.4% and 90.3%, respectively. It could be interpreted from the results that SA retains its activity after the encapsulation into nanofibrous matrix and is not affected by the forcespinning process. The nanofiber samples showed higher cytotoxicity against HCT116 colon cancer cells compared to bare SA powder. It can be inferred that The polymeric nanofibers acted as a preservative agent for SA, improving its physiochemical stability and protecting it from premature breakdown. As a result, SA loaded nanofibers showed enhance activity compared to SA powder. Due to the biodegradability of PL, surgical removal is not necessary once drug release has been completed.

4.4 Discussion

FS technology enabled the successful fabrication of nanofiber membranes comprised of Danshen extract containing Salvianolic acid B (SA). Citric acid was used to crosslink the nanofibrous membranes in order to make them more stable in water.With increasing concentrations of SA, nanofibers exhibited a continuous homogeneous fiber structure with decreasing diameter. Increasing amount of SA increased the thermal stability of the nanofibrous membranes. The high surface area made it a potential candidate for drug loading in high concentration. Cell-based results indicate that nanofibers containing SA promotes cell growth and are not detrimental to the fibroblast cells. The anticancer study reveal that SA loaded nanofiber showed better inhibition to the cell proliferation of HCT116 colon cancer cells. After tumor removal, nanofibers loaded with chemotherapeutic drugs like SA can be placed on the removed tumor site to prevent colon cancer microdeposits from developing. Microdeposits of cancer always remain after surgery and those areas become difficult to penetrate. Once the nanofibers are placed on the tumor site it will slowly degrade and release the SA. These results suggest that SA-containing nanofibers may provide an innovative strategy for targeted delivery of anticancer agents in tumor sites.

CHAPTER V

CONCLUSION

FS technology enabled the successful fabrication of fine fiber based membranes containing the following bioactive compounds, OA, OM and SA. Two concentrations of OA,OM and SA were evaluated, 20 and 33 wt%. Comprehensive thermo-physical, and biological analysis was conducted for all systems. All systems prove the ability to develop, high yield of fiber membranes. For OA loaded fibers, High drug loading efficiency (>80%) was observed and cellular studies showed a non-cytotoxic behavior from the developed fiber membranes on fibroblast cells. Our cell-based results indicate that while, fibers containing OM are not cytotoxic to mammalian cells after 48 hrs, longer incubation with high concentration of OM-containing fibers elicits decreased cell viability relative to uncoated fibers. The anticancer study revealed that high concentration of OM loaded nanofiber showed inhibition to cell proliferation of HCT116 colon cancer cells. Cell-based results indicate that nanofibers containing SA promotes cell growth and are not detrimental to fibroblast cells while also providing inhibition to cell proliferation of HCT116 colon cancer cells. These results suggest that fiber containing SA and OM may provide an innovative strategy for targeted delivery of anticancer agents to tumor sites. Lining remaining tissues with nanofibers embedded with chemotherapeutic drugs such as OM and SA after tumor resection have the potential to deter colon cancer microdeposits left behind. These microdeposits are migratory and aggressive. These developed membranes have the potential to be used on the tumor site to deter further tumor development.

CHAPTER VI

FUTURE PROSPECTS

The study shows that nanofiber suitable for drug delivery can be produced using multiple polymers through forcespinning method. The in-vitro release studies show that the nanofibers can effectively suppress the proliferation of cancer cell and has the caliber to control/prolong the release of therapeutic agents. The future studies should focus on the in-vivo anti cancer studies of the nanofibers on the cancer cells using mice models to verify the effectiveness of the drug delivery method for therapeutic use.

REFERENCES

Akduman, Cigdem, Işik Özgüney, and E. Perrin Akcakoca Kumbasar. 2016. "Preparation and Characterization of Naproxen-Loaded Electrospun Thermoplastic Polyurethane Nanofibers as a Drug Delivery System." *Materials Science and Engineering C* 64: 383–90.

Akgün, Mert, Ihsan Başaran, Salih C. Suner, and Ayhan Oral. 2019. "Geraniol and Cinnamaldehyde as Natural Antibacterial Additives for Poly(Lactic Acid) and Their Plasticizing Effects." *Journal of Polymer Engineering*.

Alavarse, Alex Carvalho et al. 2017. "Tetracycline Hydrochloride-Loaded Electrospun Nanofibers Mats Based on PVA and Chitosan for Wound Dressing." *Materials Science and Engineering C* 77: 271–81. http://dx.doi.org/10.1016/j.msec.2017.03.199.

Almajhdi, Fahad N. et al. 2014. "In-Vitro Anticancer and Antimicrobial Activities of PLGA/Silver Nanofiber Composites Prepared by Electrospinning." *Journal of Materials Science: Materials in Medicine* 25(4): 1045–53.

Amarjargal, Altangerel et al. 2019. "On-Demand Drug Release from Tailored Blended Electrospun Nanofibers." *Journal of Drug Delivery Science and Technology* 52(December 2018): 8–14. https://doi.org/10.1016/j.jddst.2019.04.004.

Bahadoran, Maedeh, Amir Shamloo, and Yeganeh Dorri Nokoorani. 2020. "Development of a Polyvinyl Alcohol/Sodium Alginate Hydrogel-Based Scaffold Incorporating BFGF-Encapsulated Microspheres for Accelerated Wound Healing." *Scientific Reports* 10(1): 7–9. http://dx.doi.org/10.1038/s41598-020-64480-9.

Bansal, Vipin et al. 2011. "Applications of Chitosan and Chitosan Derivatives in Drug Delivery." *Biological Research* 5(1): 28–37.

Barbosa, Raul et al. 2021. "Aloe Vera Extract-Based Composite Nanofibers for Wound Dressing Applications." *Materials Science and Engineering C* 124(March): 112061. https://doi.org/10.1016/j.msec.2021.112061.

Basu, Sumit et al. 2012. “Colloidal Gold-Loaded, Biodegradable, Polymer-Based Stavudine Nanoparticle Uptake by Macrophages: An in Vitro Study.” *International Journal of Nanomedicine* 7: 6049–61.

BERNIER, B. 1958. “The Production of Polysaccharides by Fungi Active in the Decomposition of Wood and Forest Litter.” *Canadian journal of microbiology* 4(3): 195–204.

Blasi, Paolo et al. 2007. “Ketoprofen Poly(Lactide-Co-Glycolide) Physical Interaction.” *AAPS PharmSciTech* 8(2): 1–8.

Böncü, Tugba Eren, and Nurten Ozdemir. 2022. “Effects of Drug Concentration and PLGA Addition on the Properties of Electrospun Ampicillin Trihydrate-Loaded PLA Nanofibers.” *Beilstein Journal of Nanotechnology* 13: 245–54.

Cao, Wei et al. 2012. “Current Progress of Research on Pharmacologic Actions of Salvianolic Acid B.” *Chinese Journal of Integrative Medicine* 18(4): 316–20.

Catley, Brian J., Alison Ramsay, and Catherine Servis. 1986. “Observations on the Structure of the Fungal Extracellular Polysaccharide, Pullulan.” *Carbohydrate Research* 153(1): 79–86.

Chai, Ning Li et al. 2012. “Oxymatrine Liposome Attenuates Hepatic Fibrosis via Targeting Hepatic Stellate Cells.” *World Journal of Gastroenterology* 18(31): 4199–4206.

Chen, Hui et al. 2013. “Antiangiogenic Effects of Oxymatrine on Pancreatic Cancer by Inhibition of the NF-KB-Mediated VEGF Signaling Pathway.” *Oncology Reports* 30(2): 589–95.

Chen, Jian et al. 2015. “PAK6 Increase Chemoresistance and Is a Prognostic Marker for Stage II and III Colon Cancer Patients Undergoing 5-FU Based Chemotherapy.” *Oncotarget* 6(1): 355–67.

Chen, Tao et al. 2011. “Salvianolic Acid B Attenuates Brain Damage and Inflammation after Traumatic Brain Injury in Mice.” *Brain Research Bulletin* 84(2): 163–68. http://dx.doi.org/10.1016/j.brainresbull.2010.11.015.

Chen, Yong Hong, Guan Hua Du, and Jun Tian Zhang. 2000. “Salvianolic Acid B Protects Brain against Injuries Caused by Ischemia- Reperfusion in Rats.” *Acta Pharmacologica Sinica* 21(5): 463–66.

Cheng, Kuan Chen, Ali Demirci, and Jeffrey M. Catchmark. 2010. “Effects of Plastic Composite Support and PH Profiles on Pullulan Production in a Biofilm Reactor.” *Applied Microbiology and Biotechnology* 86(3): 853–61.

———. 2011. “Pullulan: Biosynthesis, Production, and Applications.” *Applied Microbiology and Biotechnology* 92(1): 29–44.

Chi, H. Y. et al. 2020. “Fabrication of Polylactic Acid/Paclitaxel Nano Fibers by Electrospinning for Cancer Therapeutics.” *BMC Chemistry* 14(1): 1–12. https://doi.org/10.1186/s13065-020-00711-4.

Cui, Zhixiang et al. 2018. “Electrospinning and Crosslinking of Polyvinyl Alcohol/Chitosan Composite Nanofiber for Transdermal Drug Delivery.” *Advances in Polymer Technology* 37(6): 1917–28.

Dai, Zhibo et al. 2018. “Oxymatrine Induces Cell Cycle Arrest and Apoptosis and Suppresses the Invasion of Human Glioblastoma Cells through the EGFR/PI3K/Akt/MTOR Signaling Pathway and STAT3.” *Oncology Reports* 40(2): 867–76.

Danhier, Fabienne et al. 2012. “PLGA-Based Nanoparticles: An Overview of Biomedical Applications.” *Journal of Controlled Release* 161(2): 505–22. http://dx.doi.org/10.1016/j.jconrel.2012.01.043.

Dharmappa, Kattepura K. et al. 2009. “Anti-Inflammatory Activity of Oleanolic Acid by Inhibition of Secretory Phospholipase A2.” *Planta Medica* 75(3): 211–15.

Eskitoros-Togay, Melda et al. 2019. “Fabrication of Doxycycline-Loaded Electrospun PCL/PEO Membranes for a Potential Drug Delivery System.” *International Journal of Pharmaceutics* 565(November 2018): 83–94.

Estevez-Areco, Santiago, Lucas Guz, Roberto Candal, and Silvia Goyanes. 2018. “Release Kinetics of Rosemary (Rosmarinus Officinalis) Polyphenols from Polyvinyl Alcohol (PVA) Electrospun Nanofibers in Several Food Simulants.” *Food Packaging and Shelf Life* 18(June): 42–50. https://doi.org/10.1016/j.fpsl.2018.08.006.

Fan, Jie Ping et al. 2021. “Preparation and Characterization of Oleanolic Acid-Based Low-Molecular-Weight Supramolecular Hydrogels Induced by Heating.” *ACS Applied Materials and Interfaces* 13(24): 29130–36.

Fathollahipour, Shahrzad, Ali Abouei Mehrizi, Azadeh Ghaee, and Mojtaba Koosha. 2015. “Electrospinning of PVA/Chitosan Nanocomposite Nanofibers Containing Gelatin Nanoparticles as a Dual Drug Delivery System.” *Journal of Biomedical Materials Research - Part A* 103(12): 3852–62.

Freire, Tania F. et al. 2021. “Thermal, Mechanical and Chemical Analysis of Poly(Vinyl

Alcohol) Multifilament and Braided Yarns." *Polymers* 13(21).

Fricain, Jean Christophe et al. 2013. "A Nano-Hydroxyapatite - Pullulan/Dextran Polysaccharide Composite Macroporous Material for Bone Tissue Engineering." *Biomaterials* 34(12): 2947–59. http://dx.doi.org/10.1016/j.biomaterials.2013.01.049.

Fu, Hsuan et al. 2021. "Oleanolic Acid Nanofibers Attenuated Particulate Matter-Induced Oxidative Stress in Keratinocytes." *Antioxidants* 10(9): 1–17.

Fukumura, Motonori et al. 2009. "Achyranthoside H Methyl Ester, a Novel Oleanolic Acid Saponin Derivative from Achyranthes Fauriei Roots, Induces Apoptosis in Human Breast Cancer MCF-7 and MDA-MB-453 Cells via a Caspase Activation Pathway." *Journal of Natural Medicines* 63(2): 181–88.

Gadhave, Ravindra V., Pratik Sanjiv Kasbe, Prakash A. Mahanwar, and Pradeep T. Gadekar. 2018. "To Study the Effect of Boric Acid Modification on Starch–Polyvinyl Alcohol Blend Wood Adhesive." *Journal of the Indian Academy of Wood Science* 15(2): 190–98. https://doi.org/10.1007/s13196-018-0225-2.

Gao, Dawei et al. 2007. "Antidiabetic Potential of Oleanolic Acid from Ligustrum Lucidum Ait." *Canadian Journal of Physiology and Pharmacology* 85(11): 1076–83.

Gao, Meng et al. 2016. "Oleanolic Acid-Loaded PLGA-TPGS Nanoparticles Combined with Heparin Sodium-Loaded PLGA-TPGS Nanoparticles for Enhancing Chemotherapy to Liver Cancer." *Life Sciences* 165: 63–74.

Gao, Nannan, Mengran Guo, Qiang Fu, and Zhonggui He. 2017. "Application of Hot Melt Extrusion to Enhance the Dissolution and Oral Bioavailability of Oleanolic Acid." *Asian Journal of Pharmaceutical Sciences* 12(1): 66–72. http://dx.doi.org/10.1016/j.ajps.2016.06.006.

Gatti, John W. et al. 2013. "Using Electrospun Poly(Ethylene-Oxide) Nanofibers for Improved Retention and Efficacy of Bacteriolytic Antibiotics." *Biomedical Microdevices* 15(5): 887–93.

Gentile, Piergiorgio, Valeria Chiono, Irene Carmagnola, and Paul V. Hatton. 2014. "An Overview of Poly(Lactic-Co-Glycolic) Acid (PLGA)-Based Biomaterials for Bone Tissue Engineering." *International Journal of Molecular Sciences* 15(3): 3640–59.

Ghosh, Santanu, Nabanita Kar, and Tanmoy Bera. 2016. "Oleanolic Acid Loaded Poly Lactic Co- Glycolic Acid- Vitamin E TPGS Nanoparticles for the Treatment of Leishmania

Donovani Infected Visceral Leishmaniasis." *International Journal of Biological Macromolecules* 93: 961–70. http://dx.doi.org/10.1016/j.ijbiomac.2016.09.014.

Gouda, M., A. A. Hebeish, and A. I. Aljafari. 2014. "Synthesis and Characterization of Novel Drug Delivery System Based on Cellulose Acetate Electrospun Nanofiber Mats." *Journal of Industrial Textiles* 43(3): 319–29.

Grenha, Ana, and Susana Rodrigues. 2013. "Pullulan-Based Nanoparticles: Future Therapeutic Applications in Transmucosal Protein Delivery." *Therapeutic Delivery* 4(11): 1339–41.

Guimarães, Pedro P.G. et al. 2015. "PLGA Nanofibers Improves the Antitumoral Effect of Daunorubicin." *Colloids and Surfaces B: Biointerfaces* 136: 248–55.

Guo, Piaoting et al. 2018. "Salvianolic Acid B Reverses Multidrug Resistance in Nude Mice Bearing Human Colon Cancer Stem Cells." *Molecular Medicine Reports* 18(2): 1323–34.

Guzman, Javier Rivera et al. 2013. "Oxymatrine Prevents NF-KB Nuclear Translocation and Ameliorates Acute Intestinal Inflammation." *Scientific Reports* 3: 1–9.

Han, D., S. Filocamo, R. Kirby, and A. J. Steckl. 2011. "Deactivating Chemical Agents Using Enzyme-Coated Nanofibers Formed by Electrospinning." *ACS Applied Materials and Interfaces* 3(12): 4633–39.

Hao, Yubin et al. 2009. "Salvianolic Acid B Inhibits Growth of Head and Neck Squamous Cell Carcinoma in Vitro and in Vivo via Cyclooxygenase-2 and Apoptotic Pathways." *International Journal of Cancer* 124(9): 2200–2209.

Hasegawa, Urara et al. 2005. "Nanogel-Quantum Dot Hybrid Nanoparticles for Live Cell Imaging." *Biochemical and Biophysical Research Communications* 331(4): 917–21.

He, Guanghua et al. 2011. "Synthesis, Characterization and Antibacterial Activity of Salicyloyl Chitosan." *Carbohydrate Polymers* 83(3): 1274–78. http://dx.doi.org/10.1016/j.carbpol.2010.09.034.

He, Qianjun et al. 2010. "An Anti-ROS/Hepatic Fibrosis Drug Delivery System Based on Salvianolic Acid B Loaded Mesoporous Silica Nanoparticles." *Biomaterials* 31(30): 7785–96. http://dx.doi.org/10.1016/j.biomaterials.2010.07.008.

Hu, Jun, Junchao Wei, Wanyun Liu, and Yiwang Chen. 2013. "Preparation and Characterization of Electrospun PLGA/Gelatin Nanofibers as a Drug Delivery System by Emulsion Electrospinning." *Journal of Biomaterials Science, Polymer Edition* 24(8): 972–85.

Hua, S. et al. 2021. "Oxymatrine Reduces Expression of Programmed Death-Ligand 1 by

Promoting DNA Demethylation in Colorectal Cancer Cells." *Clinical and Translational Oncology* 23(4): 750–56.

Irene, Bonadies, Veronica Ambrogi, Ascione Laura, and Carfagna Cosimo. 2014. "A Hyperbranched Polyester as Antinucleating Agent for Artemisinin in Electrospun Nanofibers." *European Polymer Journal* 60: 145–52. http://dx.doi.org/10.1016/j.eurpolymj.2014.09.005.

"J Biomed Mater Res - 2004 - Katti - Bioresorbable Nanofiber-based Systems for Wound Healing and Drug Delivery Optimization.Pdf."

"J of Applied Polymer Sci - 2012 - Padron - Production and Characterization of Hybrid BEH-PPV PEO Conjugated Polymer.Pdf."

Janković, Biljana et al. 2013. "The Design Trend in Tissue-Engineering Scaffolds Based on Nanomechanical Properties of Individual Electrospun Nanofibers." *International Journal of Pharmaceutics* 455(1–2): 338–47.

Ji, Xin Yan, Benny K.H. Tan, and Yi Zhun Zhu. 2000. "Salvia Miltiorrhiza and Ischemic Diseases." *Acta Pharmacologica Sinica* 21(12): 1089–94.

Jiang, Xiaotao et al. 2018. "Oral Oxymatrine for Hepatitis B Cirrhosis A Systematic Review Protocol." *Medicine (United States)* 97(49): 1–5.

Jie, Liu. 1995. "Pharmacology of Oleanolic Acid and Ursolic Acid." *Journal of Ethnopharmacology* 49(2–1): 57–68.

Jin, Nan, Yong Xing Zhao, Shu Hua Deng, and Qian Sun. 2011. "Preparation and in Vitro Anticancer Activity of Oxymatrine Mixed Micellar Nanoparticles." *Pharmazie* 66(7): 506–10.

Jing, Zhao et al. 2016. "Salvianolic Acid B, a Novel Autophagy Inducer, Exerts Antitumor Activity as a Single Agent in Colorectal Cancer Cells." *Oncotarget* 7(38): 61509–19.

Kadajji, Veeran Gowda, and Guru V. Betageri. 2011. "Water Soluble Polymers for Pharmaceutical Applications." *Polymers* 3(4): 1972–2009.

Kajdič, Saša, Odon Planinšek, Mirjana Gašperlin, and Petra Kocbek. 2019. "Electrospun Nanofibers for Customized Drug-Delivery Systems." *Journal of Drug Delivery Science and Technology* 51(January): 672–81.

Kamath, S. Manjunath et al. 2020. "Fabrication of Tri-Layered Electrospun Polycaprolactone Mats with Improved Sustained Drug Release Profile." *Scientific Reports* 10(1): 1–13.

https://doi.org/10.1038/s41598-020-74885-1.

Khampieng, Thitikan, Gary E. Wnek, and Pitt Supaphol. 2014. "Electrospun DOXY-h Loaded-Poly(Acrylic Acid) Nanofiber Mats: In Vitro Drug Release and Antibacterial Properties Investigation." *Journal of Biomaterials Science, Polymer Edition* 25(12): 1292–1305. http://dx.doi.org/10.1080/09205063.2014.929431.

Khwaza, Vuyolwethu, Opeoluwa O. Oyedeji, and Blessing A. Aderibigbe. 2018. "Antiviral Activities of Oleanolic Acid and Its Analogues." *Molecules* 23(9).

Kim, Jeong Hwa et al. 2016. "Juniperus Chinensis Extracts Loaded PVA Nanofiber: Enhanced Antibacterial Activity." *Materials Letters* 181: 367–70. http://dx.doi.org/10.1016/j.matlet.2016.05.164.

Kim, Sejeong et al. 2015. "Antimicrobial Action of Oleanolic Acid on Listeria Monocytogenes, Enterococcus Faecium, and Enterococcus Faecalis." *PLoS ONE* 10(3): 1–11.

Kimoto, T., T. Shibuya, and S. Shiobara. 1997. "Safety Studies of a Novel Starch, Pullulan: Chronic Toxicity in Rats and Bacterial Mutagenicity." *Food and Chemical Toxicology* 35(3–4): 323–29.

Kong, Lingbao et al. 2013. "Oleanolic Acid and Ursolic Acid: Novel Hepatitis C Virus Antivirals That Inhibit NS5B Activity." *Antiviral Research* 98(1): 44–53. http://dx.doi.org/10.1016/j.antiviral.2013.02.003.

Kuang, Haizhu et al. 2018. "A Method for Preparation of an Internal Layer of Artificial Vascular Graft Co-Modified with Salvianolic Acid B and Heparin." *ACS Applied Materials and Interfaces* 10(23): 19365–72.

Lay, Ing Shiow et al. 2003. "Salvianolic Acid B Enhances in Vitro Angiogenesis and Improves Skin Flap Survival in Sprague-Dawley Rats." *Journal of Surgical Research* 115(2): 279–85.

Lewandowska, Katarzyna. 2009. "Miscibility and Thermal Stability of Poly(Vinyl Alcohol)/Chitosan Mixtures." *Thermochimica Acta* 493(1–2): 42–48.

Li, Bin et al. 2021. "Coamorphous System of Florfenicol-Oxymatrine for Improving the Solubility and Dissolution Rate of Florfenicol: Preparation, Characterization and Molecular Dynamics Simulation." *Journal of Pharmaceutical Sciences* 110(6): 2544–54.

Li Bin, Yi Hu, Ting Wu, Ying Feng, Cuiping Jiang, Hongzhi Du, Shan Lu,Apigenin-oxymatrine binary co-amorphous mixture: Enhanced solubility, bioavailability, and anti-inflammatory effect,Food Chemistry,Volume 373, Part B,2022,131485,ISSN 0308-

8146,https://doi.org/10.1016/j.foodchem.2021.131485.

Li, Hongquan et al. 2016. "Cellular Uptake and Anticancer Activity of Salvianolic Acid B Phospholipid Complex Loaded Nanoparticles in Head and Neck Cancer and Precancer Cells." *Colloids and Surfaces B: Biointerfaces* 147: 65–72. http://dx.doi.org/10.1016/j.colsurfb.2016.07.053.

Li, Huanan et al. 2011. "Superabsorbent Polysaccharide Hydrogels Based on Pullulan Derivate as Antibacterial Release Wound Dressing." *Journal of Biomedical Materials Research - Part A* 98 A(1): 31–39.

Liang, Li, and Jiean Huang. 2016. "Oxymatrine Inhibits Epithelial-Mesenchymal Transition through Regulation of NF-KB Signaling in Colorectal Cancer Cells." *Oncology Reports* 36(3): 1333–38.

Liang, Ya Hui et al. 2009. "Salvianolic Acid B in Vitro Inhibited Matrix Metalloproteinases-1, -2, and-9 Activities." *Journal of Chinese Integrative Medicine* 7(2): 145–50.

Liang, Yongping et al. 2019. "PH-Responsive Injectable Hydrogels with Mucosal Adhesiveness Based on Chitosan-Grafted-Dihydrocaffeic Acid and Oxidized Pullulan for Localized Drug Delivery." *Journal of Colloid and Interface Science* 536: 224–34. https://doi.org/10.1016/j.jcis.2018.10.056.

Liao, Hsien Shun et al. 2016. "Self-Assembly Mechanisms of Nanofibers from Peptide Amphiphiles in Solution and on Substrate Surfaces." *Nanoscale* 8(31): 14814–20.

Lin, Sien et al. 2019. "PLGA/β-TCP Composite Scaffold Incorporating Salvianolic Acid B Promotes Bone Fusion by Angiogenesis and Osteogenesis in a Rat Spinal Fusion Model." *Biomaterials* 196: 109–21. https://doi.org/10.1016/j.biomaterials.2018.04.004.

Liu, Chang Suo et al. 2006. "Comparison of Antioxidant Activities between Salvianolic Acid B and Ginkgo Biloba Extract (EGb 761)." *Acta Pharmacologica Sinica* 27(9): 1137–45.

Liu, Hanqing et al. 2010. "The Analgesic Effect and Mechanism of the Combination of Sodium Ferulate and Oxymatrine." *Neurochemical Research* 35(9): 1368–75.

Liu, He et al. 2018. "A Functional Chitosan-Based Hydrogel as a Wound Dressing and Drug Delivery System in the Treatment of Wound Healing." *RSC Advances* 8(14): 7533–49. http://dx.doi.org/10.1039/C7RA13510F.

Liu, Meifeng, Sha Jin, Hao Yan, and Song Du. 2017. "Effect of Oxymatrine HSPC Liposomes on Improving Bioavailability, Liver Target Distribution and Hepatoprotective Activity of

Oxymatrine." *European Journal of Pharmaceutical Sciences* 104(December 2016): 212–20. http://dx.doi.org/10.1016/j.ejps.2017.03.048.

Liu, Qi et al. 2021. "Antibacterial Activity and Drug Loading of Moxifloxacin-Loaded Poly(Vinyl Alcohol)/Chitosan Electrospun Nanofibers." *Frontiers in Materials* 8(February): 1–9.

Liu, Qingchao et al. 2013. "Synthesis and Antitumor Activities of Naturally Occurring Oleanolic Acid Triterpenoid Saponins and Their Derivatives." *European Journal of Medicinal Chemistry* 64: 1–15. http://dx.doi.org/10.1016/j.ejmech.2013.04.016.

Liu, Shujie et al. 2020. "Polymer Template Synthesis of Flexible SiO2Nanofibers to Upgrade Composite Electrolytes." *ACS Applied Materials and Interfaces* 12(28): 31439–47.

Liu, Xiaodong, Dong Wang, Wenping Yang, and Xiaomeng Wu. 2020. "Oxymatrine Exerts Anti-Fibrotic Effects in a Rat Model of Hepatic Fibrosis by Suppressing Endoplasmic Reticulum Stress." *Journal of International Medical Research* 48(10).

Liu, Xin Hu et al. 2012. "Analysis and Identification of Chinese Drugs by Three-Step Infrared Spectroscopy - A Case Study of Danshen." *Analytical Methods* 4(10): 3344–50.

Liu, Yan et al. 2014. "Anti-Tumor Activities of Matrine and Oxymatrine: Literature Review." *Tumor Biology* 35(6): 5111–19.

Löbmann, Korbinian et al. 2013. "Amino Acids as Co-Amorphous Stabilizers for Poorly Water-Soluble Drugs - Part 2: Molecular Interactions." *European Journal of Pharmaceutics and Biopharmaceutics* 85(3 PART B): 882–88.

Lou, Lihua et al. 2019. "Functional PVA/VB2/TiO2 Nanofiber Webs for Controlled Drug Delivery." *ACS Applied Bio Materials* 2(12): 5916–29.

Lu, Mei Li, Xiao Hui Xiang, and Shi Hai Xia. 2016. "Potential Signaling Pathways Involved in the Clinical Application of Oxymatrine." *Phytotherapy Research* 1112(February): 1104–12.

Ma, Zhi Jie et al. 2013. "Combining Oxymatrine or Matrine with Lamivudine Increased Its Antireplication Effect against the Hepatitis B Virus in Vitro." *Evidence-based Complementary and Alternative Medicine* 2013. https://www.hindawi.com/journals/ecam/2013/186573/.

Maiza, Mounira, Mohamed Tahar Benaniba, Guilhem Quintard, and Valerie Massardier-Nageotte. 2015. "Biobased Additive Plasticizing Polylactic Acid (PLA)." *Polimeros* 25(6): 581–90.

Malik, Rafi, Tarun Garg, Amit K. Goyal, and Goutam Rath. 2015. "Polymeric Nanofibers: Targeted Gastro-Retentive Drug Delivery Systems." *Journal of Drug Targeting* 23(2): 109–24.

Mansur, Herman S., Carolina M. Sadahira, Adriana N. Souza, and Alexandra A.P. Mansur. 2008. "FTIR Spectroscopy Characterization of Poly (Vinyl Alcohol) Hydrogel with Different Hydrolysis Degree and Chemically Crosslinked with Glutaraldehyde." *Materials Science and Engineering C* 28(4): 539–48.

Martínez-Martínez, Mayte et al. 2018. "Ionic Hydrogel Based on Chitosan Cross-Linked with 6-Phosphogluconic Trisodium Salt as a Drug Delivery System." *Biomacromolecules* 19(4): 1294–1304.

McGuire, Shelley. 2016. "World Cancer Report 2014. Geneva, Switzerland: World Health Organization, International Agency for Research on Cancer, WHO Press, 2015." *Advances in Nutrition* 7(2): 418–19.

Meng, Z. X. et al. 2011. "Preparation and Characterization of Electrospun PLGA/Gelatin Nanofibers as a Potential Drug Delivery System." *Colloids and Surfaces B: Biointerfaces* 84(1): 97–102.

Mengoni, Fabio et al. 2002. "In Vitro Anti-HIV Activity of Oleanolic Acid on Infected Human Mononuclear Cells." *Planta Medica* 68(2): 111–14.

Mir, Maria, Naveed Ahmed, and Asim ur Rehman. 2017. "Recent Applications of PLGA Based Nanostructures in Drug Delivery." *Colloids and Surfaces B: Biointerfaces* 159: 217–31. https://doi.org/10.1016/j.colsurfb.2017.07.038.

Mirzaee, Homaira, Faramarz Khodaiyan, John F. Kennedy, and Seyed Saeid Hosseini. 2020. "Production, Optimization and Characterization of Pullulan from Sesame Seed Oil Cake as a New Substrate by Aureobasidium Pullulans." *Carbohydrate Polymer Technologies and Applications* 1(July): 100004. https://doi.org/10.1016/j.carpta.2020.100004.

Mishra, Bishwambhar, Vuppu Suneetha, and Kalyani Rath. 2011. "The Role of Microbial Pullulan, a Biopolymer in Pharmaceutical Approaches: A Review." *Journal of Applied Pharmaceutical Science* 1(6): 45–50.

Molki, Banafsheh et al. 2019. "Properties Investigation of Polyvinyl Alcohol Barrier Films Reinforced by Calcium Carbonate Nanoparticles." *Materials Research Express* 6(5).

Mondal, Kunal et al. 2014. "Highly Sensitive Biofunctionalized Mesoporous Electrospun TiO2

Nanofiber Based Interface for Biosensing." *ACS Applied Materials and Interfaces* 6(4): 2516–27.

Moydeen, A. Meera et al. 2018. "Fabrication of Electrospun Poly(Vinyl Alcohol)/Dextran Nanofibers via Emulsion Process as Drug Delivery System: Kinetics and in Vitro Release Study." *International Journal of Biological Macromolecules* 116: 1250–59. https://doi.org/10.1016/j.ijbiomac.2018.05.130.

Nakahashi-Ouchida, Rika, Yoshikazu Yuki, and Hiroshi Kiyono. 2018. "Cationic Pullulan Nanogel as a Safe and Effective Nasal Vaccine Delivery System for Respiratory Infectious Diseases." *Human Vaccines and Immunotherapeutics* 14(9): 2189–93. https://doi.org/10.1080/21645515.2018.1461298.

Nataraj, Divya, Roopa Reddy, and Narendra Reddy. 2020. "Crosslinking Electrospun Poly (Vinyl) Alcohol Fibers with Citric Acid to Impart Aqueous Stability for Medical Applications." *European Polymer Journal* 124(January): 109484. https://doi.org/10.1016/j.eurpolymj.2020.109484.

Nataraj, Divya, Seema Sakkara, Murlidhar Meghwal, and Narendra Reddy. 2018. "Crosslinked Chitosan Films with Controllable Properties for Commercial Applications." *International Journal of Biological Macromolecules* 120: 1256–64. http://dx.doi.org/10.1016/j.ijbiomac.2018.08.187.

Nii, Teruki. 2021. "Strategies Using Gelatin Microparticles for Regenerative Therapy and Drug Screening Applications." *Molecules* 26(22): 1–45.

Padron, Simon, Arturo Fuentes, Dumitru Caruntu, and Karen Lozano. 2013. "Experimental Study of Nanofiber Production through Forcespinning." *Journal of Applied Physics* 113(2).

Pant, Bishweshwar, Mira Park, and Soo Jin Park. 2019. "Drug Delivery Applications of Core-Sheath Nanofibers Prepared by Coaxial Electrospinning: A Review." *Pharmaceutics* 11(7).

Parwe, Sharad P. et al. 2014. "Synthesis of Ciprofloxacin-Conjugated Poly (L-Lactic Acid) Polymer for Nanofiber Fabrication and Antibacterial Evaluation." *International Journal of Nanomedicine* 9(1): 1463–77.

Peng, Hongsen et al. 2008. "In Vitro Degradation and Release Profiles for Electrospun Polymeric Fibers Containing Paracetanol." *Colloids and Surfaces B: Biointerfaces* 66(2): 206–12.

Peng, Liangquan et al. 2019. "Characterization of a Novel Polyvinyl Alcohol/Chitosan Porous

Hydrogel Combined with Bone Marrow Mesenchymal Stem Cells and Its Application in Articular Cartilage Repair." *BMC Musculoskeletal Disorders* 20(1): 1–12.

Peng, Qiang et al. 2008. "Enhanced Oral Bioavailability of Salvianolic Acid B by Phospholipid Complex Loaded Nanoparticles." *Pharmazie* 63(9): 661–66.

"Phytotherapy Research - 2010 - Yong-gang - Antiarrhythmic Effects and Ionic Mechanisms of Oxymatrine from Sophora.Pdf."

Pınar, O, Filiz Yangılar, Pınar Oğuzhan, and Filiz Yangılar. 2013. "Pullulan : Production and Usage in Food Industry." *African Journal of Food Science and Technology* 4(3): 57–63.

Pollier, Jacob, and Alain Goossens. 2012. "Oleanolic Acid." *Phytochemistry* 77: 10–15. http://dx.doi.org/10.1016/j.phytochem.2011.12.022.

Rahmani, Fatemeh et al. 2021. "Electrospun Pvp/Pva Nanofiber Mat as a Novel Potential Transdermal Drug-Delivery System for Buprenorphine: A Solution Needed for Pain Management." *Applied Sciences (Switzerland)* 11(6).

Raimi-Abraham, Bahijja Tolulope et al. 2015. "Development and Characterization of Amorphous Nanofiber Drug Dispersions Prepared Using Pressurized Gyration." *Molecular Pharmaceutics* 12(11): 3851–61.

Reddy, A. Babul et al. 2016. "5-Fluorouracil Loaded Chitosan–PVA/Na+MMT Nanocomposite Films for Drug Release and Antimicrobial Activity." *Nano-Micro Letters* 8(3): 260–69.

Rishabha, Malviya, Srivastava Pranati, Bansal Mayank, and P. K. Sharma. 2010. "Preparation and Evaluation of Disintegrating Properties of Cucurbita Maxima Pulp Powder." *International Journal of Pharmaceutical Sciences* 2(1 A): 395–99.

Roberts, George A. F. 1992. "Solubility and Solution Behaviour of Chitin and Chitosan." *Chitin Chemistry*: 274–329.

Rodriguez, Cristobal et al. 2022. "Cell Proliferative Properties of Forcespinning® Nopal Composite Nanofibers." *Journal of Bioactive and Compatible Polymers* 37(1): 28–37.

Sanchez, M. A., A. P. Rodriguez, L. N. Monsalve, and S. Georgiadou. 2020. "Emulsion Electrospinning for Drug Delivery : Two Encapsulation Methods." *Austin Journal of Pharmacology and Therapeutics* 8(1): 1–8. www.austinpublishinggroup.com.

Santos, Carla et al. 2014. "Preparation and Characterization of Polysaccharides/PVA Blend Nanofibrous Membranes by Electrospinning Method." *Carbohydrate Polymers* 99: 584–92. http://dx.doi.org/10.1016/j.carbpol.2013.09.008.

Sarkar, Kamal et al. 2010. “Electrospinning to Forcespinning™.” *Materials Today* 13(11): 12–14.

Saxena, S K. 2004. “POLYVINYL ALCOHOL (PVA) Chemical and Technical Assessment (CTA) First Draft Prepared By.” *Chemical and Technical Assessment 61st JECFA* 1(3).

Semnani, Koroush et al. 2018. “Antifungal Activity of Eugenol Loaded Electrospun PAN Nanofiber Mats Against Candida Albicans.” *Current Drug Delivery* 15(6): 860–66.

Shanmugam, Muthu K. et al. 2014. “Oleanolic Acid and Its Synthetic Derivatives for the Prevention and Therapy of Cancer: Preclinical and Clinical Evidence.” *Cancer Letters* 346(2): 206–16. http://dx.doi.org/10.1016/j.canlet.2014.01.016.

Shawe, J, R Riesen, J Widmann, and M Schubnell. 2000. “UserCom.” *Mettler Toledo*: 1–28.

Shi, H. J. et al. 2019. “Oxymatrine Therapy Inhibited Epidermal Cell Proliferation and Apoptosis in Severe Plaque Psoriasis.” *British Journal of Dermatology* 181(5): 1028–37.

Shi, Rui et al. 2008. “The Effect of Citric Acid on the Structural Properties and Cytotoxicity of the Polyvinyl Alcohol/Starch Films When Molding at High Temperature.” *Carbohydrate Polymers* 74(4): 763–70.

Shoba, Ekambaram, Rachita Lakra, Manikantan Syamala Kiran, and Purna Sai Korrapati. 2017. “Fabrication of Core-Shell Nanofibers for Controlled Delivery of Bromelain and Salvianolic Acid B for Skin Regeneration in Wound Therapeutics.” *Biomedical Materials (Bristol)* 12(3).

Shukry, N A Abdullah, K Ahmad Sekak, M R Ahmad, and T J Bustami Effendi. 2014. “Proceedings of the International Colloquium in Textile Engineering, Fashion, Apparel and Design 2014 (ICTEFAD 2014).” *Proceedings of the International Colloquium in Textile Engineering, Fashion, Apparel and Design 2014 (ICTEFAD 2014)* (September).

Siegel, Rebecca, Jiemin Ma, Zhaohui Zou, and Ahmedin Jemal. 2014. “Cancer Statistics, 2014.” *CA: A Cancer Journal for Clinicians* 64(1): 9–29.

Singh, R. S., and G. K. Saini. 2008. “Pullulan-Hyperproducing Color Variant Strain of Aureobasidium Pullulans FB-1 Newly Isolated from Phylloplane of Ficus Sp.” *Bioresource Technology* 99(9): 3896–99.

Singh, R.S., Saini, G.K. (2012). Biosynthesis of Pullulan and Its Applications in Food and Pharmaceutical Industry. In: Satyanarayana, T., Johri, B. (eds) Microorganisms in Sustainable Agriculture and Biotechnology. Springer, Dordrecht.

https://doi.org/10.1007/978-94-007-2214-9_24

Singh, Ram S., Gaganpreet K. Saini, and John F. Kennedy. 2009. “Downstream Processing and Characterization of Pullulan from a Novel Colour Variant Strain of Aureobasidium Pullulans FB-1.” *Carbohydrate Polymers* 78(1): 89–94. http://dx.doi.org/10.1016/j.carbpol.2009.03.040.

Singh, Ram Sarup, and Navpreet Kaur. 2010. “Microbial Biopolymers for Edible Film and Coating Applications.” *Advances in Industrial Biotechnology* (December): 187–216.

Singh, Ram Sarup, Navpreet Kaur, Muhammad Hassan, and John F. Kennedy. 2021. “Pullulan in Biomedical Research and Development - A Review.” *International Journal of Biological Macromolecules* 166: 694–706. https://doi.org/10.1016/j.ijbiomac.2020.10.227.

Singh, Ram Sarup, Navpreet Kaur, Vikas Rana, and John F. Kennedy. 2017. “Pullulan: A Novel Molecule for Biomedical Applications.” *Carbohydrate Polymers* 171: 102–21. http://dx.doi.org/10.1016/j.carbpol.2017.04.089.

Song, Botao, Chengtie Wu, and Jiang Chang. 2012. “Controllable Delivery of Hydrophilic and Hydrophobic Drugs from Electrospun Poly(Lactic-Co-Glycolic Acid)/Mesoporous Silica Nanoparticles Composite Mats.” *Journal of biomedical materials research. Part B, Applied biomaterials* 100(8): 2178–86.

Song, Song Ie, and Byoung Chul Kim. 2004. “Characteristic Rheological Features of PVA Solutions in Water-Containing Solvents with Different Hydration States.” *Polymer* 45(7): 2381–86.

Sonker, Amit Kumar, Kalpana Rathore, Rajaram Krishna Nagarale, and Vivek Verma. 2018. “Crosslinking of Polyvinyl Alcohol (PVA) and Effect of Crosslinker Shape (Aliphatic and Aromatic) Thereof.” *Journal of Polymers and the Environment* 26(5): 1782–94.

Sutherland, Ian W. 1998. “Novel and Established Applications of Microbial Polysaccharides.” *Trends in Biotechnology* 16(1): 41–46.

Tacx, J. C.J.F., H. M. Schoffeleers, A. G.M. Brands, and L. Teuwen. 2000. “Dissolution Behavior and Solution Properties of Polyvinylalcohol as Determined by Viscometry and Light Scattering in DMSO, Ethyleneglycol and Water.” *Polymer* 41(3): 947–57.

Taepaiboon, Pattama, Uracha Rungsardthong, and Pitt Supaphol. 2006. “Drug-Loaded Electrospun Mats of Poly(Vinyl Alcohol) Fibres and Their Release Characteristics of Four Model Drugs.” *Nanotechnology* 17(9): 2317–29.

Taepaiboon P, Rungsardthong U, Supaphol P. Vitamin-loaded electrospun cellulose acetate nanofiber mats as transdermal and dermal therapeutic agents of vitamin A acid and vitamin E. Eur J Pharm Biopharm. 2007 Sep;67(2):387-97. doi: 10.1016/j.ejpb.2007.03.018. Epub 2007 Mar 31. PMID: 17498935.

Tang, Guoke et al. 2020. "Recent Advances of Chitosan-Based Injectable Hydrogels for Bone and Dental Tissue Regeneration." *Frontiers in Bioengineering and Biotechnology* 8(September): 1–15.

Tang, Minke et al. 2006. "Salvianolic Acid B Improves Motor Function after Cerebral Ischemia in Rats." *Behavioural Pharmacology* 17(5–6): 493–98.

Teixeira, Ana C.T. et al. 2010. "Phase Behaviour of Oleanolic Acid, Pure and Mixed with Stearic Acid: Interactions and Crystallinity." *Chemistry and Physics of Lipids* 163(7): 655–66.

Tian, Tian et al. 2017. "Synthesis of Novel Oleanolic Acid and Ursolic Acid in C-28 Position Derivatives as Potential Anticancer Agents." *Archives of Pharmacal Research* 40(4): 458–68.

Upadhyay, Kamal K. et al. 2010. "The Intracellular Drug Delivery and Anti Tumor Activity of Doxorubicin Loaded Poly(γ-Benzyl l-Glutamate)-b-Hyaluronan Polymersomes." *Biomaterials* 31(10): 2882–92.

Venkatesh, D. Nagasamy et al. 2015. "Fabrication and in Vivo Evaluation of Nelfinavir Loaded PLGA Nanoparticles for Enhancing Oral Bioavailability and Therapeutic Effect." *Saudi Pharmaceutical Journal* 23(6): 667–74. http://dx.doi.org/10.1016/j.jsps.2015.02.021.

Wang, Y., Meng, G.D.L., Zheng, W.Y., Liu, Q.D. 2003. "Pharmacokinetics of Oxymatrine Injection Healthy Volunteers." *Chin. J. Clin. Pharmacol.*: 301–5.

Wang, Qun, Zhanfeng Dong, Yumin Du, and John F. Kennedy. 2007. "Controlled Release of Ciprofloxacin Hydrochloride from Chitosan/Polyethylene Glycol Blend Films." *Carbohydrate Polymers* 69(2): 336–43.

Wang, Xin et al. 2010. "Antioxidant Activities of Oleanolic Acid in Vitro: Possible Role of Nrf2 and MAP Kinases." *Chemico-Biological Interactions* 184(3): 328–37. http://dx.doi.org/10.1016/j.cbi.2010.01.034.

Wang X, Liu R, Zhang W, Zhang X, Liao N, Wang Z, Li W, Qin X, Hai C. Oleanolic acid improves hepatic insulin resistance via antioxidant, hypolipidemic and anti-inflammatory

effects. Mol Cell Endocrinol. 2013 Aug 25;376(1-2):70-80. doi:10.1016/j.mce.2013.06.014.

Wang, Yingsa et al. 2019. "Amphiphilic Carboxylated Cellulose-g-Poly(L-Lactide) Copolymer Nanoparticles for Oleanolic Acid Delivery." *Carbohydrate Polymers* 214(January): 100–109. https://doi.org/10.1016/j.carbpol.2019.03.033.

Wang, Yu Ping et al. 2011. "Oxymatrine Inhibits Hepatitis B Infection with an Advantage of Overcoming Drug-Resistance." *Antiviral Research* 89(3): 227–31. http://dx.doi.org/10.1016/j.antiviral.2011.01.005.

Wang, Zhi hong, Cheng chin Hsu, Chien ning Huang, and Mei chin Yin. 2010. "Anti-Glycative Effects of Oleanolic Acid and Ursolic Acid in Kidney of Diabetic Mice." *European Journal of Pharmacology* 628(1–3): 255–60. http://dx.doi.org/10.1016/j.ejphar.2009.11.019.

Wegiel, Lindsay A., Lisa J. Mauer, Kevin J. Edgar, and Lynne S. Taylor. 2013. "Crystallization of Amorphous Solid Dispersions of Resveratrol during Preparation and Storage-Impact of Different Polymers." *Journal of Pharmaceutical Sciences* 102(1): 171–84.

Wen, Jian Bo et al. 2014. "Oxymatrine Improves Intestinal Epithelial Barrier Function Involving NF-KB-Mediated Signaling Pathway in CCl4-Induced Cirrhotic Rats." *PLoS ONE* 9(8): 2–8.

Wong, Victor W. et al. 2011. "Engineered Pullulan-Collagen Composite Dermal Hydrogels Improve Early Cutaneous Wound Healing." *Tissue Engineering - Part A* 17(5–6): 631–44.

Wu, Chun Song et al. 2005. "Treatment of Pig Serum-Induced Rat Liver Fibrosis with Boschniakia Rossica, Oxymatrine and Interferon-α." *World Journal of Gastroenterology* 11(1): 122–26.

Wu, Cunzao et al. 2015. "Oxymatrine Inhibits the Proliferation of Prostate Cancer Cells in Vitro and in Vivo." *Molecular Medicine Reports* 11(6): 4129–34.

Wu, Jia et al. 2013. "Preparation and Characterization of Pullulan-Chitosan and Pullulan-Carboxymethyl Chitosan Blended Films." *Food Hydrocolloids* 30(1): 82–91. http://dx.doi.org/10.1016/j.foodhyd.2012.04.002.

Wu, Jie et al. 2017. "Oxymatrine Promotes S-Phase Arrest and Inhibits Cell Proliferation of Human Breast Cancer Cells in Vitro through Mitochondria-Mediated Apoptosis." *Biological and Pharmaceutical Bulletin* 40(8): 1232–39.

Xi, Keli et al. 1996. "Liver Targeting of Interferon through Pullulan Conjugation." *Pharmaceutical Research* 13(12): 1846–50.

Xiao, Zhuo Bing, Man Man Guo, and Rui Ke Guo. 2014. "Thermal Decomposition Mechanism and Kinetics of Ursolic Acid and Caffeic Acid." *Chemistry and Industry of Forest Products* 34(2): 33–39.

Xie, Jingwei, and Chi Hwa Wang. 2006. "Electrospun Micro- and Nanofibers for Sustained Delivery of Paclitaxel to Treat C6 Glioma in Vitro." *Pharmaceutical Research* 23(8): 1817–26.

Xie, Li Xia et al. 2010. "The Effect of Salvianolic Acid B Combined with Laminar Shear Stress on TNF-α-Stimulated Adhesion Molecule Expression in Human Aortic Endothelial Cells." *Clinical Hemorheology and Microcirculation* 44(4): 245–58.

Xiong, Xiao Hong et al. 2016. "Absorption Mechanism of Oxymatrine in Cultured Madin–Darby Canine Kidney Cell Monolayers." *Pharmaceutical Biology* 54(10): 2168–75.

Xu, Fenghua et al. 2015. "Development of Tannic Acid/Chitosan/Pullulan Composite Nanofibers from Aqueous Solution for Potential Applications as Wound Dressing." *Carbohydrate Polymers* 115: 16–24. http://dx.doi.org/10.1016/j.carbpol.2014.08.081.

Xu, Jiqing, Yanpeng Jiao, Xiaohong Shao, and Changren Zhou. 2011. "Controlled Dual Release of Hydrophobic and Hydrophilic Drugs from Electrospun Poly (l-Lactic Acid) Fiber Mats Loaded with Chitosan Microspheres." *Materials Letters* 65(17–18): 2800–2803. http://dx.doi.org/10.1016/j.matlet.2011.06.018.

Xue, Jiajia, Jingwei Xie, Wenying Liu, and Younan Xia. 2017. "Electrospun Nanofibers: New Concepts, Materials, and Applications." *Accounts of Chemical Research* 50(8): 1976–87.

Yang, Jianfeng liu Jinjian liu hongyan Xu Yumin Zhang liping chu Qingfen liu Naling song cuihong, and Tianjin. 2014. "Peptide Nanofiber as a Carrier for Effective Curcumin Delivery." *international journal of Nanomedicine* 9: 197–207.

Yao, Yihan et al. 2020. "Nanoparticle-Based Drug Delivery in Cancer Therapy and Its Role in Overcoming Drug Resistance." *Frontiers in Molecular Biosciences* 7(August): 1–14.

Ying, Xin Jiang et al. 2015. "Oxymatrine Downregulates HPV16E7 Expression and Inhibits Cell Proliferation in Laryngeal Squamous Cell Carcinoma Hep-2 Cells in Vitro." *BioMed Research International* 2015.

Yu, Deng-Guang, Li-Min Zhu, Kenneth White, and Chris Branford-White. 2009. "Electrospun Nanofiber-Based Drug Delivery Systems." *Health* 01(02): 67–75.

Yu, Dong et al. 2021. "Fabrication, Characterization, and Antibacterial Properties of Citric Acid

Crosslinked PVA Electrospun Microfibre Mats for Active Food Packaging." *Packaging Technology and Science* 34(6): 361–70.

Yue, Peng Fei et al. 2010. "Process Optimization, Characterization and Evaluation in Vivo of Oxymatrine-Phospholipid Complex." *International Journal of Pharmaceutics* 387(1–2): 139–46. http://dx.doi.org/10.1016/j.ijpharm.2009.12.008.

Zhang, Xiaoli, Keyong Tang, and Xuejing Zheng. 2016. "Electrospinning and Crosslinking of COL/PVA Nanofiber-Microsphere Containing Salicylic Acid for Drug Delivery." *Journal of Bionic Engineering* 13(1): 143–49.

Zhang, Y., G. Talmon, and J. Wang. 2015. "MicroRNA-587 Antagonizes 5-FU-Induced Apoptosis and Confers Drug Resistance by Regulating PPP2R1B Expression in Colorectal Cancer." *Cell Death and Disease* 6: 1–12.

Zhao, Hanqing et al. 2013. "Efficient Synthesis and Anti-Fungal Activity of Oleanolic Acid Oxime Esters." *Molecules* 18(3): 3615–29.

Zhao, Peng et al. 2015. "Oxymatrine Attenuated Hypoxic-Ischemic Brain Damage in Neonatal Rats via Improving Antioxidant Enzyme Activities and Inhibiting Cell Death." *Neurochemistry International* 89: 17–27. http://dx.doi.org/10.1016/j.neuint.2015.06.008.

Zhao, Yuan et al. 2010. "Combination Effects of Salvianolic Acid B with Low-Dose Celecoxib on Inhibition of Head and Neck Squamous Cell Carcinoma Growth in Vitro and in Vivo." *Cancer Prevention Research* 3(6): 787–96.

Zhou, Limin, Zhong Zuo, and Moses Sing Sum Chow. 2005. "Danshen: An Overview of Its Chemistry, Pharmacology, Pharmacokinetics, and Clinical Use." *Journal of Clinical Pharmacology* 45(12): 1345–59.

BIOGRAPHICAL SKETCH

Salahuddin Ahmed has acquired his bachelor's degree in Mechanical Engineering from Bangladesh University of Engineering and Technology in 2017 and joined the department of Mechanical Engineering at the University of Texas Rio Grande Valley in Spring 2021 for pursuing a Master's. He worked as a research assistant at the Polymer and Nanofiber Development lab under Dr. Karen Lozano and completed his Master of Science in Mechanical Engineering in December 2022. He earned his Master of Science in Mechanical Engineering at The University of Texas Rio Grande Valley in December 2022. His research interests are focused on nano bio materials for drug delivery and tissue engineering. During his Master's, he was awarded the Presidential Graduate Research Assistantship award for all two years. He has co-authored one article in a prestigious journal, one poster presentation, and is on the verge of submitting three articles. He will pursue Ph.D at Pennsylvania State University after completion of his master's degree. He can be reached at s.ahmed.me156@gmail.com.